UNIVERSITY OF CALIFORNIA
RIVERSIDE

Genetic and Bioinformatic Characterization of Mammalian Antiviral RNA Interference

A Dissertation submitted in partial satisfaction
of the requirements for the degree of

Doctor of Philosophy

in

Genetics, Genomics and Bioinformatics

by

Jinfeng Lu

December 2015

Dissertation Committee:
Dr. Shou-wei Ding, Chairperson
Dr. Jason E. Stajich
Dr. Weifeng Gu

The Dissertation of Jinfeng Lu is approved:

Committee Chairperson

University of California, Riverside

Acknowledgements

I would like to express my deepest gratitude to my advisor, Dr. Shou-wei Ding, for his excellent guidance and caring. My research would not have been possible without his contributions of funds, time, ideas and experimental assistance during the past five years. It has been an honor to become a PhD student working in such a great lab under Dr. Ding's excellent leadership, and I benefited a lot from not only his academic knowledge but also his life philosophy.

I would like to thank Dr. Jason E. Stajich and Dr. Weifeng Gu, who kindly served as my dissertation committee members and gave me lots of great suggestions to help me finish this work. I also want to thank Dr. A.L.N. Rao, Dr. Peter Atkinson, Dr. Wenbo Ma and Dr. Yinsheng Wang, who together with Dr. Jason E. Stajich kindly served as my qualifying exam committee. I also want to thank the advisors of Genetics, Genomics and Bioinformatics (GGB) program: Dr. Hailing Jin, Dr. Thomas Girke, and Dr. Shizhong Xu, who have provided me an excellent platform to combine my programming training with my research. Special thank goes to GGB student service advisor Ms. Deidra Kornfeld, who has helped me a lot during my study in University of California, Riverside.

I would like to thank my collaborators in this work and all other former and current members in Ding lab: Ms. Wanxiang Li, Dr. Yang Li, Dr. Yanhong Han, Dr. Xiaoxu Fan, Ms. Shuwei Dong, Dr. Qingxia Han, Dr. Xin Zhong, Ms. Stephanie Coffman, *et al*. They have given me great assistance and guidance during my research, and it has been a great

pleasure to work with them in such great academic atmosphere.

Finally, I would like to thank my parents, Xin Che and Guobin Lu, and other members in my family, for their warm support during my study abroad.

This dissertation thesis contains the results (illustrated by Figures 2.3, 2.4, 2.5, 2.6, 2.7, 2.8, and 2.9, and Tables 2.1 and 2.2) that were included in the report <RNA Interference Functions as an Antiviral Immunity Mechanism in Mammals> published in *Science* in 2013, of which I am a co-first author.

Jinfeng Lu
University of California, Riverside
December, 2015

ABSTRACT OF THE DISSERTATION

Genetic and Bioinformatic Characterization of Mammalian Antiviral RNA Interference

by

Jinfeng Lu

Doctor of Philosophy, Graduate Program in Genetics, Genomics and Bioinformatics
University of California, Riverside, December 2015
Dr. Shou-wei Ding, Chairperson

Diverse eukaryotic hosts produce virus-derived small interfering RNAs (siRNAs) to direct antiviral immunity by RNA interference (RNAi). However, it has been controversial in the past decade whether the mammalian RNAi pathway has a natural antiviral function. In this dissertation, I demonstrate the production of canonical virus-derived siRNAs processed by endoribonuclease Dicer from viral double-stranded RNA (dsRNA) precursors in cultured hamster and human somatic cells and in mice infected by two distinct RNA viruses after their cognate viral suppressor of RNA silencing (VSR) is rendered inactive. These mammalian viral siRNAs are predominantly 22 nucleotides long and contain mostly uridine as the 5'-terminal nucleotide, and are therefore similar to mammalian microRNAs. I show that canonical viral siRNAs are loaded into mouse and human Argonaute proteins at high levels in the infected cells. Further analysis reveals that the VSR protein NS1 of Influenza A virus inhibits the biogenesis of viral siRNAs whereas the VSR protein B2 of Nodamura virus suppresses both the biogenesis and the Argonaute loading of viral siRNAs during infection. The

results together demonstrate that the antiviral RNAi response is conserved in mammals as found in fungi, plants, insects, and nematodes.

Table of Contents

List of Figures

Chapter 2

List of Tables

Chapter 2

Chapter 3

Chapter 1: Introduction

1.1 RNA virus and replication

Viruses are small pathogenic agents relying on host cells (*1*). Viruses are the most abundant biological entities on the earth with estimated 10^{31} species, infecting almost every cellular organism from the animals to the plants, and predominantly the bacteria (*2*). Without the cell structure of other life forms, viruses replicate inside the host cells using the host machinery to synthesize specialized self-assembled particles known as virions, and release the progeny to infect the new cells by cell lysis or budding (*3*). Among the individuals in a population the viruses can be transmitted either vertically (from mother to child) or horizontally (from person to person) (*4, 5*). Viruses cause human diseases such as shingles, influenza, SARS, AIDS and Ebola, and some species can induce cancer (*6-11*). There are three hypotheses to the origin of viruses: the regressive hypothesis, the cellular origin hypothesis and the co-evolution hypothesis, but the origin of viruses is still unclear as each hypothesis has its own problems (*12*).

Virions may be naked consisting of protein capsid and the packaged DNA or RNA as the genetic materials or enveloped with a lipid coat (*3, 13-14*). There are seven virus families according to the Baltimore classification system based on their genome types and their replication strategies: (I) double-stranded DNA (dsDNA) viruses, (II) single-stranded DNA (ssDNA) viruses, (III) double-stranded RNA (dsRNA) viruses, (IV)

positive-strand RNA (+RNA) viruses, (V) negative-strand RNA (-RNA) viruses, (VI) single-stranded RNA retro-transcription (ssRNA-RT) viruses, and (VII) double-stranded DNA retro-transcription (dsDNA-RT) viruses (*15*). RNA viruses broadly exist in the plants and animals (*1*), and have RNA as the genetic material with no DNA intermediates in the life cycle, including families III, IV and V in the Baltimore classification system (*16*). The viral RNA polymerization, including both viral replication and transcription, is catalyzed by the virus-encoded RNA-dependent RNA polymerase (RdRP) as well as other enzymes such as helicase, capping enzymes and NTPase (*16-17*). The RdRPs are believed to be the only viral protein containing motifs conserved in all RNA viruses (*18*). The three-dimensional structures available from five families of (+)RNA viruses show that the RdRPs share an overall "right-handed" structure with "fingers", "palm" and "thumb" domains conserved in other types of polymerases (*17*). RNA viruses have different replication and transcription machineries (*16*): (+)RNA viruses anchor their replication complexes to the intracellular membranes, and replicate asymmetrically ~100 times more positive RNAs than negative RNAs (*19*); (-)RNA viruses have the negative RNA genome as the template for both replication and transcription. (-)RNA viruses pack their genome into a helical-shaped, protein-coated structure known as the ribonucloeprotein complex (RNP), and in such way newly made progeny viral RNA (vRNA) and the replication intermediate (cRNA) can be stabilized in a single-stranded form immediately after the synthesis (*20*). Multiple segmented (-)RNA viruses such as the influenza A virus have conserved vRNA termini recognized and bound by the heterotrimeric polymerase (*21*), while non-segmented (-) RNA viruses undergo

conformational changes in the nucleocapsid and allow the polymerase access to RNA to initiate RNA synthesis (*22-23*); dsRNA viruses enclose their genomes and RdRPs by a viral capsid to form subviral particles, and the progeny dsRNA genomes are replicated inside the particles (*24*). During the transcription of dsRNA viruses, the asymmetrically capping to the (+)RNA strand inhibits the binding of RdRPs and allows efficient initiation of transcription from the (-)RNA strand only (*25*). The RNA polymerization initiates at or near the 3' end of the viral genome, or internally to the template strand during subgenomic synthesis (*26-27*). The initiation of RNA polymerization can be either *de novo* (primer-independent), or primer-dependent using leader RNAs synthesized by the viruses, protein-linked RNA oligonucleotides (protein-primed), oligonucleotides cleaved from the 5' end of cellular capped mRNA (cap-snatching), or back-looped 3' end of the template RNA strand as the primers (*26-29*). Although the *de novo* initiation is the most common strategy of the viral RdRPs, some viruses use different initiation strategies separately among genomic replication, transcription and subgenomic synthesis (*26-27*). During the RNA polymerization a partially double-stranded RNA structure is formed. To date the detection of such double-stranded RNA by immunofluorescence is reported upon infection by dsRNA viruses, (+)RNA viruses, (-)RNA viruses, dsDNA viruses, and ssDNA viruses (*30, 205*).

Very few viral pathogens can be effectively controlled to date possibly due to the evolution of the viruses (*31*). Besides the genomic recombinations and the segment resortments shared by all the viruses, RNA viruses particularly have a million fold higher

mutation rate compared to DNA viruses because of the lack of the proof-reading activity of the RdRPs and the instability of the RNA genomes (*32-33*). For example, the evolutionary rate of the NS gene of influenza A virus is 2×10^{-3} substitution per site per year, which is about 10^6 higher compared to the mammalian germline genes (*34*). Therefore the concept quasispecies is used to describe the mutant distribution of RNA viruses stated as "a huge swarm of mutants" derived from the "master sequence" (*31-32, 35*). Viral quasispecies allow the appearance of vaccine-escape and drug-resistant strains within short time periods by the continuous input of mutant genomes during replication, which have a major negative impact on the disease control of RNA viruses (*31*), and inspire people to explore broader-spectrum antiviral strategies targeting the fundamental machineries of RNA viruses.

1.2 Innate immunity against RNA virus

The host defense against the pathogens relies on three systems: anatomic and physiologic barriers, innate immunity and adaptive immunity (*36*). Anatomic and physiologic barriers work as the first defense line to protect the host from the infections, and include the skin, mucociliary clearance mechanisms, stomach acid, and bacteriolytic lysozyme in secretions like tears and saliva (*36*). The disruption of these barriers burdens the innate and adaptive immune systems, and usually they cannot compensate the loss of anatomic and physiologic barriers. Blood-brain barrier (BBB) functions as a physical barrier

between the peripheral circulation and the central nervous system to protect the brain against microbial invasions, and the disruption of BBB by viruses may lead to serious encephalitis accompanied with significant mortality (*37*). Adaptive immunity active in vertebrates depends on recombination of a large array of gene segments to generate the pathogen recognition receptors to mediate pathogen-specific immunologic response. After the primary response the cells involved in adaptive immunity expressing the recognition receptors retain the immunologic memory and respond rapidly to the pathogen upon re-exposure (*38-40*). Adaptive immune responses include cellular immunity by T lymphocytes from the thymus and humoral immunity by B lymphocytes from the bone marrow (*38*). T cells are activated by the recognition of T-cell receptors (TCRs) to antigen peptide fragments presented within the major histocompatibility complex (MHC) on cell surfaces, to trigger the immune response by killing the infected cells, providing cognate or cytokine signals to enhance both B cell and T cell responses, and motivating mononuclear phagocytes (*38-39*). In gnathostomes (jawed vertebrates) the variety of TCRs is achieved by assembly of the array of V (variable), D (diversity) and J (joining) segments from the original TCR loci by V(D)J recombinase composed of proteins encoded by recombinase-activating genes 1 and 2 (RAG1 and RAG2) (*38*), while in agnathans (jawless vertebrates) it's made by inserting diverse LRR modules from flanking genomic cassettes to the original variable lymphocyte receptor (VLR) gene (*39-40*). B cells activated by T-independent antigens (by themselves or facilitated by signals provided by cytokines or dendritic cells) or T-dependent antigens can change the production type of immunoglobulins, as well as activating nucleotide substitution in the

immunoglobulin heavy and light chain variable regions (*38, 41-42*). These processes, known as class-switching and somatic hypermutation (SHM), lead to the production of antibodies with higher affinity to the antigen (*38*). The cognate interaction between T cells and B cells activates the latter to be differentiated into memory cells for response upon next exposure, or plasma cells producing large amounts of antibodies (*38*).

Innate immunity responds to the pathogen-associated molecular patterns (PAMPs) by the function of pattern-recognition receptors (PRRs) (*43*). Unlike adaptive immunity which requires the rearrangement to the gene segments for the production of various pathogen-specific receptors, innate immunity relies on a limited number of receptors encoded by germline genes (*44*). Though adaptive immunity allows the recognition to almost all the pathogens by the diversity of receptors and the immunological memory for future responses, it takes three to five days for the colonial expansion of the T cells and B cells with the specific receptors to execute a robust clearance of the pathogen, with the risk of autoimmune diseases. By contrast, innate immunity reacts much faster within minutes after the exposure to the pathogen (*36, 44*). Moreover, the PAMPs recognized by innate immunity are usually conserved structures or components essential to the pathogens or common biologic consequences of infection, preventing viruses and other pathogens from escaping innate immune detection by their rapid evolution (*36*). Therefore, innate immunity functions as a universal and ancient host defense mechanism against pathogen infections, and the fact that plants and invertebrates which have no adaptive immunity and rely only on innate immunity indicates the critical importance of

innate immunity (*39-40, 44-45*).

There are several classes of PRRs to recognize viruses, bacteria and fungi in innate immunity, including Toll-like receptors (TLRs) for cell-extrinsic recognition, the nucleotide binding and oligomerization domain (NOD)-like receptors (NLRs) and the retinoic acid inducible gene I (RIG-I)-like receptors (RLRs) for cell-intrinsic recognition (*43*). TLRs are type I transmembrane proteins composed of an ectodomain which contains leucine-rich repeats (LRR) for the recognition of PAMPs, a transmembrane region, and cytosolic Toll-IL-1 receptor (TIR) domains to activate downstream signaling pathways (*46*). TLRs are expressed on the cell surface or associated with intracellular vesicles to recognize the components from viruses and other pathogens in the extracellular space or in the phagosome or endosomes without direct infection (*43, 46*). Each member of TLRs detects distinct PAMPs. Upon RNA viruse infections, TLR3 recognizes viral double-stranded RNAs, while TLR7 and TLR8 recognize viral single-stranded RNAs as PAMPs, in addition to the recognition of structural or componential proteins of certain viruses by TLR2 and TLR4 (*46*). Activated TLRs trigger myeloid differentiation primary response gene 88 (MyD88)-dependent pathway or TIR-domain-containing adapter-inducing interferon-β (TRIF)-dependent pathway, leading to induce the production of type I interferons (IFNs) and inflammatory cytokine via the activation of nuclear factor NF-κB, mitogen-activated protein (MAP) kinase and interferon regulatory factors (IRFs) (*46-47*). Type I IFNs bind to IFN-αβ receptor (IFNAR) to activate the cytokine-activated Janus kinase (JAK)-signal transducer and activator of transcription

(STAT) pathway and induce over 300 IF-stimulated genes (ISGs), thereby establishing an antiviral state (*43, 47-49*). TLRs also have interplay with other PRRs in the antiviral immunity. Plasmacytoid dendritic cells (pDCs) that express TLR7 and TLR9 can produce abundant IFNs in rapid response to virus infection and may function as a backup antiviral response when RLR pathways are blocked by viruses (*46*). NLRs have a tripartite structure composed of a variable N-terminal protein-protein interaction domain critical for downstream signaling, a central NOD domain for activation, and a C-terminal LRR for PAMP recognition (*50*). Most NLRs are located within the cytoplasm except few members that reside in the mitochondria or in part in the nucleus (*50*). Members of NLRs, including NLRP3, NLRC2, NLRC5 and NLRX1, are found to be involved in the antiviral immunity, some of which are activated by RNA viruses or viral ssRNAs and dsRNAs to stimulate caspase-1 and IRF3 activation and downstream production of IL-1β, IL-18 and IFNs, and regulate inflammation during virus infection, while others are suggested to have an interaction with RLR pathway (*51-53*). However, though the crystal structure of NLRX1 suggests its binding ability to ssRNA and dsRNA, the upstream activation mechanism of NLRs by viruses, whether directly or indirectly via other innate immunity pathways like RLRs, as well as the *in vivo* relevance of NLRs in antiviral immunity upon virus infection, are not clear to date (*51, 54*).

RLRs are a family of DExD/H box RNA helicases that function as cytoplasmic PRRs to recognize viral RNAs as the PAMPs (*55*). To date three members are identified and two of them, RIG-I and melanoma differentiation associated factor 5 (MDA5), are composed

of an N-terminal tandem caspase-activation and recruitment domains (CARDs) essential for downstream signaling activation, a central DExD/H box RNA helicase/ATPase domain for RNA binding and the ATP hydrolysis ability, and a C-terminal repressor domain (RD) participated in autoregulation (*55, 206*). RIG-I and MDA5 are involved in the antiviral innate immunity by recognizing the RNA components of RNA viruses and triggering intracellular signaling pathways and downstream production of IFNs and proinflammatory cytokines via binding to IFN-β promoter stimulator 1 (IPS-1, also known as MAVS) (*43, 55*). RNA viruses are differentially recognized by either RIG-I or MDA5 (*56*). The antiviral immunity to Sendai virus, vesicular stomatitis virus (VSV), influenza A and B virus, Ebola and hepatitis C virus, for example, require RIG-I, picornaviridae viruses are detected by MDA5, whereas some viruses such as Dengue virus, West Nile virus (WNV) and reovirus are recognized by both RIG-I and MDA5 (*55-56*). Short dsRNAs and 5'-triphosphate or 5'-diphosphate RNA derived from RNA viruses are recognized by RIG-I, while long dsRNAs over 2kb such as polyinosinic polycytidylic acid (poly I:C) are the preferred PAMPs of MDA5 (*43, 56-59*). The antiviral function of the third member of RLRs, D11Lgp2 (Laboratory of Genetics and Physiology 2, LGP2), remains controversial (*207*). With a similar structural domains to RIG-I and MDA5 but lacking any CARD domain which is essential for IFN induction and inflammation, LGP2 was originally considered as a negative regulator of RLR signaling pathway via competition for dsRNA binding, however studies using lgp2 deficient cells and mice detected reduction in IFN production and high susceptibility to infections by RNA viruses except for influenza virus, suggesting that LGP2 may facilitate viral RNA

recognition by RIG-I and MDA5 via its ATPase domain (*60-61*).

Innate immunity also plays an important role in the regulation of adaptive immunity. RNA viruses or other pathogens recognized by the TLRs expressed on dendritic cells are further processed and presented to T cells by MHC molecules, and the signals induced by TLRs in this event including co-stimulatory signals and cytokines are required for naïve T cell activation, and IFNs are involved in the proliferation of memory T cells and the isotype switch and differentiation of B cells into plasma cells (*62-63*). RIG-I and MDA5 can induce $CD8^+$ T cell effector responses to certain virus infection via MAVS signaling pathway independently of TLRs, but they are insufficient for $CD4^+$ T cell induction and antibody responses, which require TLR signaling pathways (*64*). Natural killer (NK) cells show features of both innate immunity, such as the rapid response to tumor cells and the secretion of effector cytokines during inflammation in response to IFN or IL-12 and IL-18, and adaptive immunity such as immunological memory to cytomegalovirus infection in mice (*65*).

1.3 siRNAs and RNA interference

Small silencing RNAs are a group of short non-coding RNAs with the size range from 20 to 30 nucleotides (nt) (*66*). Small RNAs distinguish from random degradation products with specific size preference and properties corresponding to their biogenesis machinery. Small RNAs control transcriptional and post transcriptional regulations such as chromatin

modification, translational repression and mRNA degradation in a sequence-specific manner, which are collectively referred as RNA interference (RNAi) (*67*). The phenomenon of RNAi was originally described as co-suppression in transgenic plants in which the introduced transgenes and the homologous endogenous genes were inhibited from expression (*68-69*), but its mechanism of activation by dsRNA was first illustrated in *Caenorhabditis elegans* in 1998 (*89*). According to the biogenesis, properties and gene silencing activities, small RNAs are classified into three categories: microRNAs (miRNAs), small interfering RNAs (siRNAs) and Piwi-interacting RNAs (piRNAs) (*66*). To date small RNAs are found to directly target at least 30% of host genes and regulate various biological activities including cell fate, host development, metabolism and the control of transposable elements (*71*).

The biogenesis of canonical miRNAs requires two sequential steps, including the processing of the primary precursor (pri-miRNA) to the hairpin structured precursor (pre-miRNA) and the maturation into miRNA product (*72*). However, some pre-miRNAs are spliced directly from messenger RNA (mRNA) introns, which are called mirtrons (*73-75*). miRNA genes are transcribed to pri-miRNAs by RNA polymerase II, capped and polyadenylated like mRNAs, and one single pri-miRNA transcription product may by processed into multiple miRNAs in clusters (*76-77*). Self-complementary sequences on pri-miRNAs form an imperfectly paired stem-loop (hairpin) structure recognized by an RNase III endonuclease known as Drosha in mammals and flies or Dicer-like protein 1 (DCL1) in plants, facilitated by their double-stranded RNA binding domain (dsRBD)

partner (DGCR8 in mammals, Pasha in flies and HYL1 in plants) (66*, 78, 116-117*). The recognition of RNase III to pri-miRNAs in the nucleus leads to cleavage at the stem and generates 60-70 nt long stem-loop pre-miRNAs with 2-nt overhangs at 3' ends and phosphated 5' ends, which are important features for RNase III products (*79*). For miR-30a the termini of pre-miRNA are identical to the mature miRNAs, indicating that the sequences for the final products are predetermined at this step (*78*). Pre-miRNAs are exported to the cytoplasm, where they are processed by another RNase III Dicer (Dcr), or the same DCL1 in plants, into mature products facilitated by another dsRBD partern (TRBP in mammals and Loqs in flies) (*66, 72, 116*). A typical structure of Dicer includes a DExD helicase domain, a DUF283 domain, a piwi argonaute zwille (PAZ) domain for binding to the 2-nt 3' overhang end, two RNase III domains (RIIIDs) for cleavage and a dsRBD (*79*). The cleavage by Dicer generates a duplex with 2-nt overhang at the 3' ends, composed by two small RNA strands defined as mature miRNA and miRNA* (*80*).

miRNAs are assembled into RNA induced silencing complex (RISC) to perform the RNA silencing function (*80-82*). Argonaute protein (AGO) is the core component of RISC and contains an amino-terminal (N) domain required for small RNA loading and unwinding, a middle (MID) domain and a PAZ domain to respectively anchor the 5' and 3' end of small RNA, and a PIWI domain which is structurally similar to RNase H and functions as endonucleases (*81*). miRNA and the corresponded miRNA* processed by Dicer and dsRBD partners are loaded together as a duplex to AGO to form pre-RISC, a process facilitated by a second function of Dicer and other components in a RISC-loading

complex (RLC) (*80-81, 83*). The two strands of miRNA and miRNA* are dissociated and further asymmetrically selected by AGO to form mature RISC according to their 5' end stability and the preference by the AGO involved in the miRNA pathway, leading to a strong 1U bias of mature miRNAs (*80, 84*). miRNAs* are normally degraded, but some miRNAs* can also have biological functions like miRNAs (*85*). miRNAs in RISC target mRNAs with sequences imperfectly complementary to their seeds (from 2^{nd} to 7^{th} nt) to trigger direct slicing or translation repression by binding to 3' untranslated region (UTR), and the target prediction methods following this principle by such short seeds have uncovered widespread genes regulated by miRNAs, which are available at online database (*71, 85-86*). The Dicer-AGO mechanism in miRNA pathway is commonly shared among species with variation in details, however in few specific cases like the process of miR-451 in mice and zebrafish is found to be independent of Dicer and requires AGO cleavage activity instead (*87-88*).

Unlike miRNAs that are processed from a single-strand RNA as the precursor, siRNAs are usually derived from endogenous or exogenous long dsRNAs, or dsRNAs synthesized by the host from exogenous sources in plants by their RDRs (*89-91*). Similar to the biogenesis of mature miRNAs from pre-miRNAs, the dsRNA structure is recognized by Dicer and cleaved into siRNA duplexes with 2-nt overhang at 3' end (*89, 92*). The discovery of successive siRNA duplexes in plants which are called phased siRNAs suggests that Dicer can move along the dsRNA to process the cleavage, potentially relying on its ATPase activity of the helicase domain which is not required for

cleavages at dsRNA termini (*93-95*). The siRNA duplex is asymmetrically loaded into RISC, where the passenger strand of the duplex is destroyed, leaving the guide strand of siRNA to the RNA target by AGO (*81*). Targets of siRNAs are originally considered to include only perfect complementary mRNAs for slicing and degradation (*96-97*), however, recent studies reveal the "off-target" silencing by siRNAs in a mechanism that may also depend on the seed region and repress mRNA translation by binding to 3'-UTRs (*98-99*). In *C. elegans* and plants the siRNAs can be amplified in which the degradation products of mRNA targeted by miRNAs or primary siRNAs recruit the RdRP complex to synthesize secondary siRNAs (*100, 122*).

miRNA and siRNA pathways share the same or homologous components. In human and other mammals the single Dicer processes both miRNAs and siRNAs 22-nt in length (*101-102*). miRNAs are sorted randomly into the four AGOs in the AGO subfamily, among which only AGO2 has the slicer activity (*103-106*). *Drosophila melanogaster* has two Dicers with distinct roles for miRNAs and siRNAs. Dcr-1 is required for the biogenesis of miRNAs predominantly 22-nt in length, whereas Dcr-2 processes long dsRNAs to siRNAs predominantly 21-nt in length (*107*). However, both Dcr-1 and Dcr-2 are required for siRISC assembly (*107*). In *C. elegans* the single Dcr produces both miRNAs and siRNAs. The primary siRNAs in *C. elegans* induce the production of secondary siRNAs, which exhibit 1G and 22-nt size preference (*100, 115*). In plants miRNAs and siRNAs loaded in AGO1 and AGO2 show preference of 1U and 1A, respectively, while AGO4 loaded 24-nt siRNAs cleaved by DCL3 induce both

post-transcriptional and transcriptional silencing (*109, 116-121*). 22-nt siRNAs processed by DCL2 trigger the production of secondary siRNAs due to their specific size (*119, 122-123*).

The third type of small RNAs, piRNAs, is responsible for suppression of transposable elements like transposons in reproductive tissues to maintain the integrity of genome, as well as the function in early development (*124*). Insect and mammalian piRNAs are derived from clusters and are longer than miRNAs and siRNAs in size (*124*). Deficiency in piRNA pathway generally results in high activity of transposable elements corresponding to DNA damage and sterility (*125*). PIWI proteins are preferentially expressed in the germline, and the amplification of piRNAs may involve distinct PIWI proteins in a ping-pong model (*126*). However, how primary piRNAs are generated is not completely elucidated yet. Though the nuclease zucchini (Zuc) was found to process the 5' end of primary piRNAs, the component cleaving the 3' end has not been understood (*81*). In flies the PIWI/Aubergine complex and AGO3 complex are involved in the ping-pong amplification, and mouse MILI and MIWI2 may have similar roles (*124*). piRNAs loaded in PIWI proteins guide the complementary and silencing to the target transposable elements (*81, 124*). In *C. elegans* there is a unique pathway of piRNA biogenesis, in which an endogenous capped-small RNA species (csRNAs) generated by Pol II polymerase can be processed into mature piRNAs by cap removing and trimming (*127*).

1.4 Viral siRNA-dependent antiviral RNAi: a new innate immunity across species

In the last two decades the antiviral activity of RNAi was discovered as a new host innate immunity mechanism against RNA virus infection, in which host RNAi machinery recognizes the dsRNA intermediates of viral replication and processes the dsRNAs into viral siRNAs (vsiRNAs) to guide specific antiviral RNA silencing (*128*). The correlation between gene silencing and virus resistance was first observed in transgenic plants (*129*). It was soon followed by the first detection of virus derived siRNAs in *Nicotiana benthamiana* plants infected by potato virus X (PVX) (*130*). With specific size preferences in distinct host organisms, sense and antisense vsiRNAs often accumulated to similar levels even though the accumulation of viral genomic RNAs and mRNAs exhibits strong strand bias (*131*). Moreover, vsiRNAs cloned from infected cells overlap in sequence and can be assembled into contigs covering the entire length of the virus genomes (*132*). These properties of vsiRNAs are consistent with the model in which vsiRNAs are processed from dsRNAs precursors, rather than from hairpin-like secondary structures found in specific genomic loci of the single-strand viral RNAs similar to precursor miRNAs (*128*). *Drosophila* vsiRNAs have 5' monophosphates and are methylated at the 3'-end, and are similar to the endogenous siRNAs, but distinct from miRNAs and random degradation products (*128, 131*). Genetic mutants of fungi, plants, flies, and worms defective in the biogenesis or functionality of vsiRNAs exhibit enhanced susceptibility to distinct RNA viruses, revealing that antiviral RNAi functions as a broadly conserved innate immunity against virus infection in diverse eukaryotic species

(*133-136*). Some DNA viruses encode virus-derived miRNAs, which may regulate expression of host genes to facilitate virus infection without direct viral targets (*137*). Virus-derived piRNAs were found firstly in *Drosophila* ovarian somatic sheet (OSS) cells and subsequently in mosquitoes (*132, 138-139*). Early genetic studies suggested an antiviral role for the piRNA pathway in *Drosophila*. Recent studies have illustrated the biogenesis of viral piRNAs and their antiviral functions in mosquitoes. However, whether this antiviral function is direct or indirect via interacting with the vsiRNA pathway remains to be determined (*140-141*).

In *Cryphonectria parasitica* fungi infected by the positive-stranded RNA virus hypovirus the generation of predominantly 21-nt vsiRNAs is dependent on Dicer-2, which is also induced upon virus infection (*133*). In *Drosophila*, antiviral RNAi is mediated by the dsRNA-siRNA pathway of RNAi controlled by Dcr-2, R2D2, and AGO2 (*132, 142-143*). The dsRNA uptake pathway is also found to suppress the virus replication, which was proposed to function in building up the systemic immunity based on antiviral RNAi (*140, 144*). In *C. elegans* antiviral RNAi is induced by either the artificially launched replication or natural infection of RNA viruses (*145-147*). *C. elegans* vsiRNAs are predominantly 22G secondary siRNAs, consistent with the dominant role of the siRNA amplification pathway in antiviral RNAi (*147*). Genetic studies have shown that the biogenesis of vsiRNAs relies on the single Dicer in *C. elegans* facilitated by RDE-4, and antiviral RNAi requires the loading of vsiRNAs in RDE-1 and the amplification by RdRP like RRF-1 as well as other components such as DRH-1, RDE-2 and MUT-7

(*145-150*). In *Arabidopsis thaliana* DCL4-dependent 21-nt vsiRNAs are the most dominant upon (+)RNA virus infection although 22- and 24-nt vsiRNAs made respectively by DCL2 and DCL3 become detectable when DCL4 is inactive (*151*). Both DCL4 and DCL2 can mediate independent antiviral RNAi as the double knockout mutant plants support the highest virus accumulation compared to either single knockout mutant (*136, 151*). In contrast, an antiviral function of DCL3 is detectable only when the DCL4 function is compromised (*208*). Among all the ten AGO proteins of *A. thaliana*, AGO1 and AGO2 cooperate to mediate antiviral RNAi (*209*), while the other AGOs may also be involved, as the deficiency of AGO7 led to a higher virus accumulation, and AGO5 can bind vsiRNAs (*152-155*). As found in *C. elegans*, the amplification of secondary vsiRNAs by RDR1 and RDR6 plays an important role in antiviral RNAi in plants (*156*). Unlike *Drosophila*, siRNAs are systemically mobile in plants, which may also contributes to antiviral RNAi (*157-158*). In plants infected by DNA viruses, DCL3-dependent 24-nt vsiRNAs become the most dominant and are loaded in AGO4 to mediate a viral DNA methylation pathway to repress virus infection (*159-160*).

To counteract the host antiviral RNAi immunity, viruses have evolved to encode diverse viral suppressors of RNA silencing (VSRs) (*161*). The repression of host antiviral RNAi by VSRs is essential for the infection and virulence of plant and invertebrate viruses. VSRs may target almost every step in the host antiviral RNAi pathway, including binding to viral dsRNAs to inhibit the biogenesis of vsiRNAs, sequestering duplex vsiRNAs to prevent their loading into AGOs or their systemic spreading, degrading

vsiRNAs, and interacting with the protein components required for dicing, slicing and secondary vsiRNA amplification to interrupt their functions (*161*). For example, VSR B2 protein encoded by FHV suppresses antiviral RNAi in *Drosophila* and is also active in the non-host *N. benthamiana* plants (*162*). B2 binds dsRNAs with two positively charged antiparallel α helices (α2/α2') in a homodimer, forming a four-helix bundle that binds to one face of an A-form RNA duplex independently of sequence or length. Functional analysis indicates dual modes of the VSR function by B2 to block both the dicing of long dsRNAs by Dicer and the loading of duplex vsiRNAs into RISC (*163-164*).

1.5 vsiRNA-dependent antiviral RNAi in mammals: an issue remaining controversial

Although antiviral RNAi is conserved in invertebrates and plants, whether it is also active in mammals remains controversial in the past decade. Proteins encoded by mammalian viruses have been shown to encode the activity to suppress experimentally induced RNAi, including B2 of Nodamura virus (NoV), NS1 of influenza A virus, VP35 of Ebola virus, Tat of HIV-1, and NS4B of Dengue virus, all of which are indispensable for infection (*168-173*). Deficiency of RNAi components in mammalian cells is correlated with an increase of virus accumulation (*174-176*). Although these results suggest an antiviral function of RNAi in mammals against viruses, it is unclear if the antiviral effect is mediated by virus-derived miRNAs or siRNAs, or host miRNAs (*177*). Previous efforts

to clone small RNAs from mammalian cells infected by some DNA viruses have identified viral miRNAs. However, virus-derived small RNAs from mammalian cells infected with many RNA viruses show no clear size preference and are likely to be degradation products (*137, 178-180*), except those from HIV and HCV showing features similar to siRNAs (*172, 179*). These unsuccessful attempts to find mammalian vsiRNAs have led to a popular hypothesis that with the mature interferon system and the adaptive immunity, mammals may have evolved to abandon antiviral RNAi. This dissertation aims to characterize the role of antiviral RNAi in mammals according to the insights into the mechanism of antiviral RNAi from the previous studies carried out in Ding lab in the fruit fly model.

Chapter 2: Characterization of antiviral RNAi response in cultured Baby Hamster Kidney cells and mice

2.1 Introduction

Previous effort in characterization of antiviral RNAi response in mammalian system returned no supportive evidence to the hypothesis due to the failure in identification of vsRNAs with canonical siRNA properties as defined in other model organisms. We hypothesized that the failure from previous studies in detecting viral siRNAs was due to the impediment to host RNAi machinery by VSRs, which may prevent the biogenesis or Argonaute loading of vsiRNAs. Suppression of antiviral RNAi also ensures robust virus replication, leading to high accumulation of virus RNA degradation products as the noise covering vsiRNA signals. Therefore, use of VSR deficient virus mutants may facilitate the detection of the canonical vsiRNAs in mammals.

Nodamura virus (NoV) was employed in this study. NoV lethally infects both suckling mice and suckling hamsters, and can replicate in cultured mosquito cells and baby hamster kidney (BHK-21) cells (*181, 214*). NoV belongs to the *Alphanodavirus* genus of the *Nodaviriade* family, which includes Flock house virus (FHV) that has served as a model for the characterization of antiviral RNAi in the fruit fly (*162-164, 194*). The Nodaviral B2 proteins encode VSR activity. The B2 protein of NoV can suppress experimental RNAi in both *Drosophila* cells and human embryonic kidney (293T) cells

and exhibits dsRNA-binding activity similar to B2 of FHV (*131, 182-183*). The crystal structure of NoV B2 shows a four-helix bundle structure capped by two short helices at the C-termini also similar to FHV B2 protein even though the amino acid sequences of the two B2 proteins share less than 30% identity (*169*). Notably, NoV B2 also enhances the accumulation of NoV in mammalian cells (*181*), suggesting that the B2 protein of NoV may suppress antiviral RNAi in mammals as which has been illustrated for B2 of FHV in *Drosophila* infection.

2.2 Materials and Methods

2.2.1 Nodamura virus (NoV) and B2-deficient NoV mutant (NoVΔB2)

NoV and its B2-deficient mutant (NoVΔB2) were initially rescued from the infectious *in vitro* transcripts of full-length cDNA clones in BHK-21 cells as described (*213*). The genome of NoV consists of two positive RNA segments, RNA1 and RNA2, encoding RdRP and the coat protein respectively (*181*). The subgenomic RNA3 from RNA1 (nucleotide position 2732 to 3204) encodes three extra proteins, B1 and two isoforms of B2. B1 shares the same open reading frame (ORF) with the RdRP encoded by RNA1, and the two isoforms of B2 are translated from the +1 ORF of the RdRP and B1 (*181*). NoVΔB2 contains three point mutations on RNA1 (*181*), U2745C, U2754C and C2757G, as new stop codons to terminate the translation of both isoforms of B2 without affecting the amino acid sequences of the RdRP and B1 due to codon synonyms (Fig 2.1).

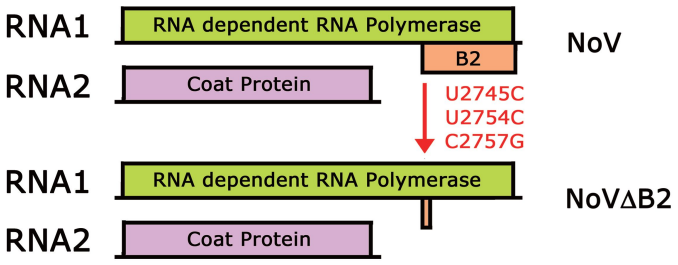

Figure 2.1 The genomic structures of NoV and NoVΔB2. NoVΔB2 strain was derived from NoV by introducing three point mutations to deplete the expression of B2 protein which is a virus encoded VSR, without changing the ORFs of the RdRP and B1 protein.

2.2.2 Infection of cultured BHK-21 cells

BHK-21 cells were obtained from American Type Culture Collection (ATCC) and were propagated in complete growth medium (Dulbecco's Modified Eagle's Medium (DMEM) + 10% Fetal Bovine Serum) at 37°C, 5% CO_2. NoV was propagated in BHK-21 cells whereas NoVΔB2 was amplified in the stable BHK-21 cell line expressing B2 of NoV due to its defective infection, which was constructed and selected using pseudotyped murine leukemia viruses for transduction as described (*181, 190*). The copy number of the viral genome RNA1 in the stock preparations of NoV and NoVΔB2 were determined by a real-time RT-PCR protocol previously reported (*191-192*), in which a 10-fold dilution series of NoV RNA1 with known concentrations were synthesized *in vitro* by T7 polymerase and used to establish a standard curve by real-time RT-PCR to amplify nucleotides 595-732 of RNA1 by primers 5'-CCGTTCATGGCTTACACCTT-3' (NoV Replicase_Fwd) and 5'-GCACCAGTCCCAAACTTCAT-3' (NoV Replicase_Rev). Virion RNAs extracted from a defined volume of each of the virus stock preparations were quantified by the same real-time RT-PCR using the standard curve as the reference.

For infection in cell culture, BHK-21 cells seeded in 6-well plate were infected in each well by NoV or NoVΔB2 with the same amount of viral genome copies.

2.2.3 Infection of mice

Suckling BALB/c mice of 6 to 8 days old after birth or adult mice (Jackson Lab, Bar Harbor, ME) were inoculated by intraperitoneal injection (IP) as described (*193*) with the same amount of viral genome copies of NoV or NoVΔB2. Total RNA was extracted separately from individual fore (2 samples) and hind (2 samples) limb tissues of one anesthetized suckling mouse using TRIzol (Invitrogen, Carlsbad, CA) according to manufacturer's instructions at different days post inoculation (dpi). Animals were housed in the Animal Resources Facility according to the guidelines described under the federal Animal Welfare Regulations Act. All animal procedures were approved by the Institutional Animal Care and Use Committee at the University of California, Riverside.

2.2.4 Quantification of NoVΔB2 titer by real-time PCR in suckling mice

The virus accumulation in suckling mice was determined by quantitative PCR using iScript™ Select cDNA Synthesis Kit and iQ SYBR green Supermix (Bio-Rad, Richmond, CA) using the extracted RNA samples described above. One μg of total RNA from individual fore or hind limb tissue of each inoculated mouse was used for cDNA synthesis

and 1/100 of the cDNA products obtained were used for real-time PCR using NoV Replicase_Fwd and NoV Replicase_Rev primers to amplify nucleotides 595-732 of NoV RNA1. The relative abundance of the viral RNA 1 was normalized to β-actin mRNA as the internal control and was estimated by the ΔCT method as described (*194*).

2.2.5 Small RNA library construction

Libraries of small RNAs from cultured cells or mice were constructed using the method that depends on the 5' monophosphate of small RNAs as described previously with minor modifications (*194*). Total small RNAs from BHK-21 cells 2 or 3 days after inoculation with NoV or NoVΔB2 were used to construct libraries with a barcode added to the 5' ligation adaptors. Libraries of total small RNAs from the hind limb tissues of mice at different days after inoculation with NoVΔB2 or NoV were constructed using TruSeq Small RNA Sample Preparation Kit of Illumina (San Diego, CA). The libraries were sequenced by Illumina HiSeq 2000 at the Core Facility of the Institute for Integrative Genome Biology on campus.

Co-immunoprecipitation of small RNAs from mice 3 dpi with NoV or NoVΔB2 by Anti-pan Argonaute (Ago) antibody (Millipore, Billerica, MA), and from mice 3 dpi with NoV by B2 antibodies were essentially as described (*195*). Briefly, 100 μg of muscle tissue lysates in 1 ml RIPA was pre-cleared by sequential incubation with 3 μg of rabbit or mouse IgG and 15 μl of protein A/G PLUS-Agarose beads (Santa Cruz Biotechnology,

Santa Cruz, CA). Three μg of Anti-pan Ago or B2 antibodies immobilized to protein A/G PLUS-Agarose beads were then incubated with the pre-cleared cell lysates for 2 hours at 4 °C. After extensive washes, the precipitated complexes were used for RNA extraction by TRIzol and the total RNAs obtained were used for the construction of small RNA libraries as described above.

2.2.6 Deep sequencing and bioinformatics analysis of small RNAs

The libraries of small RNAs cloned from cultured cells and mice were sequenced by Illumina HiSeq 2000/2500 at the Core Facility of the Institute for Integrative Genome Biology on campus. Small RNA reads were mapped to the virus and host genome references or compared to mature miRNAs. Mapping was done by Bowtie 1.0.0 with either perfect match or 1 mismatch only for genotyping and reads origin analysis. All of the references used were downloaded from web sources as listed below. Subsequent bioinformatics analysis of virus-derived small RNAs was carried out using in-house Perl scripts. The reference sequences used in this study:

1. Nodamura Virus (NoV) RNAs 1 and 2: NCBI NC_002690.1 and NC_002691.1.
2. NoVΔB2 RNAs 1 and 2: the same as NoV except for 3 substitutions in RNA1: U2745C, U2754C and C2757G.
3. Mature miRNAs and miRNA precursors: miRBase 19 (http://www.mirbase.org/).

Specifically for the cellular miRNAs in BHK-21 cells which are not available on miRBase, the miRNA sequences from Chinese Hamster Ovary (CHO) cell lines were used as an imperfect alternative (*184*).

4. Non-coding RNAs: fRNAdb 3.0 (http://www.ncrna.org/frnadb/).

5. *Mus musculus* mRNAs: Mammalian Gene Collection (MGC) and NIA Mouse cDNA Project.

6. *Mus musculus* whole genome: the Dec. 2011 (GRCm38/mm10) assembly of the mouse genome (mm10, Genome Reference Consortium Mouse Build 38 (GCA_000001635.2)).

Pairs of complementary 22-nt vsRNAs in each library in different distance categories were computed using previously described basic principles (*126, 179*) with modifications. The program calculates the counts of pairs in each nucleotide distance category between the 5' and 3' ends of complementary 22-nt vsRNAs with the algorithm below:

$$f(x)_{x=-a,-a+1,\ldots,b-1,b} = \sum_{i=1}^{i=t} \sum_{j=1}^{j=l_{xi}} \left(\frac{n_i}{p_i} \times \frac{m_j}{q_j}\right)$$

x indicates each distance category.

a and *b* are determined by the sizes of small RNAs examined.

f(x) indicates the total number of small RNA pairs for each distance category.

i indicates a small RNA from positive strand.

t indicates the total number of positive-strand small RNAs.

j indicates a small RNA from negative-strand which overlaps with small RNA i in the distance category x.

l_{xi} indicates the total number of negative-strand small RNAs that meet the requirement determined by x and i.

n_i indicates the repeat number of the small RNA i.

p_i indicates the multiple viral genome hit number of the small RNA i.

m_j indicates the repeat number of the small RNA j.

q_j indicates the multiple viral genome hit number of the small RNA j.

2.2.7 Correlation analysis of small RNA populations

The correlation analysis of small RNA populations was done by the formulas below:

$$\text{Correlation coefficient } (r) = \frac{\sum_{i=1}^{n}(x_i - \bar{x})(y_i - \bar{y})}{\sqrt{\sum_{i=1}^{n}(x_i - \bar{x})^2} \cdot \sqrt{\sum_{i=1}^{n}(y_i - \bar{y})^2}}$$

$$\text{Regression coefficient } (a) = \frac{\sum_{i=1}^{n} x_i y_i}{\sum_{i=1}^{n} x_i^2}$$

$$\text{Average variation } (\mu) = \frac{\sum_{i=1}^{n}(y_i - x_i)}{n}$$

$$\text{Standard deviation } (\sigma) = \sqrt{\frac{\sum_{i=1}^{n}(y_i - x_i - \mu)^2}{n}}$$

n indicates the total number the total number of the unique NoVΔB2 small RNA species (18- to 28-nt) found in ago1/3/4 mutant and/or wild-type BALB/c suckling mice with/without co-IP by anti-pan-AGOs antibody.

i indicates a given small RNA species in ago1/3/4 mutant and wild-type BALB/c suckling mice.

y_i indicates the % of a given vsiRNA to the total vsiRNAs in ago1/3/4 mutant suckling mice with a value between 0 and 100%. $\bar{y}$ indicates the average % of all the vsiRNAs in ago1/3/4 mutant suckling mice.

x_i indicates the % of a given vsiRNA to the total vsiRNAs in wild-type suckling mice with/without co-IP by anti-pan-AGOs antibody with a value between 0 and 100%. $\bar{x}$ indicates the average % of all the vsiRNAs in wild-type suckling mice.

Any unique small RNA species referred as (*i*) above with a value change (y_i-x_i) beyond the interval [μ-3σ, μ+3σ] was considered as displaying significant variation between the two small RNA libraries; otherwise it was considered to display no significant variation.

2.3 Results

2.3.1 Characterization of antiviral RNAi induced by NoVΔB2 in BHK-21 cells

Previous studies in Ding lab suggested that use of NoVΔB2, a B2-deficient mutant of NoV (*213*), to challenge baby hamster kidney 21 (BHK-21) cells might facilitate detection of mammalian viral siRNAs. In two independent experiments, I compared deep sequencing profiles of 18- to 28-nt small RNAs from BHK-21 cells 2 or 3 days post inoculation (dpi) with either NoV or NoVΔB2. Reads perfectly identical to the mature cellular miRNAs were highly abundant in all the four libraries and occupied from 20% to 40% of the total reads sequenced, indicating the good quality and reliability of the small RNA cloning (Table 2.1). To confirm the genotype of NoVΔB2 used in the cell infection and library construction, reads sequenced from the BHK-21 cells challenged by NoVΔB2 were mapped to the loci on NoV genome where the three point mutations were expected (Fig 2.2). The result verified the correct genotype of NoVΔB2 used in this study.

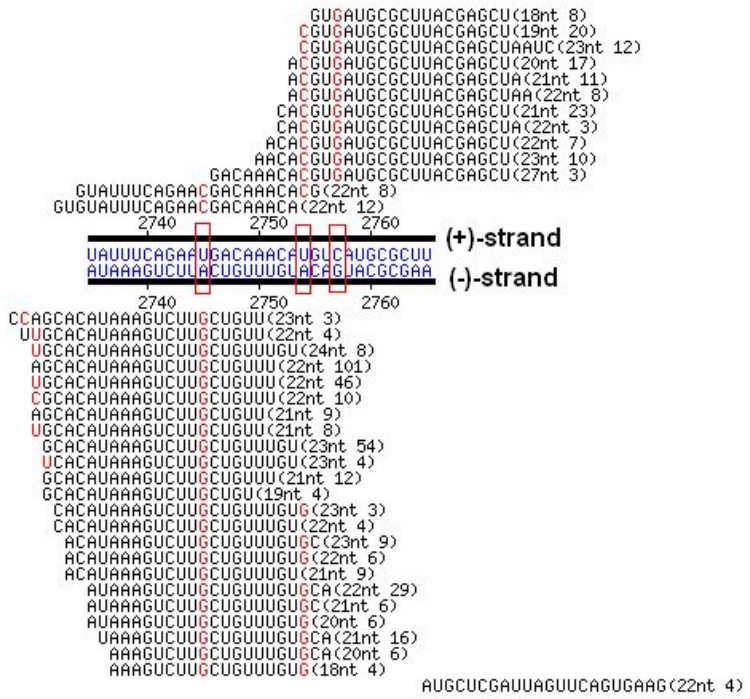

Figure 2.2 The small RNAs from NoVΔB2 infected BHK-21 cells revealing the three expected point mutations. Small RNAs from BHK-21 cells inoculated with NoVΔB2 at 3 dpi are mapped to NoV genome, and the sequence, size and raw number of each read are shown. The average coverage to the region presented is over 100 times, sufficient to provide statistically reliable results. The mismatches (shown in red) reveal the three expected mutations (indicated by red frames). To simply the figure, only reads with counts no less than 3 in the library are presented.

I found that virus-derived small RNAs (vsRNAs) from BHK-21 cells infected by NoV at either 2 dpi or 3 dpi were highly abundant, representing 22.8% and 24.9% of the total reads sequenced in the two libraries (Table 2.1). However, they displayed an overwhelming bias for positive strands (~97%) (Table 2.1), showed no size preference expected for Dicer products (Fig 2.3A, Table 2.1), and are likely breakdown products from the abundant positive-strand viral RNAs (*128*).

Table 2.1 Profiles of mammalian virus-derived small RNAs

Small RNAs from materials infected with NoV			
	BHK-21 Cells (2 dpi)	BHK-21 Cells (3 dpi)	Suckling mice (4 dpi)
Total reads	10,892,126	17,461,069	13,715,643
NoV reads[1]	2,479,591 (22.8%)	4,338,911(24.9%)	1,998,876 (14.6%)
Positive-strand	2,409,046 (97.1%)	4,213,052 (97.1%)	1,683,734 (84.2%)
Negative-strand	70,545 (2.9%)	125,859 (2.9%)	315,142 (15.8%)
Cellular miRNAs	4,015,778 (36.9%)	6,681,547 (38.3%)	2,128,066 (15.5%)
Other reads	4,396,757 (40.4%)	6,440,611 (36.9%)	9,588,701 (69.9%)

Small RNAs from materials infected with NoVΔB2				
	BHK-21 Cells (2 dpi)	BHK-21 Cells (3 dpi)	Suckling mice (1 dpi)	Suckling mice (2 dpi)
Total reads	16,424,313	9,205,304	13,728,046	14,882,576
NoVΔB2 reads[1]	12,622 (0.1%)	12,049 (0.1%)	14,664 (0.1%)	39,906(0.3%)
Positive-strand	10,772 (85.3%)	10,122 (84.0%)	12,138 (82.8%)	20,678 (51.8%)
Negative-strand	1,850 (14.7%)	1,927 (16.0%)	2,526 (17.2%)	19,228 (48.2%)
22-nt reads[2]	2,242	2,156	3,807	22,191
-2 population	636 (28.4%)	682 (31.6%)	1,452 (38.1%)	14,522 (65.4%)
+20 population	751 (33.5%)	769 (35.7%)	1,090 (28.6%)	11,232 (50.6%)
Cellular miRNAs	3,368,644 (20.5%)	3,708,149 (40.3%)	4,941,829 (36.0%)	5,086,428 (34.2%)
Other reads	13,043,047 (79.4%)	5,485,106 (59.6%)	8,771,553 (63.9%)	9,756,242 (65.6%)

1. The % of virus reads (with 100% identity/complementarity to viral genomic RNAs 1 and 2) in the total qualified reads of a library, and the % of positive- and negative-strand virus reads in the total virus reads of a library were given in brackets.

2. Two mutually non-exclusive populations were detected in the total 22-nt virus reads in each library: “-2” refers to 22-nt virus reads that are perfect base-paired duplexes with 2-nt overhang at the 3’ end of each strand; “+20” refers to immediately successive 22-nt virus reads according to their mapping positions in the viral genome. The % of each population in the total virus reads were given in brackets.

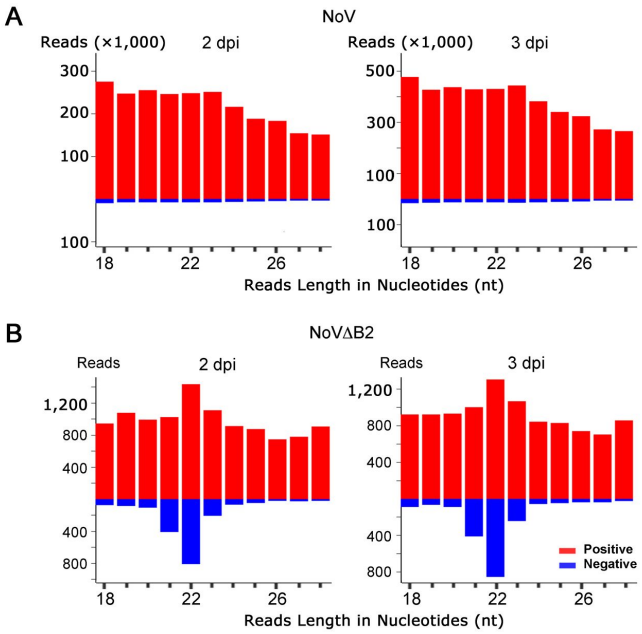

Figure 2.3 The size distribution of small RNAs from NoV or NoVΔB2 infected BHK-21 cells. Small RNAs from BHK-21 cells inoculated with **(A)** NoV or **(B)** NoVΔB2 are respectively mapped to the virus genome, and the raw reads number of each size is shown. The strand sources of viral small RNAs are indicated by colors.

By contrast, vsRNAs from NoVΔB2-infected cells were much less abundant, representing only approximate 0.1% of the total sequenced reads in both libraries (Table 2.1). The reduced abundance of viral reads was consistent with low replication levels of NoVΔB2 in cultured cells (*181*). By comparison, NoVΔB2 vsRNAs exhibited reduced positive-strand bias (~85%) compared to NoV infection (Table 2.1). Notably, I found that ~77% of the total negative-strand vsRNA reads of NoVΔB2 in both libraries were in the 21- to 23-nt size range with a major 22-nt peak (Fig 2.3B), similar to Dicer-dependent cellular miRNAs (Fig 2.4). NoVΔB2 unique negative-strand vsRNAs also had a dominant 22-nt peak, eliminating potential experimental bias to certain small RNA species caused by cloning and library construction (Fig 2.5). Such size preference of 22-nt was also

visible for NoVΔB2 positive-strand vsRNAs, although it was not as strong as that exhibited by negative-strand vsRNAs (Fig 2.3B). Therefore, NoVΔB2 vsRNAs display patterns of length distribution and strand bias expected for Dicer products as found for plant and invertebrate viral siRNAs (vsiRNAs) (*128*).

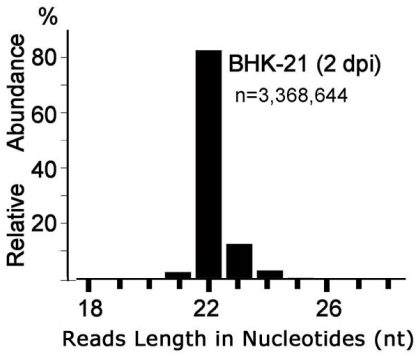

Figure 2.4 The size distribution of miRNAs from BHK-21 cells. Small RNAs from BHK-21 cells inoculated with NoVΔB2 (2 dpi) are compared with the miRNA sequences from Chinese Hamster Ovary (CHO) cell lines (*184*), and the percentage of each size to total miRNAs is shown. The total number of miRNA reads (*n*) is indicated.

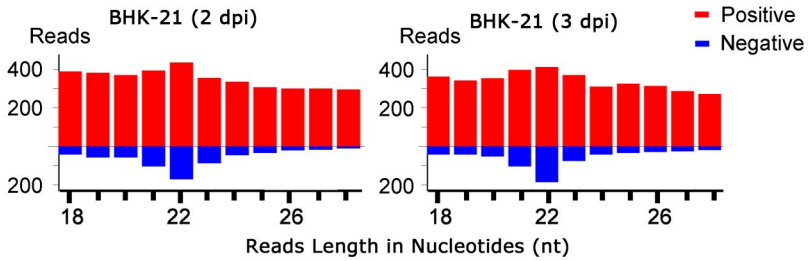

Figure 2.5 Properties of NoVΔB2 unique vsiRNA species in BHK-21 cells. Size distribution and abundance of positive- (red) or negative-strand (blue) viral unique small RNA species from BHK-21 cells infected by NoVΔB2 showing the a peak at 22-nt.

I found that NoVΔB2 vsRNAs exhibited properties of canonical siRNAs, using a program I wrote aiming to detect the most abundant vsRNA duplex patterns (Fig 2.6,

Table 2.1). First, both NoVΔB2 libraries were enriched for a population of 22-nt vsRNAs that contained a 20-nt perfectly base-paired duplex region with 2-nt 3' overhangs (Fig 2.6, peak indicated as "-2" and the small RNA pair by α and β). 28.4% and 31.6% of the total 22-nt NoVΔB2 vsRNAs in BHK-21 cells at 2 and 3 dpi, respectively, were involved in this duplex pattern, and contributed over 3,000 raw counts of pairs revealed by the program in both libraries (Table 2.1, Fig 2.6). However, such enrichment for 22-nt canonical siRNA pairs was not found for the comparably much more abundant vsRNAs of NoV (Fig 2.6). Second, I detected a more dominant population of complementary 22-nt vsRNA pairs with 20-nt 5'-end overhangs only for NoVΔB2 vsRNAs (Fig 2.6, peak indicated as "+20" and the small RNA pair by α and γ). Such duplex pattern was likely a byproduct composed of vsRNAs from two adjacent canonical siRNA pairs, representing 33.5% and 35.7% of the total 22-nt NoVΔB2 vsRNAs in cells at 2 and 3 dpi, respectively (Fig 2.6, Table 2.1). These findings together suggest Dicer-dependent processing of the same viral dsRNA precursor into successive 22-nt viral siRNA duplexes in cells infected by NoVΔB2, but not by NoV.

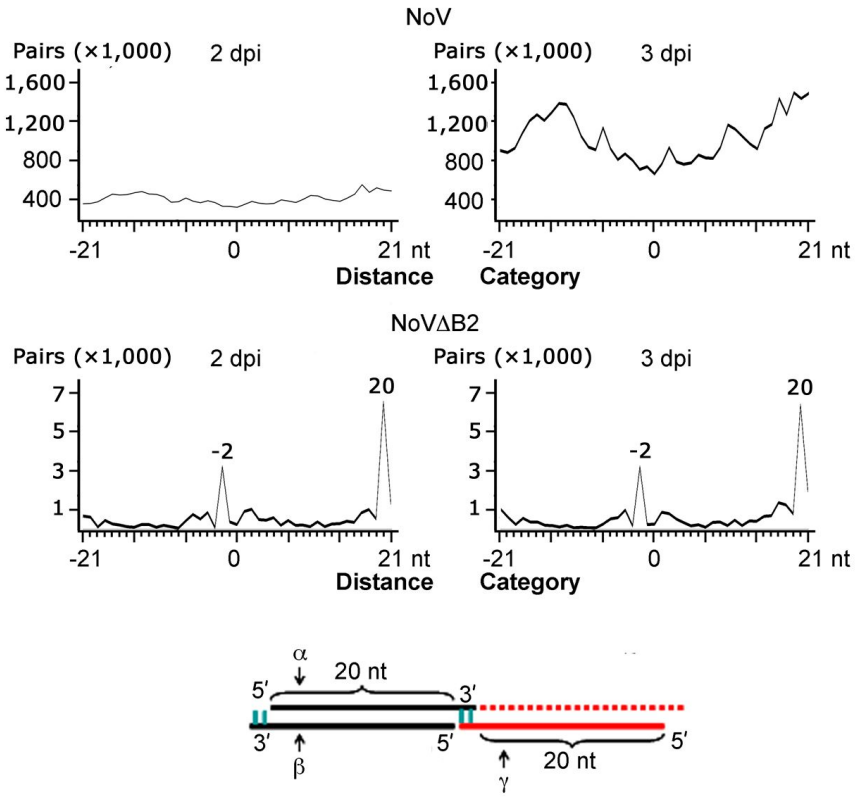

Figure 2.6 The canonical siRNA properties of NoVΔB2 22-nt small RNA duplexes in BHK-21 cells. Total counts of pairs of complementary NoV or NoVΔB2 22-nt small RNAs in each distance category (in nucleotides) between 5' and 3' ends of a complementary small RNA pair is shown. Perfect base-paired 22-nt small RNA duplexes with blunt ends are defined as a distance of 0. -2 is defined for duplexes with 2-nt overhang at the 3' end of each strand (illustrated as small RNA α and β), and +20 is defined for small RNA pairs with 2-nt overlapping (α and γ).

2.3.2 Characterization of antiviral RNAi induced by NoVΔB2 in suckling mice

Small RNA libraries were further deep-sequenced from BALB/c suckling mice 4 days after NoV inoculation and from those 1 or 2 days after NoVΔB2 inoculation. NoV vsRNAs in suckling mice were abundant, representing 14.6% of the total sequenced small RNAs (Table 2.1). Similar to results in BHK-21 cells, NoV vsRNAs in suckling mice showed no size preference, and the 22-nt vsRNAs of NoV were not enriched for

canonical siRNAs (Fig 2.7), which suggested B2 suppression of viral siRNA biogenesis in NoV-infected mice. By comparison, NoV vsRNAs cloned from mice contained more abundant negative-strand vsRNAs (~16%) than those from cell culture (~3%) (Table 2.1), which might indicate weak *in vivo* dicing of NoV dsRNA in the presence of B2.

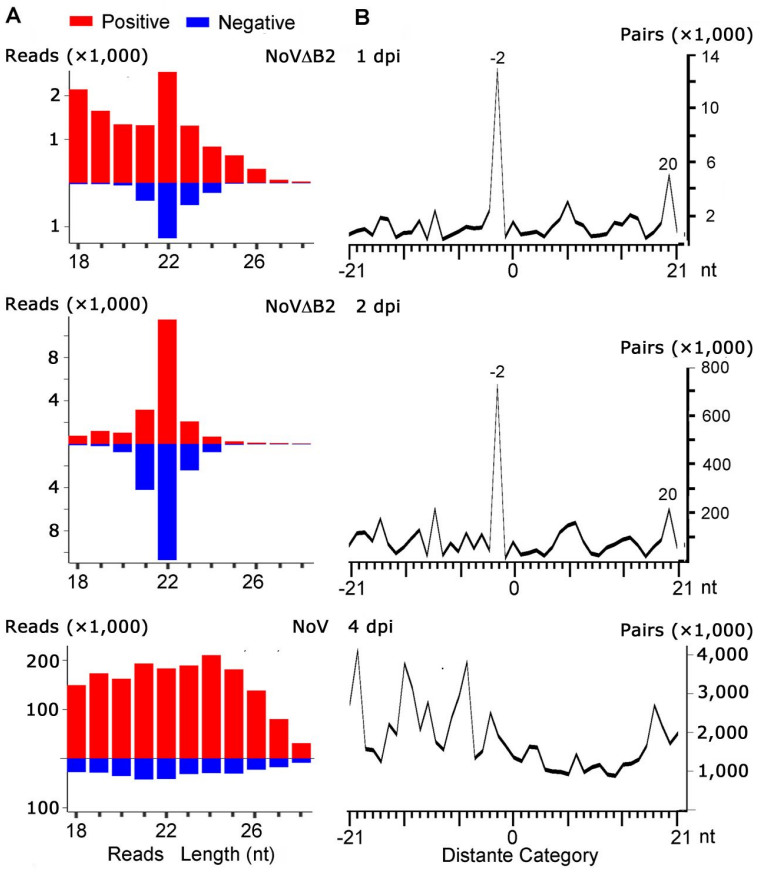

Figure 2.7 Properties of mouse vsiRNAs produced *in vivo*. (A) Size distribution and abundance of positive- (red) or negative-strand (blue) viral small RNAs from suckling mice 1 or 2 dpi with NoVΔB2 or with NoV at 4 dpi. **(B)** Total counts of pairs of complementary NoV or NoVΔB2 22-nt small RNAs in each distance category (in nucleotides) between 5' and 3' ends of a complementary small RNA pair.

The relative abundance of vsiRNAs in NoVΔB2-infected mice was 0.1% and 0.3% to the total sequenced reads in mice at 1 and 2 dpi (Table 2.1), similar to that found in fruit flies (0.5 to 0.9%) undergoing FHVΔB2 clearance (*194*). In contrast to NoV vsRNAs,

~85% of NoVΔB2 small RNAs from mice at 2 dpi were 21- to 23-nt long, with 22 nt as the predominant size for both strands (Fig 2.7, Table 2.1). A higher density of vsiRNAs was found to target the RNA3-coding region of RNA1 and the 5'-terminal region of RNAs 1 and 2 in NoVΔB2-infected mice and BHK-21 cells (Fig 2.8). NoVΔB2 siRNAs from mice at 2 dpi were divided approximately equally into positive and negative strands (51.8% and 48.2%), and 65.4% of the 22-nt vsiRNAs could form canonical siRNA duplexes with 2-nt 3' overhang (Table 2.1, Fig 2.7). I found a conserved set of successive viral canonical siRNA pairs at 5' terminal of RNA1 in both NoVΔB2-infected mice and cells (Table 2.2). Unique NoVΔB2 vsRNA species in mice also exhibited the enrichment for population within Dicer product size range and canonical vsiRNA duplexes (Fig 2.9). Together, these findings reveal that mice are able to launch a potent antiviral RNAi response without viral suppression of RNAi.

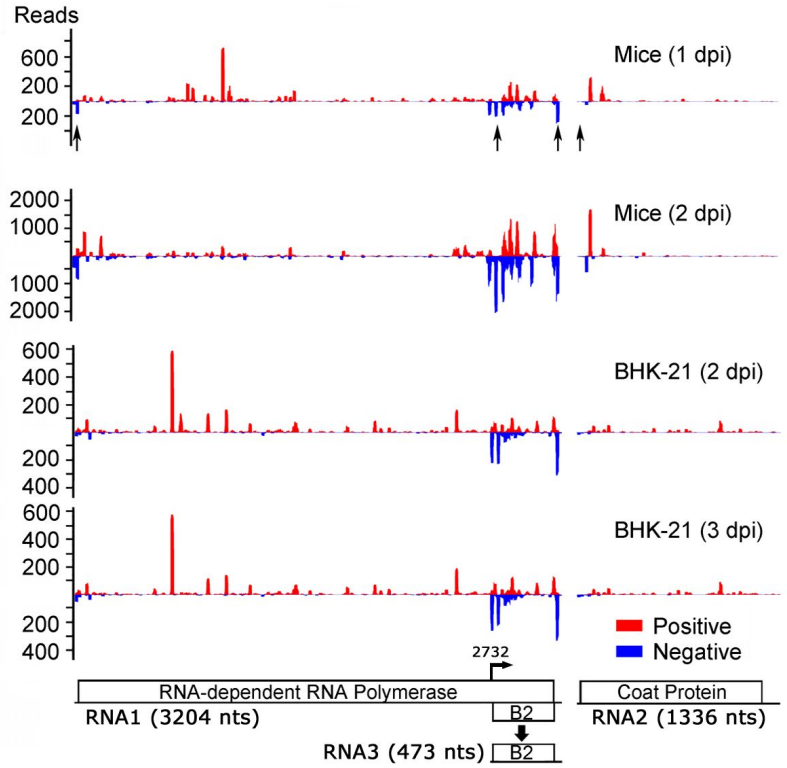

Figure 2.8 Virus genome distribution of 21- to 23-nt vsiRNAs in suckling mice and BHK-21 cells infected by NoVΔB2. The coverage of each nucleotide position along the virus genome by 21- to 23-nt vsiRNAs is shown. The strand sources of vsiRNAs are indicated by colors. Arrows indicate the regions of the enrichment of vsiRNAs. The functional proteins encoded by the viral bipartite RNA genome and transcription of B2 mRNA (RNA3) from RNA1 are shown.

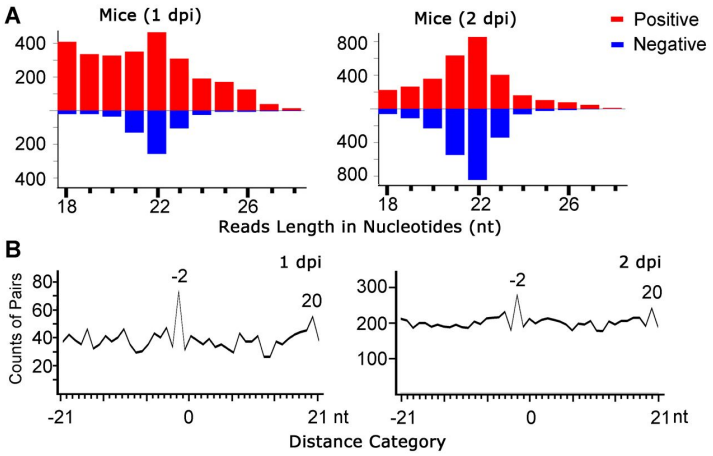

Figure 2.9 Properties of NoVΔB2 unique vsiRNA species in suckling mice. (A) Size distribution and abundance of positive- (red) or negative-strand (blue) viral unique small RNA species from suckling mice infected by NoVΔB2 showing the a peak at 22-nt. **(B)** Total counts of pairs of complementary unique 22-nt small RNA species in each distance category (in nucleotides) from suckling mice at 1 or 2 dpi with NoVΔB2, showing the -2 peak for the duplexes of 2-nt overhang at the 3' ends and the +20 peak for successive vsiRNAs.

Table 2.2 Phased viral small RNAs targeting the 5'-terminal region of NoVΔB2 RNA1

Duplex no.	BHK-21 2 dpi	BHK-21 3 dpi	Mice 1 dpi	Mice 2 dpi
1 (-)[1]	26 (nt 2-23)	47 (nt 2-23)	38 (nt 2-23)	375 (nt 2-23)
1 (+)[2]	9 (nt 4-25)	11 (nt 4-25)	2 (nt 4-25)	14 (nt 4-25)
2 (-)	9 (nt 24-45)	13 (nt 24-45)	163 (nt 24-45)	716 (nt 24-45)
2 (+)	3 (nt 26-47)	7 (nt 26-47)	15 (nt 26-47)	229 (nt 26-47)
3 (-)	—	—	—	—
3 (+)	6 (nt 48-69)	1 (nt 49-70)	7 (nt 48-70)	86 (nt 48-70)
4 (-)	2 (nt 69-90)	3 (nt 69-90)	—	3 (nt 69-90)
4 (+)	60 (nt 71-92)	52 (nt 71-92)	55 (nt 71-92)	735 (nt 71-92)
5 (-)	29 (nt 91-111)	21 (nt 91-111)	6 (nt 91-112)	56 (nt 91-112)
5 (+)	—	—	—	1 (nt 94-114)
6 (-)	—	—	—	—
6 (+)	5 (nt 114-135)	5 (nt 114-135)	14 (nt 114-135)	67 (nt 114-135)
7 (-)	—	1 (nt 134-155)	2 (nt 134-155)	4 (nt 134-155)
7 (+)	2 (nt 136-157)	6 (nt 136-157)	—	—
8 (-)	5 (nt 156-177)	3 (nt 156-177)	4 (nt 157-177)	42 (nt 156-177)
8 (+)	13 (nt 158-179)	11 (nt 158-179)	1 (nt 160-180)	9 (nt 158-179)

Read numbers of phased positive (+) and negative (-) strand 22-nt viral small RNAs targeting the 5'-terminal region (1-180 nt) of NoVΔB2 RNA1 cloned from BHK-21 cells or suckling mice after infection with NoVΔB2.

[1] Positions of small RNAs mapped to the viral negative-strand RNA1 were given from 3' to 5'.

[2] Positions of small RNAs mapped to the viral positive-strand RNA1 were given from 5' to 3'.

— indicates that phased viral small RNAs at this position were undetectable in the library.

NoVΔB2 vsRNAs in mice at 1 dpi also exhibited canonical siRNA properties as found in mice at 2 dpi, but were less enriched for positive-strand population within Dicer product size range and exhibited a stronger positive-strand bias (Fig 2.7). This suggests a time-course effect to the enrichment of vsiRNA population in mice. I next analyzed the nucleotide bias of NoVΔB2 22-nt vsiRNAs (Fig 2.10). Unlike vsiRNAs in cultured cells exhibiting preference for adenine at 3' ends (22A, ~40%), vsiRNAs cloned in mice at 1 or 2 dpi were enriched for population with uracil at 5' end (1U, ~35% or 45%, respectively, Fig 2.10). This finding suggests potential loading of NoVΔB2 vsiRNAs in AGOs in mice.

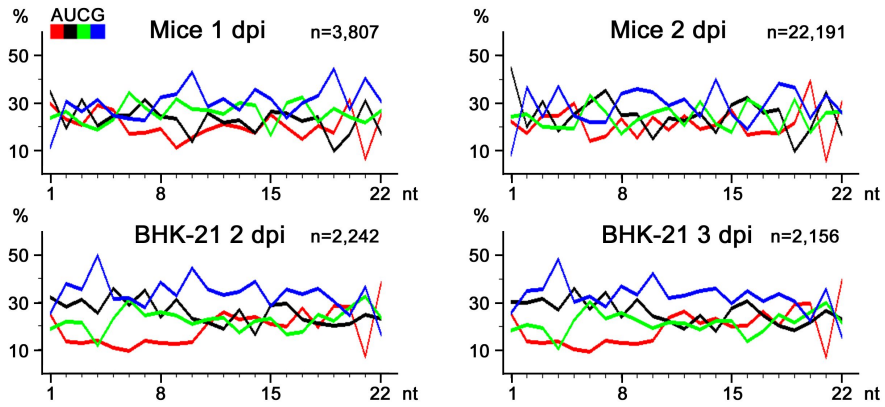

Figure 2.10 The nucleotide preference of NoVΔB2 derived vsiRNAs. The %s of each type of the four bases (indicated by colors) at each nucleotide position of NoVΔB2 derived 22-nt vsiRNAs in suckling mice or BHK-21 cells are shown. Both positive- and negative-strand vsiRNAs were included in the analysis. The raw numbers of the 22-nt vsiRNAs in each library are indicated.

2.3.3 Characterization of AGO-bound NoVΔB2 vsiRNAs in suckling mice

To directly determine if NoVΔB2 vsiRNAs were loaded into AGOs, I compared the populations of vsiRNAs obtained from NoVΔB2-inoculated suckling mice at 3 dpi before and after co-immunoprecipitation (co-IP) by an antibody specific to the four mouse AGOs (Figs 2.11 and 2.12). miRNAs, miRNAs* and imprecise products from the hairpin precursor miRNAs were abundant in both libraries and represented >90% to the total sequenced reads and indicating the good quality of small RNA cloning (Fig 2.11). All known canonical siRNA properties were found for NoVΔB2 vsRNAs bound to AGOs (Fig 2.12). NoVΔB2 vsRNAs bound to AGOs were highly enriched for population within Dicer product size range, and were predominantly 22-nt in size (Fig 2.12). Approximately equally distributed to positive and negative strands, the 22-nt NoVΔB2 vsiRNAs were enriched for canonical siRNA duplexes with 2-nt 3' overhang (Fig 2.12). Notably, 63.3%

of NoVΔB2 vsiRNAs found in AGO complexes contained 1U, exhibiting a higher preference compared to 41.0% of input vsiRNAs in mice at 3 dpi (Fig 2.12). This finding suggests 1U as a shared *in vivo* property between vsiRNAs and miRNAs in mice. I noted similar virus genome distribution patterns of vsiRNA hot spots between the total and AGO-bound populations (Fig 2.13). Therefore, mouse vsiRNAs produced in response to infection are *in vivo* loaded in AGOs, and exhibited preference of both 1U and 22-nt similar to mammalian miRNAs.

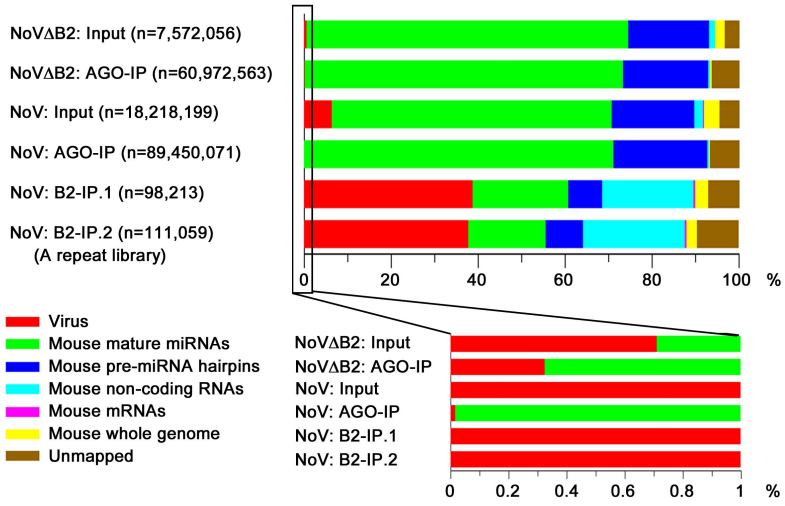

Figure 2.11 Origins of the small RNAs in each library from suckling mice. 18- to 28-nt small RNA reads sequenced from suckling mice infected by NoV or NoVΔB2 at 3 dpi were mapped to each category allowing 1-nt mismatch. For clarity, the proportion of the virus-derived small RNAs (vsRNAs) in each library was enlarged below, showing the lowest content of vsRNAs among those co-immunoprecipitated with AGOs from NoV-infected mice. Mature mouse miRNAs (& those mapped to their precursor hairpins, including microRNAs* and imprecise products) were the most abundant in both the total and AGO-bound small RNAs from NoV- and NoVΔB2-infected mice. However, vsRNAs became the most abundant in two independent small RNA libraries co-immunoprecipitated with B2 protein (B2-IP.1 was shown as the representative for the analysis in Fig 2.19).

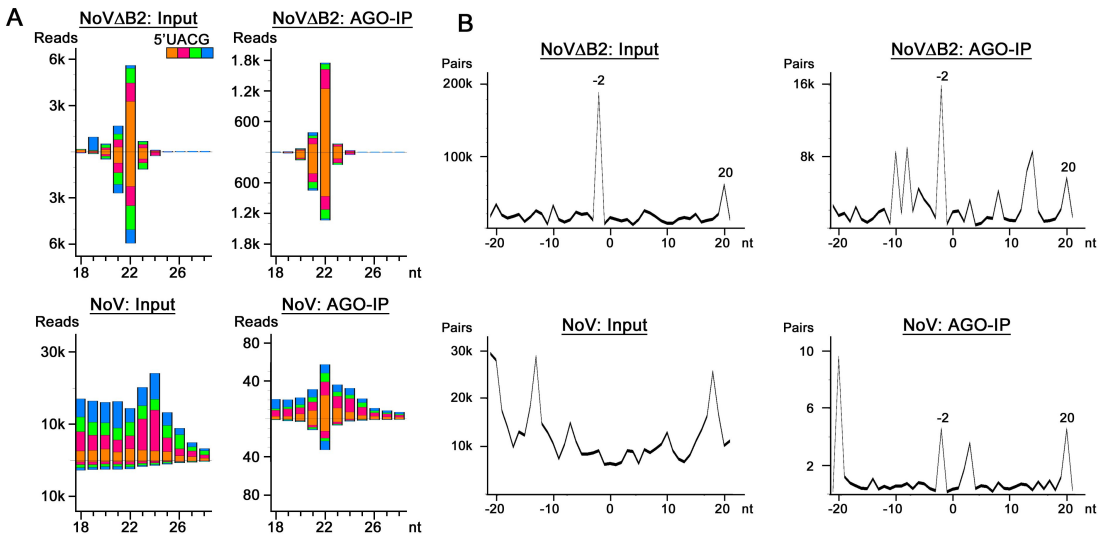

Figure 2.12 Properties of vsiRNAs and the loading to AGOs in suckling mice. (A) Size distribution and abundance (shown as reads per million of total mature miRNAs) of virus derived small RNAs sequenced from suckling mice infected with NoVΔB2 or NoV at 3 dpi, either with or without co-immunoprecipitation (co-IP) by the antibody to AGOs. The 5' terminal nucleotides of viral small RNAs are indicated by colors. **(B)** Total counts of pairs of complementary 22-nt viral small RNAs (per million of total mature miRNAs) in each distance category (in nucleotides). The enrichment for pairs of canonical vsiRNAs with 2-nt 3' overhangs (-2 peak) was detected by the infection of NoVΔB2 both before and after the co-IP.

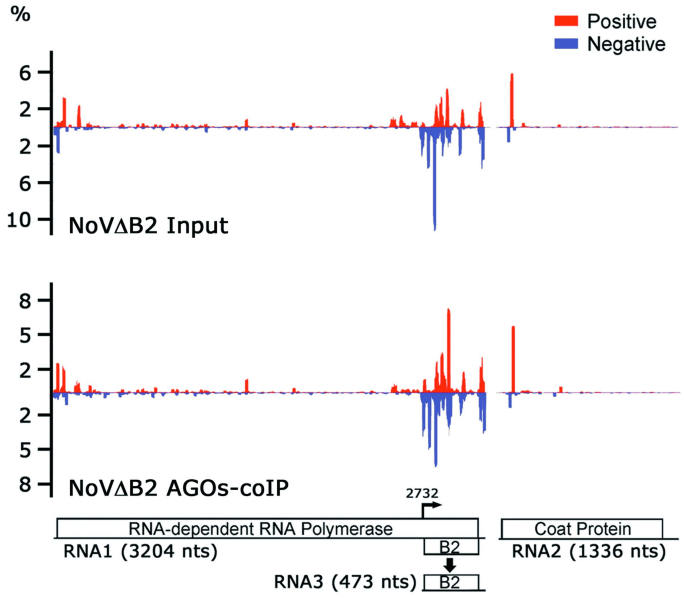

Figure 2.13 Virus genome distribution of 21- to 23-nt NoVΔB2 vsiRNAs loaded in AGOs in suckling mice. The % of the coverage of each nucleotide position to the whole virus genome by 21- to 23-nt vsiRNAs is shown. The strand sources of vsiRNAs are indicated by colors. The functional proteins encoded by the viral bipartite RNA genome and transcription of B2 mRNA (RNA3) from RNA1 are shown.

I next analyzed the population of vsRNAs in NoV-infected mice at 3 dpi before and after the co-IP by the anti-pan-AGOs (Figs 2.11 and 2.12). Although 22-nt vsiRNAs were detectable in AGOs from NoV-infected mice, AGO-loaded vsiRNAs were >30-fold less abundant and showed reduced preference for 1U compared to those from NoVΔB2-infected mice (Figs 2.11 and 2.12). Such de-enrichment of vsiRNAs was in contrast to the abundant input NoV vsRNAs in total mice, representing 6.5% of the total sequenced reads in the library (Fig 2.11). These findings indicate that the biogenesis of vsiRNAs is not completely suppressed during wild-type NoV infection, but the remaining vsiRNAs are invisible by sequencing small RNAs either with or without AGO co-IP because of the presence of abundant non-specific vsRNAs and the suppressed vsiRNA loading into AGOs.

2.3.4 Characterization of antiviral RNAi in suckling mice depleted of non-slicer AGOs

Three of the four mouse AGO proteins (AGO1, AGO3 and AGO4) do not exhibit the slicing activity unlike AGO2 (*103-106*). To investigate the role of non-slicer AGOs in mammalian antiviral RNAi response, I next analyzed the vsRNA population sequenced from ago1/3/4 triple knock-out (KO) mutant suckling mice at 3 days post inoculation by NoVΔB2 (Fig 2.14). By comparison, NoVΔB2 vsRNAs in ago1/3/4 KO mice were as abundant as those in wild-type mice (Fig 2.14). NoVΔB2 vsRNAs produced by ago1/3/4 KO mutant mice exhibited the known canonical siRNA properties, since they were

predominantly 22-nt in size, and were enriched within Dicer product size range (Fig 2.14A). Moreover, viral siRNAs were equally distributed to positive and negative strands (Fig 2.14A), and were enriched for canonical 22-nt vsiRNA duplexes with 2-nt 3' overhang (Fig 2.14B). The population of 1U vsiRNAs represented 41.2% of the total NoVΔB2 vsiRNAs in ago1/3/4 KO mutant mice, comparable to those found in wild-type suckling mice (Fig 2.14A). The result suggests that depletion of AGO1, AGO3 and AGO4 in suckling mice does not affect the canonical siRNA properties of NoVΔB2 vsiRNAs in antiviral RNAi response induced by infection.

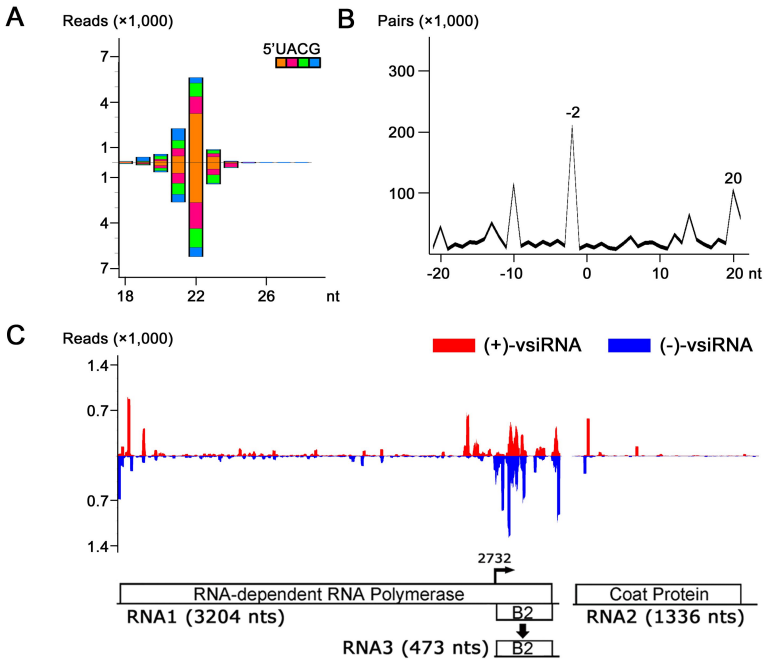

Figure 2.14 Properties of vsiRNAs in suckling mice depleted of AGO1/3/4. (A) Size distribution and abundance (shown as reads per million of total mature miRNAs) of virus derived small RNAs sequenced from ago1/3/4 suckling mice infected with NoVΔB2 at 3 dpi. The 5' terminal nucleotides of viral small RNAs are indicated by colors. **(B)** Total counts of pairs of complementary 22-nt viral small RNAs (per million of total mature miRNAs) in each distance category (in nucleotides) show the enrichment for pairs of canonical vsiRNAs with 2-nt 3' overhangs (-2 peak) and successive phasing vsiRNAs (+20 peak). **(C)** The coverage of each nucleotide position to the whole virus genome by 21- to 23-nt vsiRNAs (shown as reads per million of total mature miRNAs). The strand sources of vsiRNAs are indicated by colors. The functional proteins encoded by the viral bipartite RNA genome and transcription of B2 mRNA (RNA3) from RNA1 are shown.

NoVΔB2 vsiRNAs in ago1/3/4 KO mutant mice exhibited similar genome distribution pattern as found in wild-type mice, and were enriched at both termini of RNA1, 5' terminal of RNA2, and RNA3-coding region for both positive and negative strands (Fig 2.14C). I noted higher densities of positive-strand NoVΔB2 vsiRNAs from an upstream locus to RNA3 in ago1/3/4 KO mutant mice (Fig 2.14C). Such specific positive-strand vsiRNA hot spot attenuated the similarity between NoVΔB2 vsiRNA populations from ago1/3/4 KO mutant and wild-type mice revealed by correlation analysis (Fig 2.15). By comparison, 68 out of the total 11,613 vsRNA species exhibited significant variations in abundance between ago1/3/4 KO mutant and wild-type mice, and the abundance of 74 out of the total 13,011 vsRNA species sequenced from ago1/3/4 KO mutant mice or found in AGOs of wild-type mice were changed (Fig 2.15). I found that the majority of the variation was contributed by positive-strand vsRNAs. When only negative-strand vsRNAs were analyzed, I obtained higher regression coefficients (0.90 or 0.87, respectively) for the two comparisons between vsRNAs in ago1/3/4 KO mutant and wild-type mice, or between those in total ago1/3/4 KO mutant mice and bound to AGOs. The correlation coefficients were also increased to 0.73 or 0.79 for the two comparisons, respectively. Therefore, the depletion of non-slicer AGOs did not induce significant variation to NoVΔB2 vsiRNA population in suckling mice, suggesting that presence of AGO2 alone may support the loading and stability of the viral siRNAs *in vivo*.

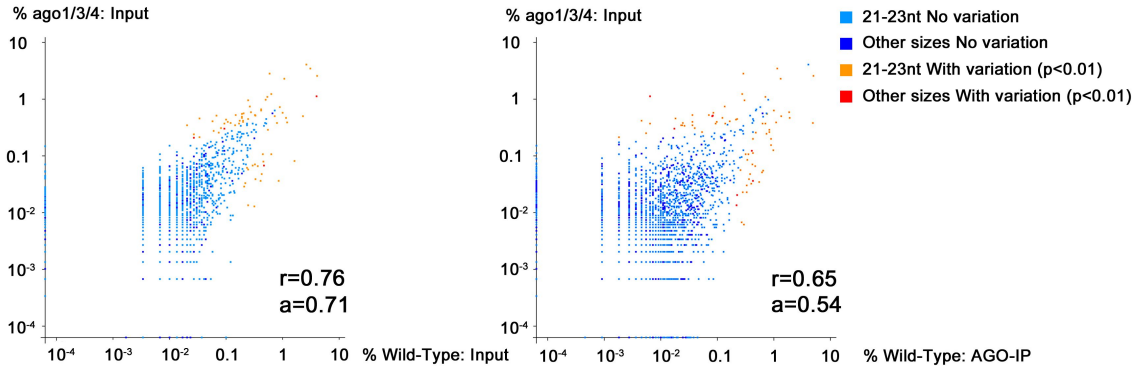

Figure 2.15 Correlation analysis between vsiRNAs in suckling mice depleted of AGO1/3/4 and wild-type suckling mice. Scatter plots of NoVΔB2 vsRNAs from total ago1/3/4 suckling mice and from wild-type mice either with or without treatment by AGO-coIP. The sizes of reads are indicated by colors. Each dot indicates the % of a given vsRNA to the total vsRNAs in either library. The correlation coefficient (r) and the regression coefficient through the origin (a) of each comparison are shown.

2.3.5 Time course analysis of NoVΔB2 vsiRNAs in suckling mice

I next investigated the change of vsiRNA properties during NoVΔB2 infection in suckling mice. NoVΔB2 was rapidly cleared by 7 dpi from its peak level of replication at 3 dpi, and became essentially undetectable at 15 dpi or later time points (Fig 2.16). Viral siRNAs accumulated to high levels in mice at 3 dpi, and were equal to approximately 0.5% of the total cellular miRNA population (Fig 2.16). A time course analysis revealed that although there was a major decrease in the abundance of NoVΔB2 vsiRNAs in mice during the process of virus clearance from 3 to 7 dpi, the population of NoVΔB2 vsiRNAs was maintained at abundant levels for 2 to 3 weeks after virus clearance (Fig 2.16). Notably, NoVΔB2 vsiRNAs detected at 7 dpi and after were as highly enriched for those with 1U as found for vsiRNAs co-immunoprecipitated with AGOs (Fig 2.16). These findings suggest stable maintenance *in vivo* of NoVΔB2 vsiRNAs in mice AGOs.

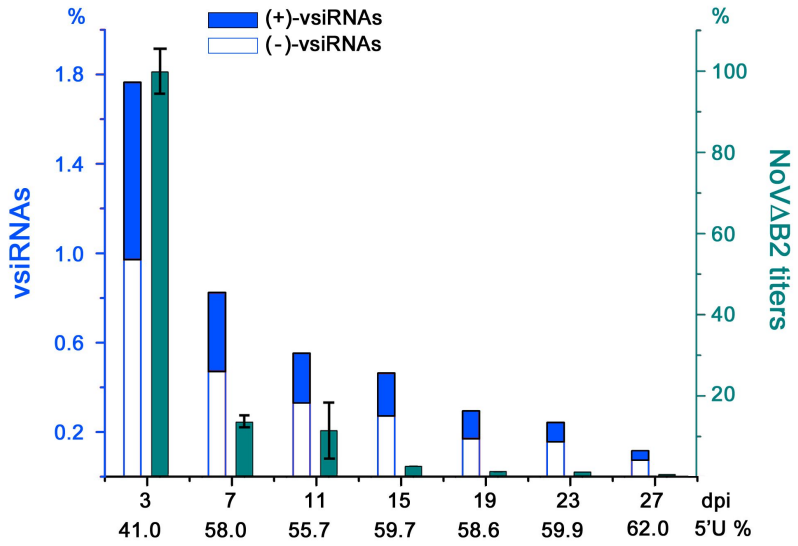

Figure 2.16 A time course analysis of NoVΔB2 vsiRNAs and the virus titer in suckling mice. The abundance of 21- to 23-nt vsiRNAs mapped to the positive- (blue) and negative-strand (white) of NoVΔB2 in suckling mice at each time point after the inoculation is shown, which is normalized as the % of the total mature miRNAs for comparison among the libraries. The accumulation of NoVΔB2 was measured by RT-qPCR of the viral genomic RNA1 normalized to β-actin mRNA (obtained from collaborators in Ding lab) and the one at 3 dpi was set as 100% (green). The 1U % of the vsiRNAs in each library is indicated at bottom.

NoVΔB2 vsRNAs were predominantly within Dicer product size range during virus infection in two repeat sets of time course libraries (~85%, Fig 2.17). Interestingly, I found that the proportion of 21-nt NoVΔB2 vsiRNAs was increased at later time points (Fig 2.17) from a low relative abundance of only ~35% to 22-nt vsiRNAs at 3 dpi. The abundance of 21-nt vsiRNAs became approximately equal to 22-nt vsiRNAs at 19 or 27 dpi in the two time course analysis (Fig 2.17). In contrast to 21-nt vsiRNAs, the relative abundance of 23-nt vsiRNAs to 22-nt vsiRNAs was unchanged, representing ~15% during the time course of virus infection (Fig 2.17). This finding suggests a size shift by 1-nt shortening in NoVΔB2 vsiRNA size distribution after virus clearance.

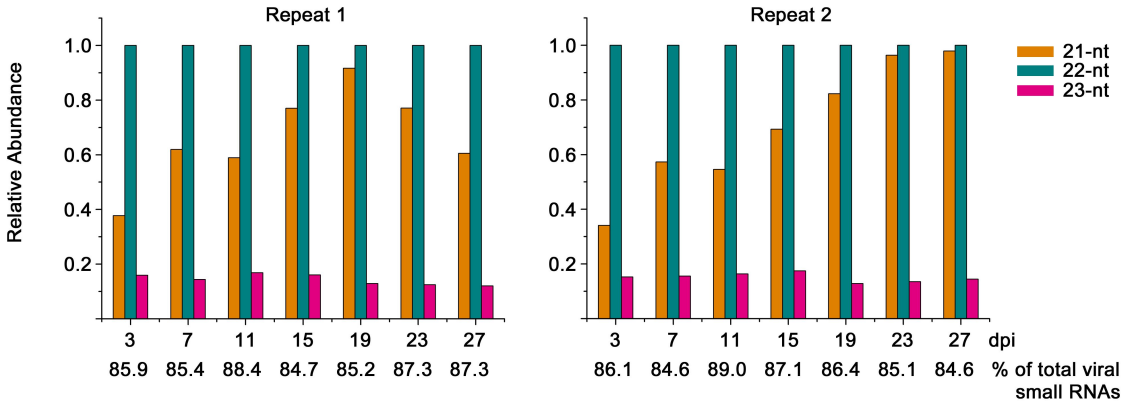

Figure 2.17 A time course analysis of NoVΔB2 vsiRNA proportions. The relative abundance of 21- and 23-nt NoVΔB2 small RNAs from both strands compared to the 22-nt vsiRNAs in suckling mice at each time point after the inoculation is shown. The % of the vsiRNAs to total viral small RNAs (18- to 28-nt) in each library is given at bottom. The library set of repeat 1 was shown as the representative for the analysis in Figs 2.16 and 2.18.

I found that the 21-nt vsiRNAs at later time points were generated from the same loci of the 22-nt vsiRNAs at earlier time points (Fig 2.18). For example, 93.8% of the 21-nt vsiRNA reads, or 84.6% of the total unique 21-nt vsiRNA species at 27 dpi, representing 867 raw reads in the library, shared sequences with 16.1% of the total unique 22-nt vsiRNA species at 3 dpi by missing a single nucleotide at either 5' or 3' end (Fig 2.18). 31.6% of the 867 21-nt vsiRNAs were shortened at their 3' ends, and only 9% were shortened at their 5' end (Fig 2.18). The remaining 59.4% of the 21-nt vsiRNAs were found to derive from two possible 22-nt vsiRNA species by one nucleotide removal from either end (Fig 2.18). Similar results were also found by comparing 21-nt vsiRNAs at 19 or 23 dpi to the 22-nt vsiRNAs at 3 dpi (Fig 2.18). This finding suggests the preference to 3' shortening in vsiRNA size shift during the time course, which could be explained by the importance of 5' nucleotide in loading and stable maintenance of vsiRNAs by AGOs.

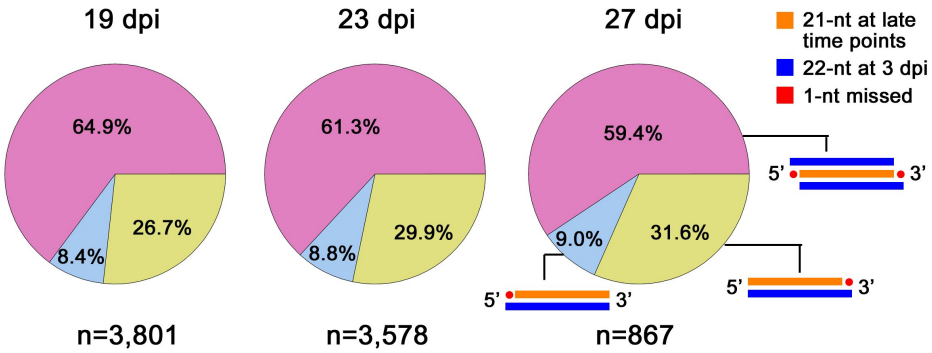

Figure 2.18 A comparison between 21-nt NoVΔB2 small RNAs at late time points and 22-nt vsiRNAs at 3 dpi in suckling mice. The %s and the total reads number of the three types of 21-nt virus reads at late time points with 1 or 2 correlated 22-nt vsiRNA species at 3 dpi in each library are shown.

2.3.6 *In vivo* sequestration of vsiRNA duplexes by VSR B2

Our previous studies *in vitro* suggested that Nodaviral B2 proteins inhibit both the dicing and loading steps of antiviral RNAi (*131, 182*). Lack of vsRNAs exhibiting canonical siRNA properties in NoV-infected mammalian cells and mice in previous results was consistent with the activity of B2 to suppress *in vitro* processing long dsRNA into siRNAs by Dicer. To investigate if NoV B2 protein binds *in vivo* to vsiRNA duplexes, I next characterized the population of NoV vsRNAs in BALB/c mice at 3 dpi after co-IP by the antibody specific to the viral B2 protein (Fig 2.19). NoV vsRNAs co-immunoprecipitated with B2 were highly abundant, representing ~40% of the total reads in two repeat libraries (Fig 2.11). In contrast to the input NoV vsRNAs that exhibited strong positive-strand bias and random size distribution, B2-bound vsRNAs were predominantly 22-nt and exhibited approximately equal strand ratios for all sizes (Fig 2.19A). B2-bound 22-nt vsRNAs were

enriched for canonical siRNA duplexes with 2-nt 3' overhangs (Fig 2.19B), but exhibited no preference for 1U population unlike AGO-bound NoVΔB2 vsiRNAs (Fig 2.19A). These findings, together with the low abundance of vsiRNAs found in AGOs in NoV-infected mice, indicate that B2 sequesters also vsiRNA duplexes to prevent their loading in AGOs in addition to the suppression of dicing. Interestingly, miRNAs and miRNAs* were significantly de-enriched in the libraries (Fig 2.11), suggesting that B2 preferentially recognizes perfect base-paired viral siRNA duplexes than the imperfect base-paired miRNA/miRNA* duplexes.

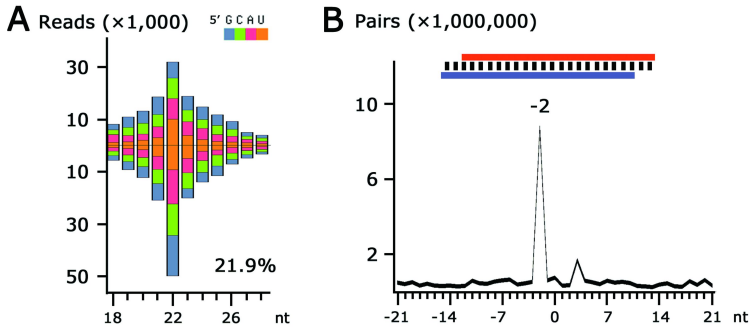

Figure 2.19 Properties of NoV derived small RNAs sequestered by B2 in suckling mice. (A) Size distribution and abundance (shown as reads per million of total reads) of virus derived small RNAs co-IPed by the antibody to B2 from suckling mice infected with NoV at 3 dpi. The 5' terminal nucleotides of viral small RNAs are indicated by colors, and the % of 1U 21- to 23-nt vsRNAs is indicated. **(B)** Total counts of pairs of complementary 22-nt vsRNAs bound to B2 (per million of total reads) in each distance category (in nucleotides) exhibiting the enrichment for pairs with 2-nt 3' overhangs (-2 peak) in suckling mice infected by NoV at 3 dpi.

2.3.7 Characterization of antiviral RNAi response in mutant mice defective in IFN signaling pathway

To investigate the crosstalk between interferon signaling pathway and antiviral RNAi in mammalian innate immunity, I next compared vsRNA populations sequenced from NoV- or NoVΔB2-infected wild-type C57 suckling mice and mutant mice defective in type I IFN signaling pathway. 22-nt NoV vsRNAs of both polarities were more abundant than other size classes of vsRNAs, and were enriched for canonical siRNA duplexes (not shown), but exhibited no enrichment of 1U population in both wild-type C57 mice and LGP-2$^{-/-}$ mice after NoV infection (Fig 2.20). This suggests that B2 is less effective to suppress the biogenesis of viral siRNAs in C57 mice than BALB/c mice. However, NoV vsRNAs in RIG-I knockout (RIG-I$^{-/-}$) or MAVS knockout (MAVS$^{-/-}$) mutant mice exhibited strong positive-strand bias and random size distribution with no canonical siRNA properties, similar to those in wild-type BALB/c mice (Fig 2.20). Viral small RNAs in NoVΔB2-infected C57, RIG-I$^{-/-}$ or MAVS$^{-/-}$ mice exhibited known canonical siRNA properties as found in BALB/c mice, including size preference for 22-nt, approximately equal strand ratio, enrichment for both 1U population and canonical siRNA duplexes (Fig 2.20). NoVΔB2 vsRNAs in RIG-I$^{-/-}$ or MAVS$^{-/-}$ mice exhibited similar genome distribution patterns to those in C57 mice (Fig 2.21). These findings suggest that the neither RIG-I nor MAVS is essential for the production of the canonical siRNAs during NoVΔB2 infection of suckling mice.

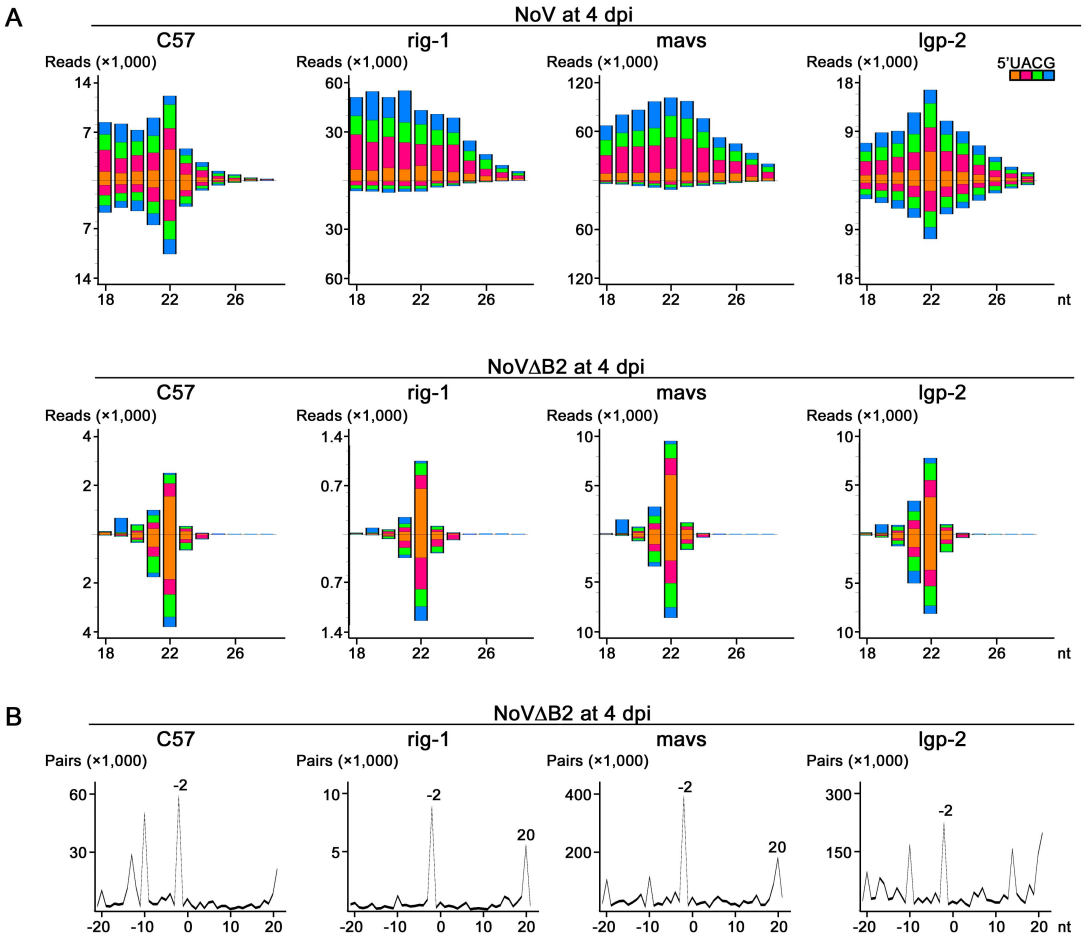

Figure 2.20 Properties of vsiRNAs in suckling mice depleted of components in IFN signaling pathway. (A) Size distribution and abundance (shown as reads per million of total mature miRNAs) of virus derived small RNAs sequenced from wild-type C57 suckling mice or mice knocked out of RIG-I, MAVS, or LGP-2 infected with NoVΔB2 or NoV at 4 dpi. The 5' terminal nucleotides of viral small RNAs are indicated by colors. **(B)** Total counts of pairs of complementary 22-nt viral small RNAs (per million of total mature miRNAs) in each distance category (in nucleotides). The enrichment for pairs of canonical vsiRNAs with 2-nt 3' overhangs (-2 peak) was shown.

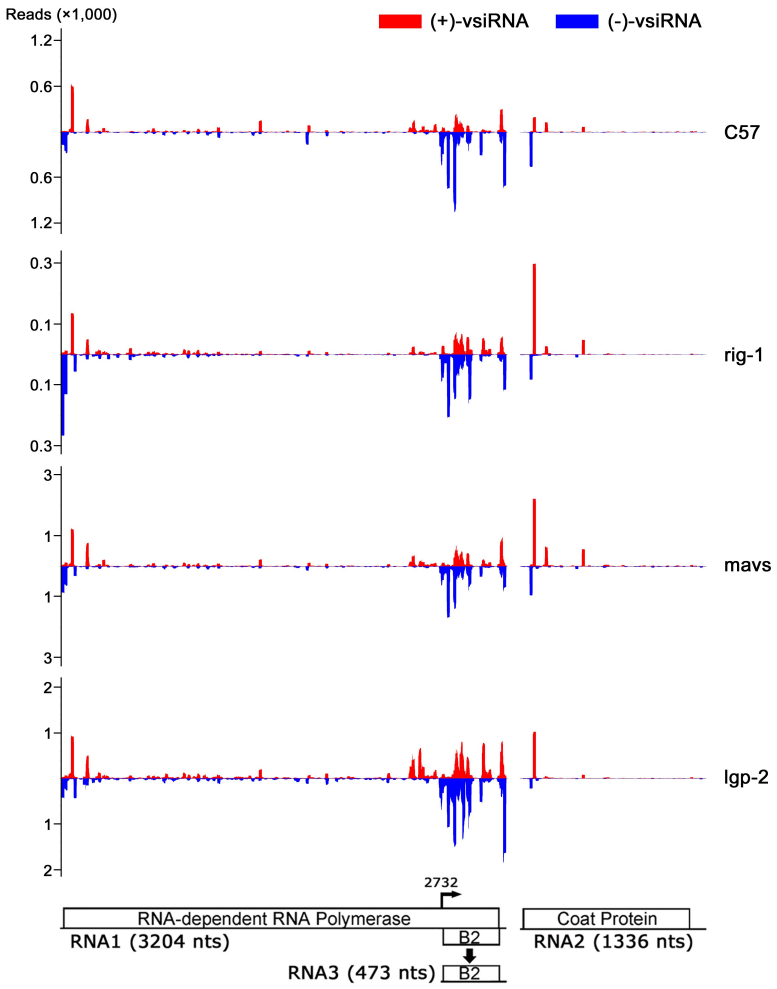

Figure 2.21 Virus genome distribution of 21- to 23-nt NoVΔB2 vsiRNAs in suckling mice depleted of components in IFN signaling pathway. The coverage of each nucleotide position to the whole virus genome by 21- to 23-nt vsiRNAs derived from wild-type C57 suckling mice or mice knocked out of RIG-I, MAVS, or LGP-2 infected with NoVΔB2 at 4 dpi (shown as reads per million of total mature miRNAs). The strand sources of vsiRNAs are indicated by colors. The functional proteins encoded by the viral bipartite RNA genome and transcription of B2 mRNA (RNA3) from RNA1 are shown.

I found that the abundance of NoVΔB2 vsiRNAs was dramatically changed in mutant mice (Fig 2.22). NoVΔB2 vsiRNA abundance in RIG-I$^{-/-}$ mice was reduced, representing only 32.5% of that in NoVΔB2-infected C57 mice (Fig 2.22). Since the abundance of vsiRNAs could correlate with the level of virus replication providing viral

dsRNA precursors, NoVΔB2 vsiRNAs in each library were further normalized by virus titers determined by RT-PCR (Fig 2.22). NoVΔB2 vsiRNA abundance in RIG-I$^{-/-}$ mice was extremely low after normalization by virus titer, representing only 0.4% compared to that in C57 mice (Fig 2.22). In contrast, although NoVΔB2 vsiRNA abundance increased in MAVS$^{-/-}$ mice by ~170%, the vsiRNA abundance after normalization by virus titer exhibited a mild decrease by ~30% compared to that in C57 mice, indicating that such change to NoVΔB2 vsiRNAs was due to a higher viral replication level (Fig 2.22). Therefore, these findings suggest that RIG-I may enhance Dicer-dependent processing of viral dsRNA into siRNAs.

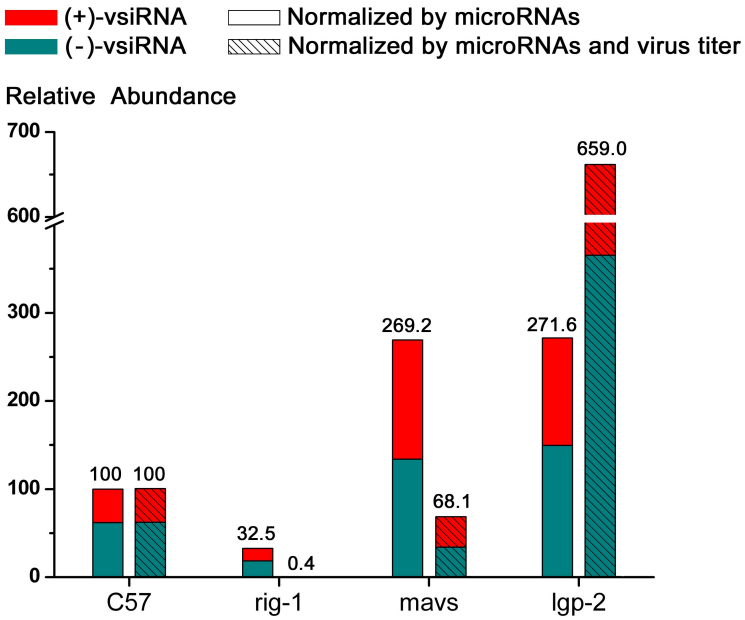

Figure 2.22 Relative abundance of 21- to 23-nt NoVΔB2 vsiRNAs in suckling mice depleted of components in IFN signaling pathway. The relative abundance of 21- to 23-nt vsiRNAs derived from wild-type C57 suckling mice or mice knocked out of RIG-I, MAVS, or LGP-2 infected with NoVΔB2 at 4 dpi is shown. Reads are normalized either by mature microRNA only or by both microRNAs and virus titer determined by RT-PCR by collaborators in Ding lab. The strand sources of vsiRNAs are indicated by colors. The value of vsiRNA abundance in wild-type C57 mice is set to 100, and the relative values of vsiRNA abundance in mutant mice compared to C57 mice are shown.

NoVΔB2 vsiRNAs were also highly abundant in LGP-2$^{-/-}$ mice at 4 dpi, suggesting LGP-2 was not essential for the vsiRNA biogenesis (Fig 2.20). Notably, the abundance of NoVΔB2 vsiRNAs increased by 2.7 and 6.6 times in LGP-2$^{-/-}$ mice compared to that in C57 mice before and after normalization by virus titer (Fig 2.22). This result suggests that LGP-2 may repress Dicer-dependent processing of viral dsRNA into vsiRNAs in contrast to RIG-I.

2.3.8 Characterization of the antiviral RNAi response in adult mice

Adult mice are resistant to NoV infection unlike suckling mice (*193*). Viral small RNAs cloned from NoVΔB2-infected BALB/c adult mice at 3 or 7 dpi were not abundant, but exhibited the canonical siRNA properties. These adult mouse vsiRNAs exhibited preference within Dicer product size range with 22-nt as the most dominant size, approximately equal strand ratio, preference of 1U, and enrichment of 22-nt canonical siRNA duplexes with 2-nt 3' overhangs (Fig 2.23). Notably, NoVΔB2 vsiRNAs in adult mice were found preferentially to target 5' terminal region of RNA1, but the vsiRNA hot spots at 5' terminal region of RNA2 reproducibly found in suckling mice became invisible (Fig 2.24). Although the RNA3-coding region was targeted by abundant NoVΔB2 vsiRNAs, the relative density of vsiRNAs from that region decreased in adult mice compared to suckling mice (Figs 2.13 and 2.24). These findings indicate that NoVΔB2 infection also induces the antiviral RNAi response in adult mice.

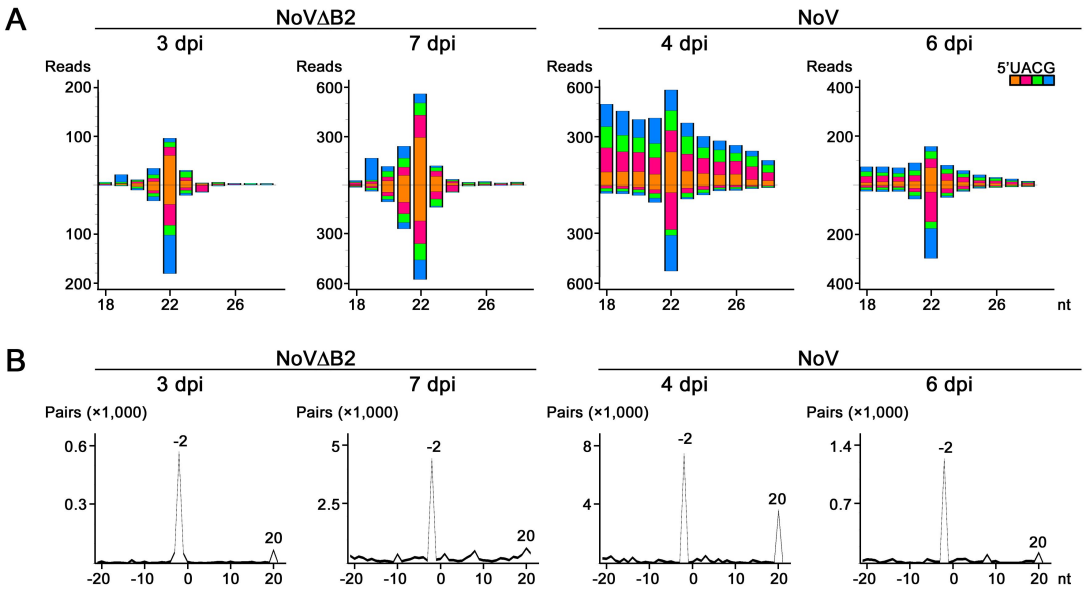

Figure 2.23 Properties of vsiRNAs in adult mice. (A) Size distribution and abundance (shown as reads per million of total mature miRNAs) of virus derived small RNAs sequenced from adult BALB/c mice at different time point post infection by NoVΔB2 or NoV. The 5' terminal nucleotides of viral small RNAs are indicated by colors. **(B)** Total counts of pairs of complementary 22-nt viral small RNAs (per million of total mature miRNAs) in each distance category (in nucleotides). The enrichment for pairs of canonical vsiRNAs with 2-nt 3' overhangs (-2 peak) and successive phasing vsiRNAs (+20 peak) was shown.

Strikingly, vsRNAs cloned from NoV-infected adult BALB/c mice were predominantly 22-nt in size (Fig 2.23). NoV vsRNAs in adult mice at 4 dpi exhibited weak positive-strand bias, but this bias disappeared for those mice at 6 dpi (Fig 2.23). NoV vsiRNAs cloned from adult mice were enriched for 22-nt canonical siRNA duplexes, but exhibited no enrichment for 1U population (Fig 2.23), suggesting that their loading into AGOs may be inhibited by B2. Notably, unlike the random genome distribution pattern of positive-strand vsiRNAs, negative-strand NoV vsiRNAs in adult mice were almost exclusively from 5' terminal region of RNA1 (Fig 2.24), which is similar to that found in mouse embryonic stem cells infected with NoVΔB2 (*196*). The negative-strand

22-nt vsiRNA species from two successive siRNA duplexes at 5' terminal of RNA1 starting from the second nucleotide of RNA1 represented 71.5% and 67.1% of the total negative-strand 22-nt vsiRNAs at 4 and 6 dpi, respectively (Figs 2.24 and 2.25). These findings demonstrate induction of the antiviral RNAi response in adult mice infected by NoV, suggesting a possible role of antiviral RNAi in the adult mouse resistance to NoV infection.

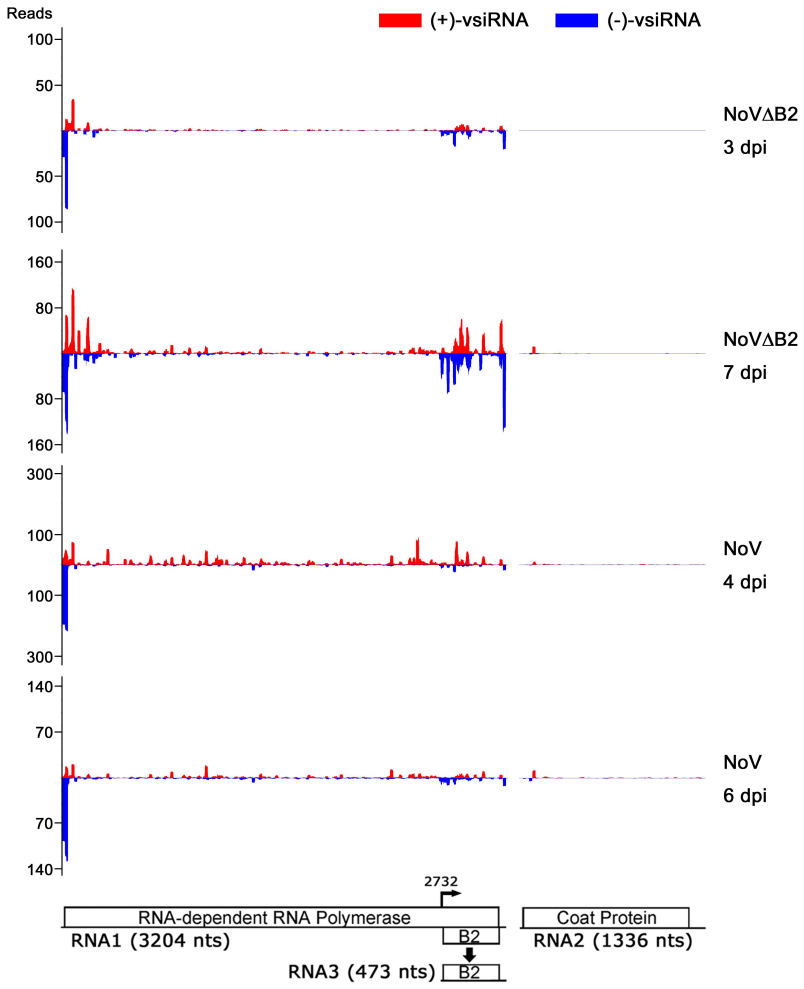

Figure 2.24 Virus genome distribution of 21- to 23-nt vsiRNAs in adult mice. The coverage of each nucleotide position to the whole virus genome by 21- to 23-nt vsiRNAs derived from adult BALB/c mice at different time points post infection by with NoVΔB2 or NoV (shown as reads per million of total mature miRNAs). The strand sources of vsiRNAs are indicated by colors. The functional proteins encoded by the viral bipartite RNA genome and transcription of B2 mRNA (RNA3) from RNA1 are shown.

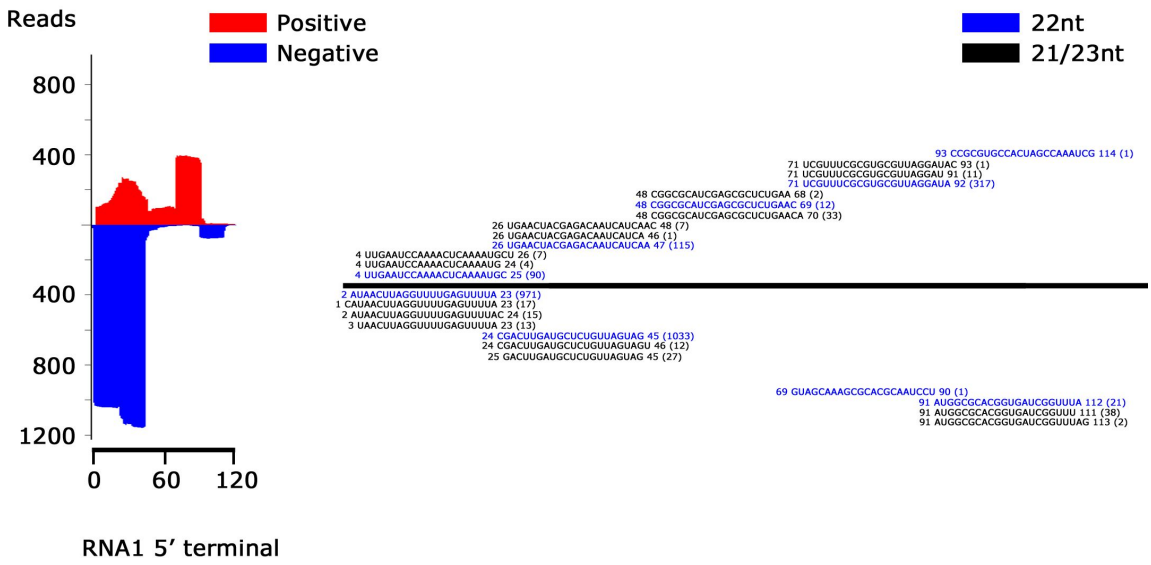

Figure 2.25 The abundant production of 21- to 23-nt vsiRNAs at 5' terminal of RNA1 in adult mice infected by NoV. The coverage of each nucleotide position to the 5' terminal of RNA1 by 21- to 23-nt vsiRNAs derived from adult BALB/c mice infected by NoV at 4 dpi (shown as raw reads). The strand sources of vsiRNAs are indicated by colors. Read sequences within this region reveal a dominant set of successive pairs of 21- to 23-nt vsiRNAs. Read counts (in brackets), read length, genomic position and sequence of each vsiRNA species are indicated.

2.4 Discussion and conclusions

Results in this chapter describe the first *in vitro* and *in vivo* characterization of the mammalian antiviral RNAi response induced by an RNA virus infection. My bioinformatics analysis of NoVΔB2 small RNAs revealed the properties of canonical siRNAs, and was supported by parallel vsiRNA detection by Northern blot hybridization by my collaborators in Ding lab (*185*). The findings here and those of Maillard *et al.* (*196*) illustrate that Dicer-dependent processing of viral dsRNA replication precursors into successive siRNAs is a conserved mammalian immune response to infection by two

distinct positive-stranded RNA viruses (Table 2.2). This work also suggests that the use of viruses incapable of inhibiting siRNA biogenesis will facilitate future detection of vsiRNAs targeting other mammalian viruses.

NoV infection both *in vitro* and *in vivo* requires the RNAi suppressor activity of its B2 protein (*185*). In particular, suckling mice become completely resistant to the lethal infection by NoVΔB2, or a NoV mutant after substitution of a single amino acid in B2 (NoVmB2) that eliminates its RNAi suppressor activity (*185*). Abundant production of vsiRNAs is detected in NoVΔB2-infected mice by deep-sequencing as presented in this chapter and by Northern blotting (*185*). Thus, the typical RNAi response induced by virus infection in mammals has potent antiviral activity. The striking similarities in the induction and suppression of antiviral RNAi by the closely related FHV and NoV in fruit flies, nematodes, and mammals (*131, 134, 145, 162-163, 194, 210-211*) highlight an evolutionary conserved role of RNAi in antiviral defense within the animal kingdom.

Viral siRNAs are *in vivo* loaded in AGOs like mammalian miRNAs and are stably maintained. Production and loading of vsiRNAs in AGOs are both dramatically repressed by dual functions of NoV B2 in viral dsRNA dicing inhibition and vsiRNA duplex sequestration. Studies in mouse embryonic stem cells by Maillard *et al*. (*196*) suggest that AGO2 is essential for *in vitro* clearance of NoVΔB2. It is not clear why the size of vsiRNAs shifts to 21-nt after NoVΔB2 clearance *in vivo*. As artificial 21-nt siRNAs efficiently inhibit infection by mammalian viruses (*212*), I propose that the *in vivo* size shift may contribute to a long lasting protection to mammalian virus infection. These

findings may facilitate future *in vivo* studies of RNAi-based antiviral immunity guided by naturally occurring vsiRNAs, and may help overcome the challenging issues of specific delivery, off-target effect and the loss of siRNA sensitivity that confronted the studies of antiviral therapies by artificial small RNA duplexes or their precursors (*165-167*).

Antiviral RNAi exhibits properties associated with adaptive and other known innate immunities as it involves rapid host recognition of a microbe-associated molecular pattern dsRNA and a mechanism of specificity determined by pathogen-derived siRNAs (*128*). Interestingly, RIG-I is required for efficient dicing of viral dsRNA in mice, suggesting a new role in mammalian antiviral RNAi immunity besides its known function in type-I IFN signaling pathway as the viral dsRNA sensor. Similarly, the observed negative regulation of the vsiRNA biogenesis by LGP-2 may provide new insights into its intriguing function in innate immunity. It is likely that the characterization of mammalian antiviral RNAi in this chapter will provide a new framework to investigate the innate and adaptive control of important human viral pathogens.

Chapter 3: Somatic role of Dicer in the biogenesis of vsiRNAs in human cells

3.1 Introduction

Chapter 2 presented the first evidence for the induction of the antiviral RNAi response in mice, which detects viral dsRNA as the non-self pathogen-associated molecular pattern. Similar to fungi, plants and invertebrates (*128*), suckling mice also are able to produce virus-derived small interfering RNAs (vsiRNAs) from viral dsRNA precursors and further load them in Argonaute proteins (AGOs) in RNA-induced silencing complex (RISC). However, controversial issues remain unresolved on mammalian antiviral RNAi despite these recent advances described in Chapter 2 and by Maillard *et al* (*196*). It is widely thought that mammalian Dicer cannot detect and process viral dsRNAs into vsiRNAs in the differentiated somatic cells that are attacked first in an infection (*215*). The sequencing of small RNAs in the past decade from a wide range of mature mammalian somatic cells after infection with diverse RNA viruses (*178-180*) detected only virus-derived small RNAs (vsRNAs), which exhibit random size distribution and strong strand bias in contrast to vsiRNAs. Our studies have demonstrated production of highly abundant vsiRNAs in mouse embryonic stem cells (mESCs) and suckling mice (*185, 196*), but the accumulation of vsiRNAs in mESCs decreases in abundance upon differentiation. Therefore it was thought that undifferentiated cells in suckling mice may play a role in

biogenesis of vsiRNAs. The absence of evidence for vsiRNA production in human cells and the presence of a rodents-specific isoform of Dicer for processing long dsRNA into siRNAs in mouse oocytes (*197*) have further led to the controversial hypothesis that humans have evolved to abandon the antiviral RNAi response (*216*).

Studies conducted in this chapter aimed to determine if human somatic cells produce canonical vsiRNAs in response to RNA virus infection. According to the mechanistic insights into the induction and suppression of the vsiRNA biogenesis by Nodamura virus (NoV), I searched for the biogenesis of vsiRNAs in human embryonic kidney 293 (293T) cells and adenocarcinomic alveolar basal epithelial (A549) cells infected by mutants of Influenza A virus (IAV) not expressing its viral suppressor of RNAi (VSR), the non-structural protein 1 (NS1). IAV belongs to the *Orthomyxoviridae* family, and is an enveloped (-)RNA virus containing eight genomic segments. IAV has a wide host range including birds and mammals and is divided into subtypes defined by the surface glycoproteins hemagglutinin (HA) and neuraminidase (NA) encoded by genome segments 4 and 6, respectively (*186-187*). IAV replicates in the nucleus, where the negative-strand viral genomic RNAs (vRNAs) are used as the template for the synthesis of both mRNAs and the full-length complementary RNAs (cRNAs) before the vRNAs copied from cRNAs are exported into the cytosol (*187*).

IAV genome segment 8 encodes two proteins, NS1 and NS2 (*187*). NS1 contains the N-terminal dsRNA-binding domain and the C-terminal effector domain and is multifunctional with main function as the IFN antagonist (*170*). NS1 also exhibits the

VSR activity in both *Drosophila* and plant cells and potently suppresses *Drosophila* antiviral RNAi against Flock house virus (FHV) (*170, 182*). Interestingly, NS1 also shares structural similarity with the B2 proteins of FHV and NoV in dsRNA binding (*219*) and both bind long dsRNA with two positively charged antiparallel α helices in a homodimer. However, differentiated mammalian cells produce only vsRNAs after infection with wild-type IAV strains that do not exhibit the properties of vsiRNAs (*180, 218*). Therefore it has not been possible to investigate the physiological role for the VSR activity of NS1 in an RNAi response induced by IAV infection (*219*).

3.2 Materials and Methods

3.2.1 Influenza A viruses and cell culture

Influenza A/Puerto Rico/8/34 (H1N1) and A/WSN/1/33 (H1N1) viruses, designated PR8-wildtype (WT) and WSN-WT, respectively, and their NS1 deletion mutants, designated PR8-delNS1 and WSN-delNS1, were kind gifts of Drs. Adolfo García-Sastre and Peter Palese (*188, 198*). The –delNS1 mutant IAVs contain a deletion of nucleotides 57 to 528 in NS segment which are located in the intron of NS2 protein but the exon of NS1. PR8-3841 mutant contains amino acid substitutions R38A and K41A known to result in defectiveness in dsRNA binding without affecting protein dimerization (*201, 217*). IAV-3841 was constructed by combining segment 1-7 from PR8-WT and segment NS from WSN-WT, containing the same mutations as referred above. Human lung

epithelial cells (A549) were maintained in F-12K medium whereas human embryonic kidney cells (293T) were cultured in Dulbecco's modified Eagle's medium (DMEM) containing 10% fetal bovine serum. hDicer knockout 293T cell line 4-25 and its parental 293T cell line were kind gifts of Dr. Bryan Cullen (*199*).

3.2.2 Plasmids and molecular cloning

The expression plasmids for human AGO1, AGO2 and Dicer were purchased from Addgene (cat no. 10820, 10822 and 19873). The cDNA clones for Drosophila Loquacious isoforms PD (Loqs PD) were from Addgene (no. 42095) whereas the plasmids encoding Drosophila proteins dDicer-2 and R2D2 were kind gifts from Dr. Qinghua Liu (*202, 203*). The ORFs of Loqs PD and R2D2 were cloned with an N-terminal Flag tag into pcDNAFlag (*195*) to generate pcDNA-Flag-PD and pcDNA-Flag-R2D2, respectively. The ORFs of dDicer-2 was cloned with an N-terminal His tag into pcDNA4HisMax (*195*) to generate pcDNA-His-dDcr2.

3.2.3 Cell culture infection, transfection and the construction of small RNA libraries.

293T and hDcrKO 293T cells were seeded in a 6-cm plate at a density of 2.5×10^6/plate one day before infection. Twenty-four hours after inoculation with serum-free DMEM (mock), PR8-WT, WSN-WT, PR8-delNS1 or WSN-delNS1 (moi=1) as previously

described (*195*), the infected cells were harvested for the extraction of total protein and RNA using TRIzol (Invitrogen, Carlsbad, CA) according to the manufacturer's protocol. To determine the role of Dicer in the biogenesis of viral siRNAs (vsiRNAs), hDicer-KO 293T cells seeded in a 6-cm plate at a density of 2.5×10^6/plate were transfected with 8 μg of the plasmid encoding hDicer, or Drosophila Dicer-2 (dDcr2), or co-transfected with 8 μg pcDNA-His-dDcr2, 4 μg pcDNA-Flag-Loqs-PD, and 4 μg pcDNA-Flag-R2D2 using TransIT®-LT1 transfection reagent (Mirus, Madison, WI) following the supplier's recommended protocol. Six hours after transfection, hDcr-KO 293T cells were infected by PR8-delNS1 (moi=1) and the infected cells were harvested for the extraction of total protein and RNA using TRIzol 24 hours after infection.

Libraries of small RNAs were constructed from total RNA extracted 24 hours after infection of 293T cells with PR8-delNS1 or WSN-delNS1 either without or with co-immunoprecipitation by Anti-pan Ago antibody (Millipore, Billerica, MA) as described in the previous chapter. Libraries of small RNAs were also constructed from (i) total RNA co-immunoprecipitated from 293T cells 24 hours after infection with PR8-WT or WSN-WT by Anti-pan Ago antibody (Millipore, Billerica, MA), (ii) total RNA from A549 cells 24 hours after infection with PR8-delNS1, (iii) total RNA from PR8-delNS1-infected hDcr-KO 293T cells without or with ectopic expression of hDicer, dDicer-2 or dDicer-2 plus Loqs-PD and R2D2, and (iv) total RNA co-immunoprecipitated from 293T cells over-expressing FLAG-tagged human AGO1 or AGO2 24 hours after infection with PR8-delNS1 or WSN-delNS1.

3.2.4 Northern blot analysis

15 μg total RNA extracted from cells 24 hours after infection and a chemical cross-linking protocol (*204*) were used as essentially described previously with one modification (*185*). Instead of using locked nucleic acid (LNA) oligonucleotides as probes (*185*), the negative- and positive-strand influenza viral RNAs were detected by the ^{32}P-labeled synthetic RNA oligo, 5'-CAUAAUGGAUCCAAACACUGUG-3' and 5'-GACACAGUGUUUGGAUCCAUUA-3', respectively.

3.2.5 Deep sequencing and bioinformatics analysis of small RNAs

Libraries of small RNAs cloned from cultured human cells were sequenced by Illumina HiSeq 2000/2500 at the Core Facility of the Institute for Integrative Genome Biology on campus. Small RNA reads were mapped to the virus and host genome references or compared to mature miRNAs. Mapping was done by Bowtie 1.0.0 with either perfect match or 1 mismatch only for genotyping and reads origin analysis. All of the references used were downloaded from web sources as listed below. Subsequent bioinformatics analysis of virus-derived small RNAs was carried out using in-house Perl scripts as described in Chapter 2. Pairs of complementary 22-nt vsiRNAs in each library with different base-pairing lengths were computed using the algorithm described in the previous chapter, which calculates the total counts of pairs in each nucleotide distance between the 5' and 3' ends of complementary 22-nt vsiRNAs (*185*). The reference

sequences used in this study:

1. A/Puerto Rico/8/34 (H1N1) (PR8-WT): NCBI AF389115.1, AF389116.1, AF389117.1, AF389118.1, AF389119.1, AF389120.1, AF389121.1 and AF389122.1.

2. PR8-delNS1: the same as PR8-WT except for the deletion of nucleotides 57 to 528 in NS segment.

3. A/WSN/1/33 (H1N1) (WSN-WT): NCBI J02179.1, J02178.1, CY034137.1, J02176.1, CY034135.1, L25817.1, L25818.1 and M12597.1 with the missing terminal sequences from the following segments completed by sequencing (nucleotides underlined are the original terminals from NCBI):

Segment PA (segment 3) 3' terminal: 3'-AGCGAAAGCAGGTACTGATT…-5'

Segment PA (segment 3) 5' terminal: 3'-…AAAAAAGTACCTTGTTTCTACT-5'

Segment NP (segment 5) 3' terminal: 3'-AGCAAAAGCAGGGTAGATAATCACTC…-5'

Segment NP (segment 5) 5' terminal: 3'-…AAAGAAAAATACCCTTGTTTCTACT-5'

Segment M (segment 7) 5' terminal: 3'…AAACTACCTTGTTTCTACT-5'

4. WSN-delNS1: the same as WSN-WT except for the deletion of nucleotides 57 to 528 in NS segment.

5. Human mature miRNAs and miRNA precursors: miRBase 19 (http://www.mirbase.org/).

6. Human non-coding RNAs: fRNAdb 3.0 (http://www.ncrna.org/frnadb/).

7. Human mRNAs: Mammalian Gene Collection (MGC).

8. Human whole genome: GRCh38 project from NCBI, released on December 24, 2013 (GCA_000001405.15).

3.2.6 Correlation analysis of small RNA populations

The correlation analysis of small RNA populations was done by the formulas below:

$$\text{Correlation coefficient } (r) = \frac{\sum_{i=1}^{n}(x_i - \bar{x})(y_i - \bar{y})}{\sqrt{\sum_{i=1}^{n}(x_i - \bar{x})^2} \cdot \sqrt{\sum_{i=1}^{n}(y_i - \bar{y})^2}}$$

$$\text{Regression coefficient } (a) = \frac{\sum_{i=1}^{n} x_i y_i}{\sum_{i=1}^{n} x_i^2}$$

$$\text{Average variation } (\mu) = \frac{\sum_{i=1}^{n}(y_i - x_i)}{n}$$

$$\text{Standard deviation } (\sigma) = \sqrt{\frac{\sum_{i=1}^{n}(y_i - x_i - \mu)^2}{n}}$$

n indicates the total number of the nucleotide positions on each strand of the PR8-delNS1 genome in the analysis for correlation between 21- and 22-nt influenza

vsiRNAs made by hDicer and dDicer2, or the total number of the unique influenza small RNA species (18- to 28-nt) found in human AGO1 and/or AGO2 co-IP libraries.

i indicates a specific nucleotide position as referred above that is covered or not covered by either 22- or 21-nt vsiRNAs from the hDicer and dDicer2 libraries, respectively, or a given small RNA species in human AGO1 and AGO2.

y_i indicates the relative coverage at position *i* by 22-nt vsiRNAs made by hDicer with a value between 0 and 1 after normalization by the maximum 22-nt vsiRNA coverage of each virion RNA segment in either polarity. $\bar{y}$ indicates the average coverage by 22-nt vsiRNAs at all nucleotide positions (n). In the analysis for small RNAs in human AGO1 and AGO2, y_i indicates the % of a given vsiRNA to the total vsiRNAs loaded in human AGO1, and $\bar{y}$ indicates the average % of all the vsiRNAs loaded in human AGO1.

x_i indicates the relative coverage at position *i* by 21-nt vsiRNAs made by dDicer2 with a value between 0 and 1 after normalization by the maximum 21-nt vsiRNA coverage of each virion RNA segment in either polarity. $\bar{x}$ indicates the average coverage by 21-nt vsiRNAs at all of the nucleotide positions (n). In the analysis for small RNAs in human AGO1 and AGO2, x_i indicates the % of a given vsiRNA to the total vsiRNAs loaded in human AGO2, and $\bar{x}$ indicates the average % of all the vsiRNAs loaded in human AGO2.

Any given nucleotide position or unique small RNA species referred as (*i*) above with a value change (y_i-x_i) beyond the interval [μ-3σ, μ+3σ] was considered as displaying

significant variation between the two small RNA libraries; otherwise it was considered to display no significant variation.

3.3 Results

3.3.1 Human 293T cells produce highly abundant vsiRNAs loaded in AGOs after infection with NS1-deletion mutant of IAV

According to the characterization of viral siRNAs (vsiRNAs) in fruit flies (*131*) and suckling mice, Argonaute co-immunoprecipitation (co-IP) enriches vsiRNAs by eliminating non-specific degradation fragments of the abundant viral genomic and messenger RNAs that accumulate during infection. These studies also show that VSRs may inhibit the processing of viral dsRNA precursor into siRNAs or destabilize the vsiRNAs by preventing their loading into Argonautes. Therefore, human vsiRNAs might become readily detectable by deep sequencing small RNAs co-immunoprecipitated with Argonaute proteins (AGOs) from cells infected with an RNA virus defective in the expression of a cognate VSR.

To test this hypothesis, the total small RNAs co-immunoprecipitated by an anti-pan-AGOs antibody from human 293T cells 24 hours post infection with a human Influenza A virus (IAV) mutant not expressing NS1 were cloned and sequenced. The AGO-bound, IAV-derived small RNAs sequenced from the human somatic cells infected

with PR8-delNS1 (Fig 3.1), a NS1-deletion mutant of IAV strain A/Puerto Rico/8/1934 (H1N1) characterized previously (*188*), exhibited several known properties of mouse vsiRNAs described in Chapter 2 and by Maillard *et al* (*196*). 93.6% of the 41,324 virus reads, cloned by a protocol requiring the presence of monophosphates at 5' termini, were in the 21- to 23-nt size range of Dicer products (Fig 3.1, Table 3.1). The most dominant size of the influenza vsiRNAs was 22-nt for both the positive and negative strands (Fig 3.1, Table 3-1). The influenza vsiRNAs were abundant, representing 0.34% of the total sequenced reads and equal to 0.81% of the total mature miRNA content (Table 3.1), and were comparable to human miR-27b-3p and miR-1307-5p in abundance in the library. By comparison, the AGO-bound 21- to 23-nt vsiRNAs reached 0.29% of the total mature miRNAs in mESCs infected with encephalomyocarditis virus (*196*). Notably, the 22-nt RNAs of IAV were highly enriched for canonical vsiRNAs with 20-nt perfect base-paired duplexes with 2-nt 3' overhangs (Fig 3.1). Therefore, the cloned influenza vsiRNAs closely resemble the mouse vsiRNAs, demonstrating production of canonical vsiRNAs in the mature human somatic cells in response to the influenza viral infection. Interestingly, 71.5% of the sequenced viral 22-nt RNAs and 62.9% of the viral 21- to 23-nt siRNAs contained uridine as the 5'-terminal nucleotide (1U) (Table 3.1), revealing shared properties between human miRNAs and the influenza vsiRNAs (*220, 221*).

Table 3.1 Contents and properties of the small RNA libraries sequenced (NS segment included)

Library	Total reads (18-28nt)	miRNAs[1] (mature)	Pre-miR hairpins[2] (of total reads)	Virus reads (18-28nt)	Virus reads of 21- to 23-nt				
					Reads (of miRNAs)	of all sizes	(+)-strand	1U	Terminal 100 nt
PR8-delNS1: Ago-IP (293T)	11,302,454	4,802,301	8,739,996 (77.3%)	41,324	38,680 (0.8%)	93.6%	68.0%	62.9%	91.8%
PR8-delNS1: Input (293T)	7,473,617	744,024	2,589,158 (34.6%)	46,102	25,170 (3.4%)	54.6%	32.5%	42.0%	56.7%
WSN-delNS1: Ago-IP (293T)	4,706,817	1,876,460	3,674,326 (78.1%)	6,176	5,615 (0.3%)	90.9%	72.9%	72.1%	88.6%
WSN-delNS1: Input (293T)	6,832,452	819,404	2,683,574 (39.3%)	32,030	13,491 (1.6%)	42.1%	57.4%	29.1%	39.1%
PR8-WT: Ago-IP (293T)	4,399,122	1,740,209	3,441,361 (78.2%)	877	304 (0.02%)	34.7%	62.5%	18.4%	37.8%
WSN-WT: Ago-IP (293T)	7,007,112	2,875,406	5,244,866 (74.9%)	1,054	370 (0.01%)	35.1%	77.0%	17.6%	27.3%
PR8-delNS1: Input (A549)	19,199,474	3,205,109	4,669,874 (24.3%)	209,896	113,446 (3.5%)	54.0%	51.0%	49.0%	49.3%

[1] Indicating the reads perfectly identical to mature microRNAs

[2] Indicating all the reads mapped to pre-microRNA hairpins, including mature microRNAs, microRNAs* and imprecise products

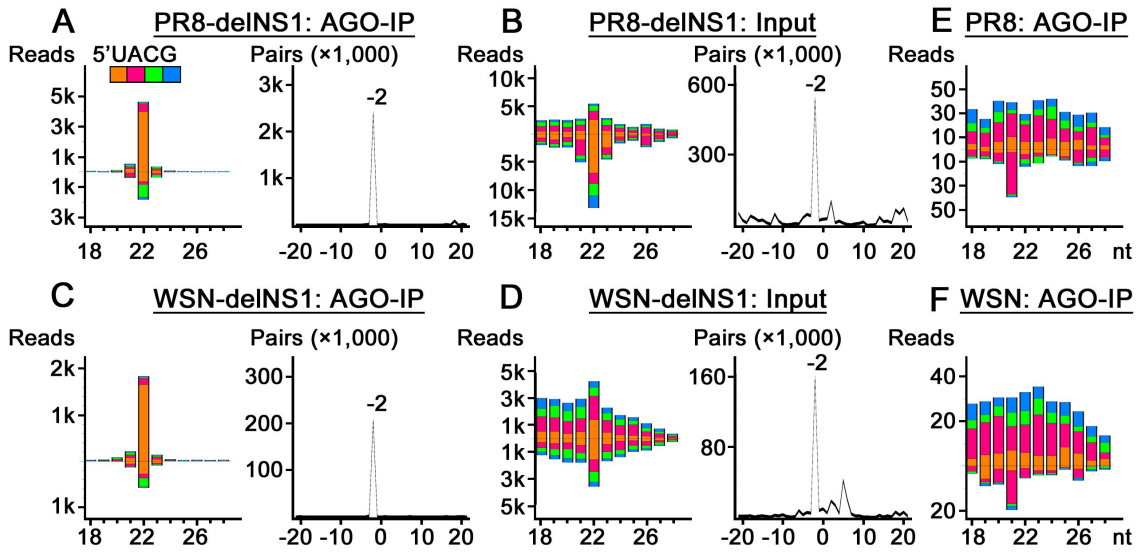

Figure 3.1 Production of IAV vsiRNAs in human 293T cells. Size distribution and abundance (shown as reads per million of total mature miRNAs) of total vsRNAs sequenced from cells 24 hours after infection with delNS1 mutants of PR8 and WSN strains without (input) or with co-IP by anti-pan AGO antibodies (AGO-IP). Strong enrichment of total and AGO-bound 22-nt RNAs of both PR8-delNS1 and WSN-delNS1 for pairs (-2 peak) of canonical vsiRNAs with 2-nt 3' overhangs was visualized by computing total pairs of 22-nt vsRNAs with different length of base-pairing. The 5' terminal nucleotide of vsRNAs is indicated by color.

In contrast, I detected abundant positive- and negative-strand virus reads outside the size range of Dicer products in the total small RNAs cloned without AGO co-IP from PR8-delNS1 infected cells (Fig 3.1). As a result, only 54.6% of the total virus reads were within the 21- to 23-nt size range (Table 3.1) and the peak at 22-nt was less dominant (Fig 3.1) compared to those cloned after AGO co-IP. Nevertheless, the 22-nt virus reads cloned either before or after AGO co-IP were similarly enriched for canonical pairs of vsiRNAs (Fig 3.1). In addition, the preference for 1U was also visible for the 22-nt virus reads in the input library cloned without AGO co-IP (Fig 3.1). These results indicate that AGO co-IP indeed selectively enrich canonical vsiRNAs produced in the human somatic cells in response to the influenza viral infection.

The canonical vsiRNAs detected in human cells after PR8-delNS1 infection differ drastically from vsRNAs detected previously during wild-type IAV infection, which exhibit random size distribution and are almost exclusively negative strands and 5' co-terminal with the virion RNAs (*180, 218*). Consistently, vsiRNAs were detectable by Northern blot hybridization in 293T cells infected with PR8-delNS1, but not in the cells infected with wild-type PR8 (Fig 3.2). Next, I further analyzed small RNAs co-immunoprecipitated with AGOs from 293T cells infected with wild-type PR8. Similar amounts of cellular miRNAs were associated with AGOs in 293T cells infected with either wild-type PR8 or PR8-delNS1 (Table 3.1). However, AGO-bound virus reads were extremely low abundant in wild-type PR8-infected cells, showed no preference either in size or for 1U (Fig 3.1), and were approximately 50-fold less abundant compared to those found in PR8-delNS1 infected cells (Table 3.1). These findings suggest suppression of either the biogenesis or the AGO loading of vsiRNAs in human cells infected by the wild-type PR8 of IAV.

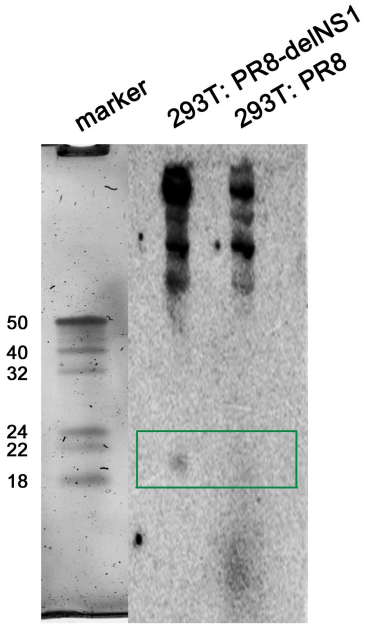

Figure 3.2 Visualization of IAV vsiRNAs by Northern blotting in human 293T cells. Northern detection of the positive-strand influenza vsiRNAs in human 293T cells 24 hours after infection with the mutant (delNS1) or wild-type (WT) viruses of PR8 strain. The lane of small RNA marker run from the same gel was stained separately. Figures were combined by the relative location of the gel to the membrane during the transfer step.

3.3.2 Infection with a distinct strain of IAV also induces vsiRNA biogenesis in human somatic cells

The subtype H1N1 (species) of influenza A viruses (genus) includes many strains with distinct pathogenesis properties. To independently verify the production of vsiRNAs during IAV infection, the total small RNAs were sequenced with and without AGO co-IP from human 293T cells 24 hours post infection with WSN-delNS1, a NS1-deletion mutant of the human IAV A/WSN/1/33 (H1N1). 90.9% of the total virus reads co-immunoprecipitated with AGOs were in the 21- to 23-nt size range of Dicer products, 72.1% of which contained 1U (Fig 3.1, Table 3.1). Similar to the vsiRNAs targeting

PR8-delNS1, 22-nt siRNAs of WSN-delNS1 were the most dominant species for both the positive and negative strands and were enriched for canonical vsiRNAs with 20-nt perfect base-paired duplexes and 2-nt 3' overhangs (Fig 3.1). In contrast to the canonical properties of AGO-bound WSN-delNS1 siRNAs, 57.9% of the total WSN-delNS1 small RNAs cloned without AGO co-IP were outside the 21- to 23-nt size range of the vsiRNAs associated with AGOs (Fig 3.1). However, the 22-nt RNAs were more abundant than other sizes of WSN-delNS1 small RNAs, and were specifically enriched for the canonical siRNA duplexes with 2-nt 3' overhangs (Fig 3.1). These findings demonstrate the production and selective AGO loading of vsiRNAs during infection of the human somatic cells by WSN-delNS1.

The AGO-bound small RNAs from 293T cells infected with the wild-type WSN strain were also sequenced. The analysis of this population of small RNAs revealed the presence of highly abundant cellular miRNAs as found for the population of small RNAs co-immunoprecipitated with AGOs from cells infected with WSN-delNS1, PR8 or PR8-delNS1 (Table 3.1). In contrast, extremely low abundant virus reads of random size distribution were associated with AGOs in WSN-infected cells (Fig 3.1), similar to the AGO-bound virus reads in PR8-infected cells. Together, these results demonstrate the production and selective AGO loading of vsiRNAs in the mature human somatic cells in response to the infection by distinct strains of IAV. Moreover, our findings indicate that VSR deletion combined with AGO co-IP will improve the identification of human vsiRNAs in the infected somatic cells (*179, 185*).

3.3.3 Influenza A virus-specific dsRNAs are precursors of the cloned human vsiRNAs

The AGO-bound 21- to 23-nt siRNAs of both PR8-delNS1 and WSN-delNS1 were next mapped to the eight genomic RNAs. For both strains, segments HA and NA were targeted only by low density of the vsiRNAs whereas the highest density of the vsiRNAs was found to target the NS segment (Fig 3.3). NS is the shortest among the eight segments and becomes 418 nt long after the introduced deletion for both PR8-delNS1 and WSN-delNS1. Approximately 65% and 56% of the total AGO-bound 21- to 23-nt vsiRNA reads from 293T cells infected respectively with PR8-delNS1 and WSN-delNS1 were mapped to NS (Figs 3.3 and 3.4). Nevertheless, the virus reads mapped to the remaining 7 genome segments of either strain also exhibited the canonical properties of vsiRNAs (Figs 3.4 and 3.5, Table 3.2) indistinguishable from those of the total virus reads.

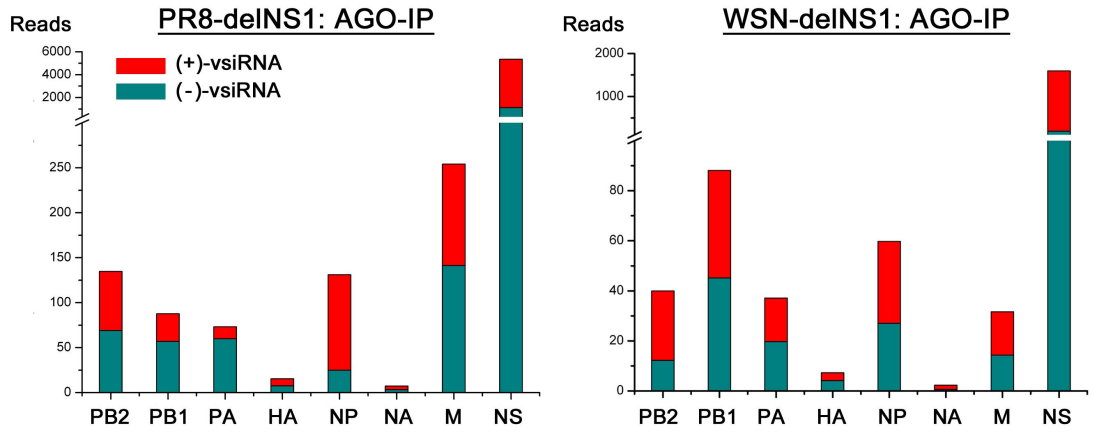

Figure 3.3 Distribution of IAV vsiRNAs among virion RNA segments in human 293T cells. 21- to 23-nt vsiRNAs from cells infected by PR8-delNS1 or WSN-delNS1 sequenced at 24 hours after the infection exhibited unequal distribution among virion RNA segments. NS segment derived vsiRNAs were the most abundant in both libraries, whereas HA and NA segments had the lowest vsiRNA production. The abundance of vsiRNAs mapped to an individual RNA segment was shown as reads per 1 kb of the RNA segment and per million of total reads.

Table 3.1 Contents and properties of the small RNA libraries sequenced (NS segment excluded)

Library	Total reads (18-28nt)	miRNAs[1] (mature)	Pre-miR hairpins[2] (of total reads)	Virus reads (18-28nt)	Virus reads of 21- to 23-nt				
					Reads (of miRNAs)	of all sizes	(+)-strand	1U	Terminal 100 nt
PR8-delNS1: Ago-IP (293T)	11,302,454	4,802,301	8,739,996 (77.3%)	15,909	13,422 (0.3%)	84.4%	47.0%	39.1%	80.0%
PR8-delNS1: Input (293T)	7,473,617	744,024	2,589,158 (34.6%)	40,896	20,340 (2.7%)	49.7%	33.5%	33.4%	61.9%
WSN-delNS1: Ago-IP (293T)	4,706,817	1,876,460	3,674,326 (78.1%)	2,995	2,470 (0.1%)	82.5%	53.7%	55.4%	75.4%
WSN-delNS1: Input (293T)	6,832,452	819,404	2,683,574 (39.3%)	29,250	11,745 (1.4%)	40.2%	57.3%	24.7%	34.5%
PR8-WT: Ago-IP (293T)	4,399,122	1,740,209	3,441,361 (78.2%)	857	292 (0.02%)	34.1%	61.3%	18.2%	39.4%
WSN-WT: Ago-IP (293T)	7,007,112	2,875,406	5,244,866 (74.9%)	850	302 (0.01%)	35.5%	73.2%	18.2%	30.8%
PR8-delNS1: Input (A549)	19,199,474	3,205,109	4,669,874 (24.3%)	150,208	60,939 (1.9%)	40.6%	55.7%	33.7%	42.8%

[1] Indicating the reads perfectly identical to mature microRNAs

[2] Indicating all the reads mapped to pre-microRNA hairpins, including mature microRNAs, microRNAs* and imprecise products

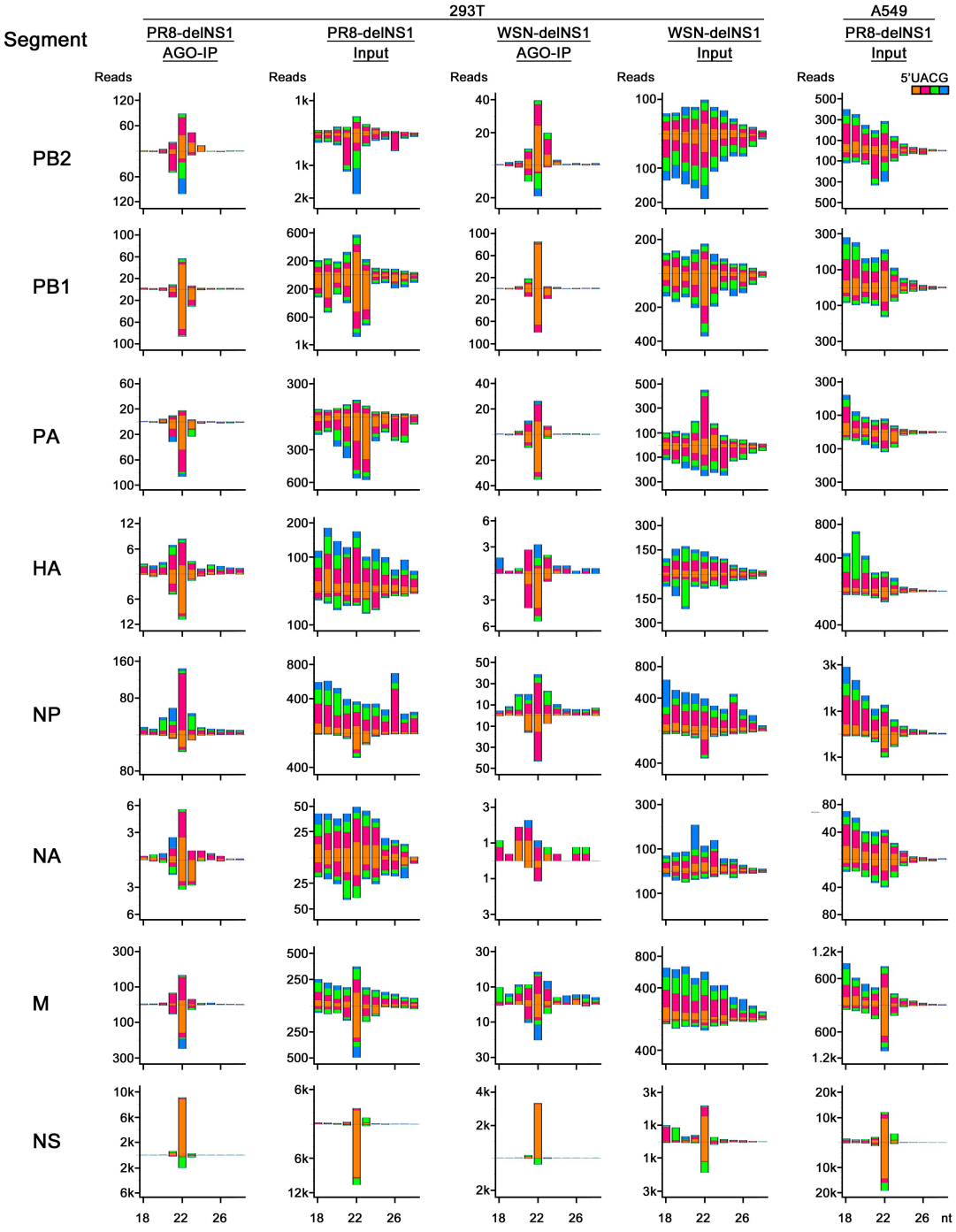

Figure 3.4 Properties of IAV vsiRNAs produced in human 293T and A549 cells. Total small RNAs were sequenced either with Argonaute co-immunoprecipitation (AGO-IP) or without (input) from human 293T or A549 cells 24 hours after infection with the indicated virus. Size distribution, abundance and 5'-terminal nucleotide (indicated by colors) of the sequenced vsRNAs mapped to each of the eight influenza virion RNA segments in five independent libraries were shown. The abundance of vsRNAs mapped to an individual RNA segment was shown as reads per 1 kb of the RNA segment and per million of total miRNAs.

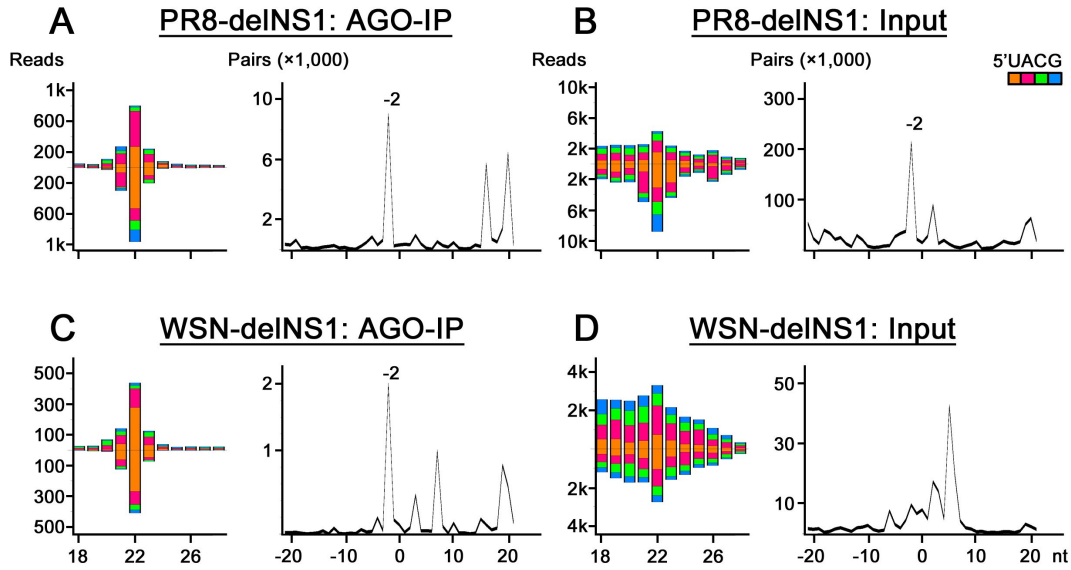

Figure 3.5 Properties of IAV vsiRNAs mapped to the RNA segments excluding NS segment in human 293T cells. The AGO-bound influenza vsiRNAs exhibit the canonical properties of vsiRNAs after removal of the NS segment-derived vsiRNAs. Size distribution, abundance (per million of total mature miRNAs), 5'-terminal nucleotide (indicated by colors), and the enrichment for pairs (-2 peak) of 22-nt vsiRNAs with 2-nt 3' overhangs of the sequenced vsiRNAs mapped to the virion RNA segments 1-7 from 293T cells 24 hours after infection with either PR8-delNS1 or WSN-delNS1 without (input) or with co-immunoprecipitation by anti-pan AGO antibodies (AGO-IP) were shown.

91.8% and 88.6% of PR8-delNS1 and WSN-delNS1 vsiRNAs, respectively, were derived from the terminal 100-nt regions of the eight virion RNA segments (Table 3.1, Figs 3.6 and 3.7). Except for segments HA and NA, high densities of the positive- and/or negative-strand vsiRNAs were mapped to one end or both ends of the genome segments (Figs 3.6 and 3.7). Notably, these terminal virus reads formed successive (or phased) complementary pairs of vsiRNAs processed from long dsRNA precursors (Figs 3.6, 3.7, and 3.8). In particular, the second pair of 22-nt vsiRNAs targeting the 3' terminus of the NS segment accumulated to extremely high levels in the human cells infected by either PR8-delNS1 or WSN-delNS1 (Figs 3.6 and 3.7). The total vsiRNAs of PR8-delNS1 and

WSN-delNS1 contained 68.0% and 72.9% positive strands, respectively (Table 3.1). After removal of the siRNAs mapped to segment NS that included a highly abundant 22-nt 1U siRNA (Figs 3.6 and 3.7), the remaining vsiRNAs exhibited approximately equal strand ratios, 47.0% and 53.7% for PR8-delNS1 and WSN-delNS1, respectively (Table 3.2). These results together indicate that IAV-specific long dsRNAs are precursors of the cloned human vsiRNAs.

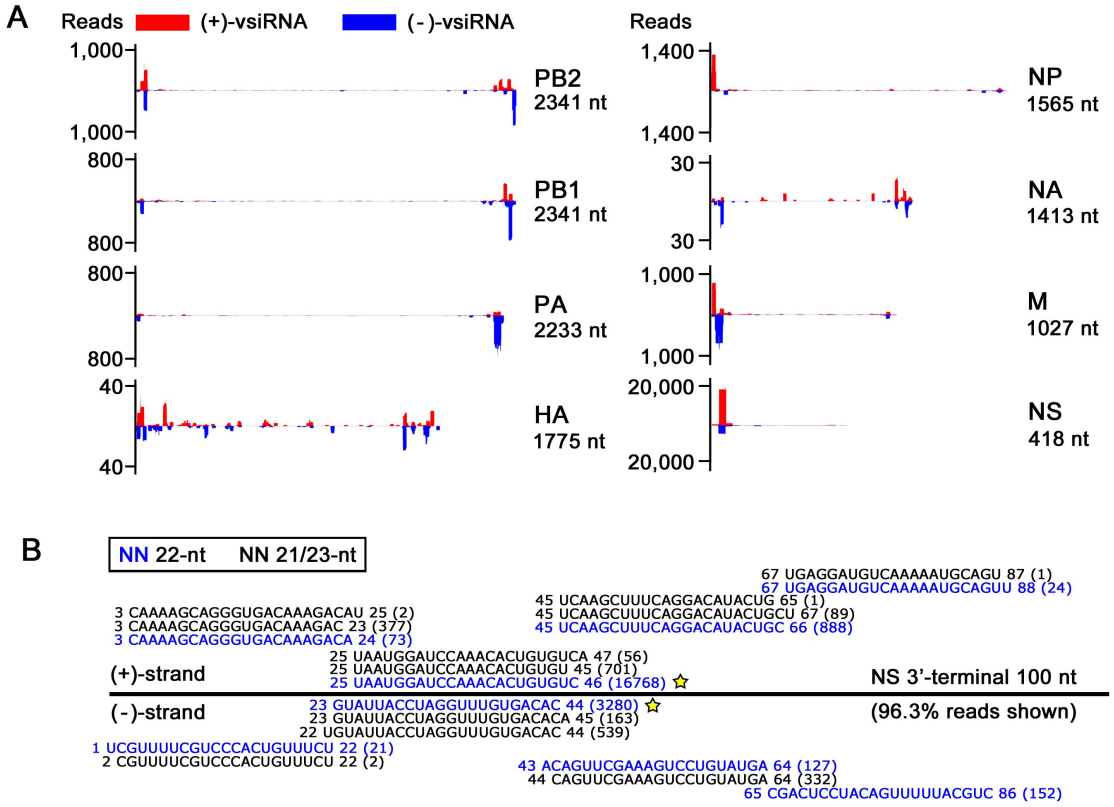

Figure 3.6 Terminal preference of PR8-delNS1 vsiRNAs along virion RNA segments in human 293T cells. (A) Relative abundance of vsiRNA hot spots mapped to the eight virion RNA segments of PR8-delNS1. The abundance of vsiRNAs was shown as total virus reads 21- to 23-nt in length co-IPed with AGOs from 293T cells 24 hours after infection. The length of each RNA segment listed from 3' end (left) to 5' end (right) is given. High density of vsiRNAs were found at the terminal regions of RNA segments except for the segments encoding the surface antigens haemagglutinin (HA) and neuraminidase (NA), both of which were targeted by extremely low density of vsiRNAs in 293T cells infected with PR8-delNS1. **(B)** Read sequences along the 3'-terminal 100 nt of PR8-delNS1 mutant genome segment NS revealed dominant sets of successive pairs of 21- to 23-nt vsiRNAs. Read counts (in brackets), read length, genomic position and % of the total reads mapped to the region are indicated. The predominant small RNA pair is marked by stars, and the small RNA complementary to the positive-strand vsiRNA species was used as the probe to detect the influenza vsiRNAs in Northern-blotting.

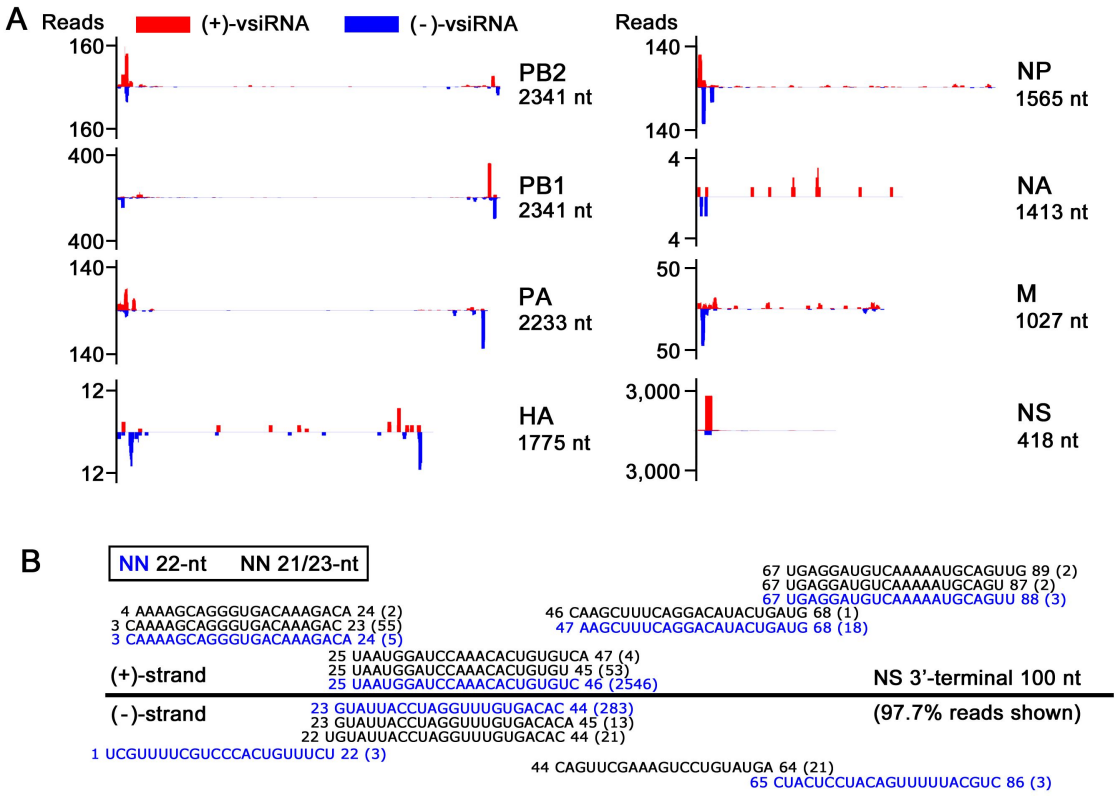

Figure 3.7 Terminal preference of WSN-delNS1 vsiRNAs along virion RNA segments in human 293T cells. (A) Relative abundance of vsiRNA hot spots mapped to the eight virion RNA segments of WSN-delNS1. The abundance of vsiRNAs was shown as total virus reads 21- to 23-nt in length co-IPed with AGOs from 293T cells 24 hours after infection. The length of each RNA segment listed from 3' end (left) to 5' end (right) is given. High density of vsiRNAs were found at the terminal regions of RNA segments except for the segments encoding the surface antigens haemagglutinin (HA) and neuraminidase (NA), both of which were targeted by extremely low density of vsiRNAs in 293T cells infected with WSN-delNS1. **(B)** Read sequences along the 3'-terminal 100 nt of WSN-delNS1 mutant genome segment NS revealed dominant sets of successive pairs of 21- to 23-nt vsiRNAs. Read counts (in brackets), read length, genomic position and % of the total reads mapped to the region are indicated.

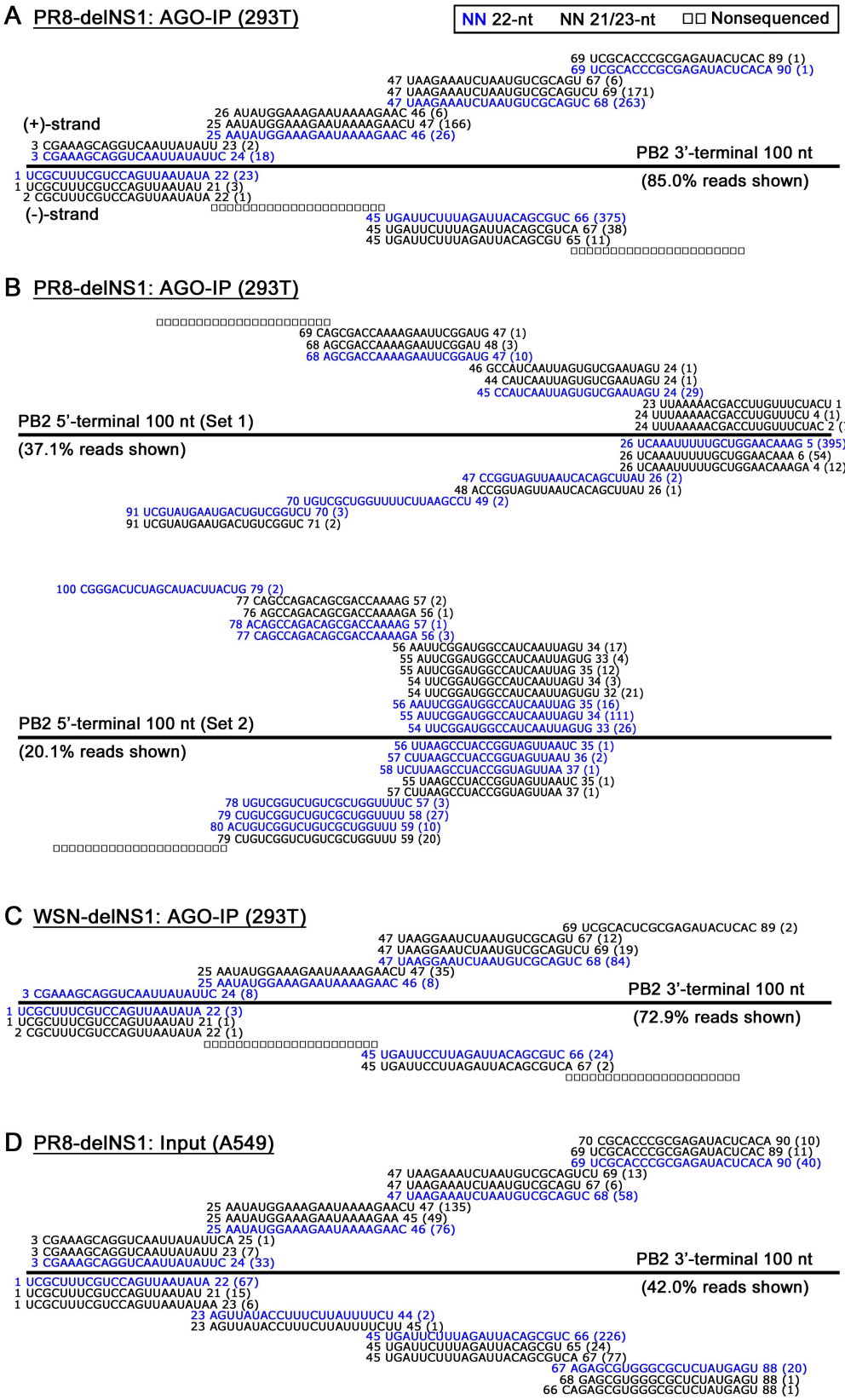

Figure 3-8 IAV phased vsiRNAs at the termini of segment PB2 in human cells. Read sequences along the 3'- or 5'-terminal 100 nt of IAV delNS1 mutant genome segments PB2 revealed dominant sets of successive pairs of 21- to 23-nt vsiRNAs. Read counts (in brackets), read length, nonsequenced reads, genomic position and % of the total reads mapped to the region are indicated.

3.3.4 Influenza vsiRNAs are loaded non-discriminatively into human AGO1 and AGO2 during infection

To verify the loading of the influenza vsiRNAs into specific AGOs, human 293T cells ectopically expressing FLAG-tagged human AGO1 or AGO2 were infected with PR8-delNS1 or WSN-delNS1. I found highly abundant small RNAs mapped to PR8-delNS1 or WSN-delNS1 in both AGO1 and AGO2 co-immunoprecipitated by the FLAG-specific antibody from the cells 24 hours after infection (Fig 3.9). The viral 21- to 23-nt RNAs, particularly those of negative polarity, were more abundant than vsRNAs of other sizes (Fig 3.9). Notably, the viral 22-nt RNAs bound by either AGO1 or AGO2 in cells infected with either PR8-delNS1 or WSN-delNS1 were enriched for the canonical siRNA duplexes with 2-nt 3' overhangs (Fig 3.9). These results indicate loading of the canonical siRNAs in both AGO1 and AGO2 during influenza viral infection of the human cells. I detected strong similarity between the populations of the viral siRNAs bound to AGO1 and AGO2 in cells infected with either PR8-delNS1 or WSN-delNS1 (Fig 3.10). This finding indicates lack of selective loading of influenza vsiRNAs into human AGO1 or AGO2, which is consistent with the loading of miRNAs among the four mammalian AGOs (*105*).

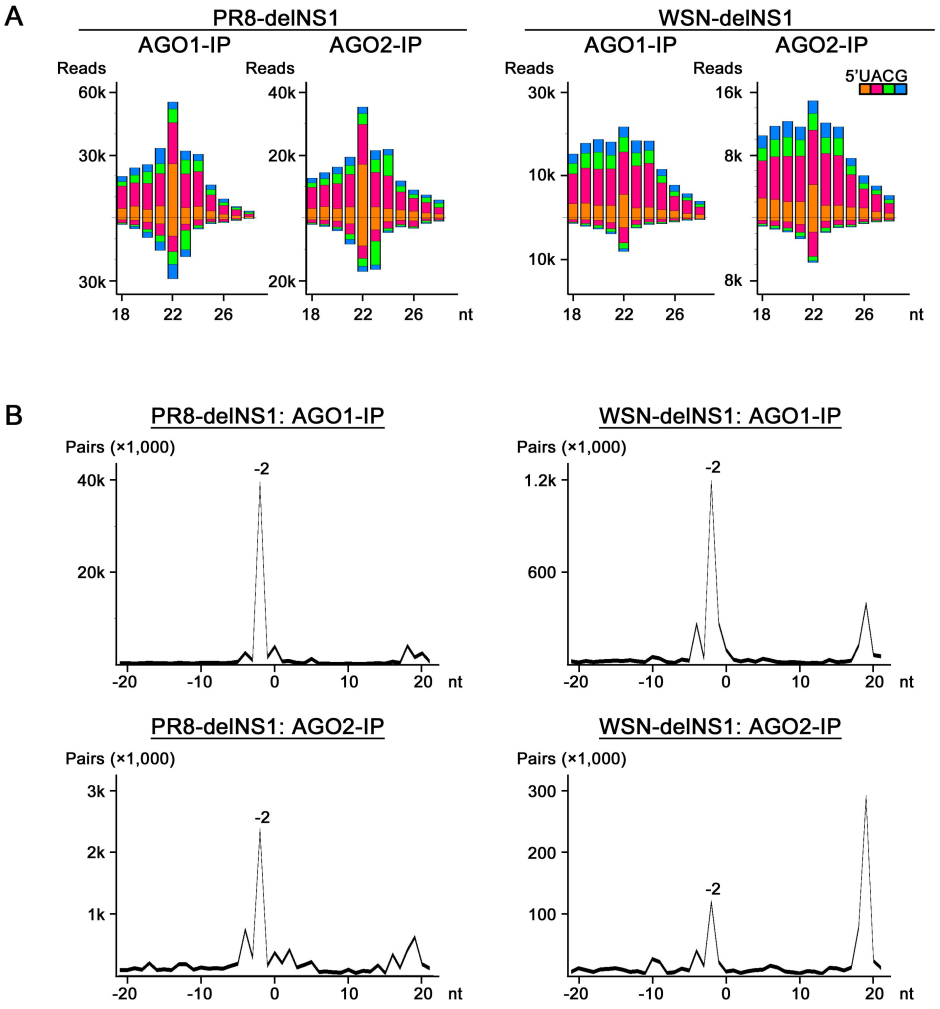

Figure 3.9 Properties of IAV vsiRNAs loaded into human AGO1 and AGO2 in human 293T cells. Human 293T cells ectopically expressing FLAG-tagged human AGO1 or AGO2 were infected with PR8-delNS1 or WSN-delNS1 and total RNAs were sequenced after co-IP by the FLAG-specific antibody from the cells 24 hours after infection. Size distribution, abundance (reads per million of total miRNAs) and 5'-terminal nucleotide (indicated by colors) of the AGO1- and AGO2-bound vsiRNAs were shown (**A**). The 22-nt vsiRNAs in both AGO1 and Ago2 exhibit strong enrichment (-2 peak) for pairs of canonical vsiRNAs with 2-nt 3' overhangs (**B**).

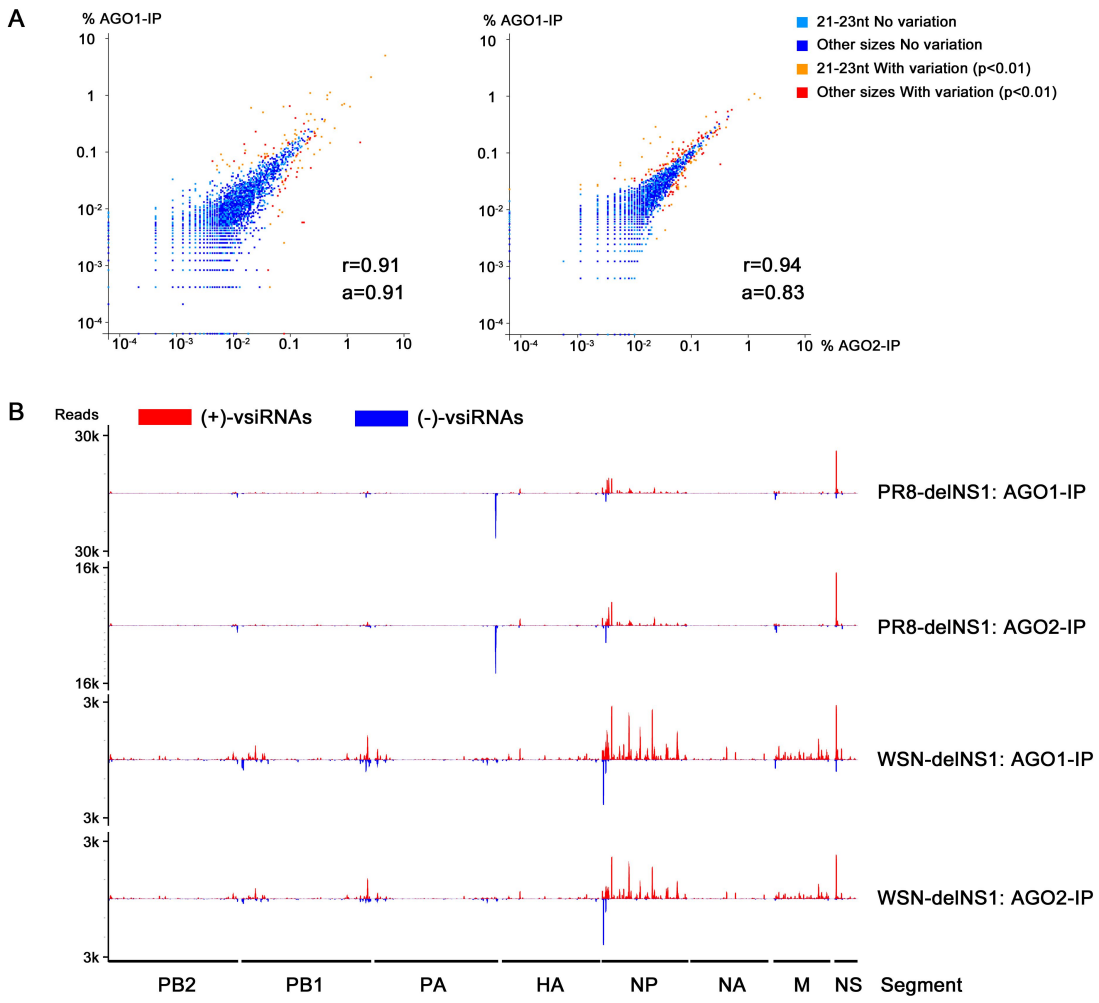

Figure 3.10 IAV vsiRNAs non-discriminatively loaded into human AGO1 and AGO2 in human 293T cells. Human 293T cells ectopically expressing FLAG-tagged human AGO1 or AGO2 were infected with PR8-delNS1 or WSN-delNS1 and total RNAs were sequenced after co-IP by the FLAG-specific antibody from the cells 24 hours after infection. **(A)** Correlation analysis by scatter plots of PR8-delNS1 or WSN-delNS1 vsRNAs either within or outside (indicated by colors) the 21- to 23-nt size range bound to AGO1 (y-axis) and AGO2 (x-axis). Each dot indicates the % of a given vsRNA to the total vsRNAs in either library. The correlation coefficient (r) and the regression coefficient through the origin (a) calculated for both viruses were close to 1, indicating strong similarity between the vsiRNA populations bound to AGO1 and AGO2. **(B)** The genome distribution showed similar patterns of vsiRNAs (21- to 23-nt reads per million of total miRNAs) loaded in human AGO1 and AGO2 along the eight virion RNA segments of PR8-delNS1 or WSN-delNS1.

3.3.5 Characterization of PR8-delNS1 derived vsiRNAs in human A549 cells

I next analyzed the small RNA populations sequenced from human lung epithelial A549 cells 24 hours post infection with PR8-delNS1 or wild-type PR8 (Fig 3.11, Table 3.1). Although the library was sequenced without AGO co-IP, PR8-delNS1 derived vsRNAs in A549 cells exhibited properties of vsiRNAs (Fig 3.11, Table 3.1) compared to those from 293T cells cloned before AGO co-IP (Fig 3.1, Table 3.1). Similarly, 49.3% of the total PR8-delNS1 vsiRNAs in A549 cells were derived from the terminal 100-nt regions of the eight virion RNA segments (Table 3.1). I found that more terminal vsiRNA species in A549 cells were involved in the formation of successive complementary vsiRNA pairs compared to those bound to AGOs in 293T cells infected by PR8-delNS1 or WSN-delNS1, but their relative abundance to the total vsiRNAs in the region was lower (Figs 3.8 and 3.11).

Several canonical siRNA properties were undetectable for vsRNAs from A549 cells infected with wild-type PR8 (Fig 3.11). However, the 22-nt vsRNAs of PR8 were enriched for the canonical siRNA duplexes, suggesting incomplete suppression of the vsiRNAs biogenesis in A549 cells during PR8 infection (Fig 3.11). Together, these findings illustrate that production of abundant vsiRNAs is a conserved immune response to IAV infection in distinct human somatic cells.

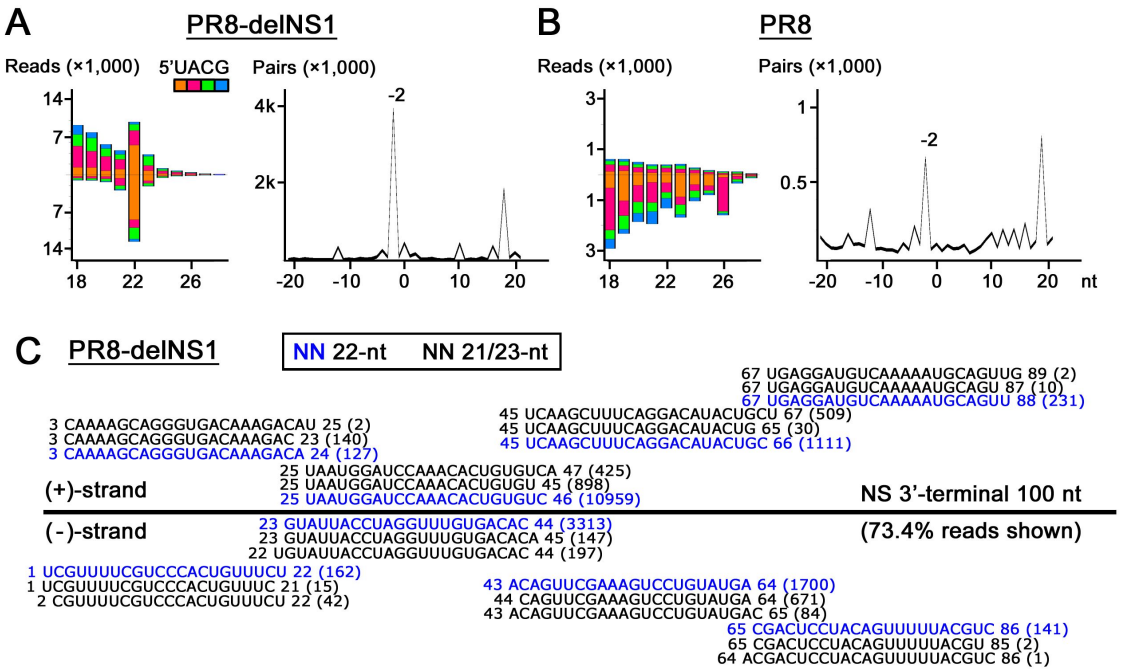

Figure 3.11 Production of PR8-delNS1 vsiRNAs in human A549 cells. Size distribution and abundance (shown as reads per million of total mature miRNAs) of total vsRNAs sequenced from human A549 cells 24 hours after infection with **(A)** PR8-delNS1 or **(B)** wild-type PR8. The 5' terminal nucleotide of vsRNAs is indicated by color. Strong enrichment of PR8-delNS1 derived 22-nt vsiRNAs for pairs (-2 peak) of canonical vsiRNAs with 2-nt 3' overhangs was visualized by computing total pairs of 22-nt vsRNAs with different length of base-pairing. **(C)** Read sequences along the 3'-terminal 100 nt of PR8-delNS1 mutant genome segment NS revealed dominant sets of successive pairs of 21- to 23-nt vsiRNAs. Read counts (in brackets), read length, genomic position and % of the total reads mapped to the region are indicated.

3.3.6 Dicer-dependent biogenesis of influenza vsiRNAs in human somatic cells

To determine if human Dicer was essential for the biogenesis of vsiRNAs, 293T cells knocked out of human Dicer (dcrKO) were challenged by PR8-delNS1. As reported previously (*199*), the abundance of miRNAs and miRNAs* in dcrKO cells dramatically reduced compared to the parental cell line, and was partially rescued by ectopically expressed human Dicer (hDicer) from a co-transfected plasmid encoding an hDicer

cDNA (Fig 3.12). *Drosophila* Dicer-2 (dDicer-2) shared the same domain architecture with hDicer, and was known to process viral dsRNA into predominantly 21-nt vsiRNAs in fruit fly somatic tissues (*128, 220*). Ectopically expressed *Drosophila* Dicer-2 did not restore the abundance of miRNAs and miRNAs* either with or without co-expression of its dsRNA-binding (RBD) partners Loqs-PD and R2D2, consistent with its specific function in siRNA processing but not in miRNA biogenesis (Fig 3.12). These results indicate successful depletion and ectopic expression of Dicer in 293T dcrKO cells.

I found that the influenza vsiRNAs became undetectable in 293T dcrKO cells, since the PR8-delNS1 vsRNAs exhibited random size distribution without enrichment for 1U population (Fig 3.12). However, vsiRNA production in 293T dcrKO cells was rescued by ectopic expression of hDicer (Fig 3.12). By comparison, PR8-delNS1 vsiRNAs produced by the ectopically expressed hDicer were more abundant, and contained a larger proportion of vsiRNAs from internal regions of virion RNAs compared to those from wild-type 293T cells infected by PR8-delNS1 (Fig 3.12). These results together reveal a new somatic function of hDicer in the production of vsiRNAs in addition to its role in the cellular miRNA biogenesis (*220, 221*).

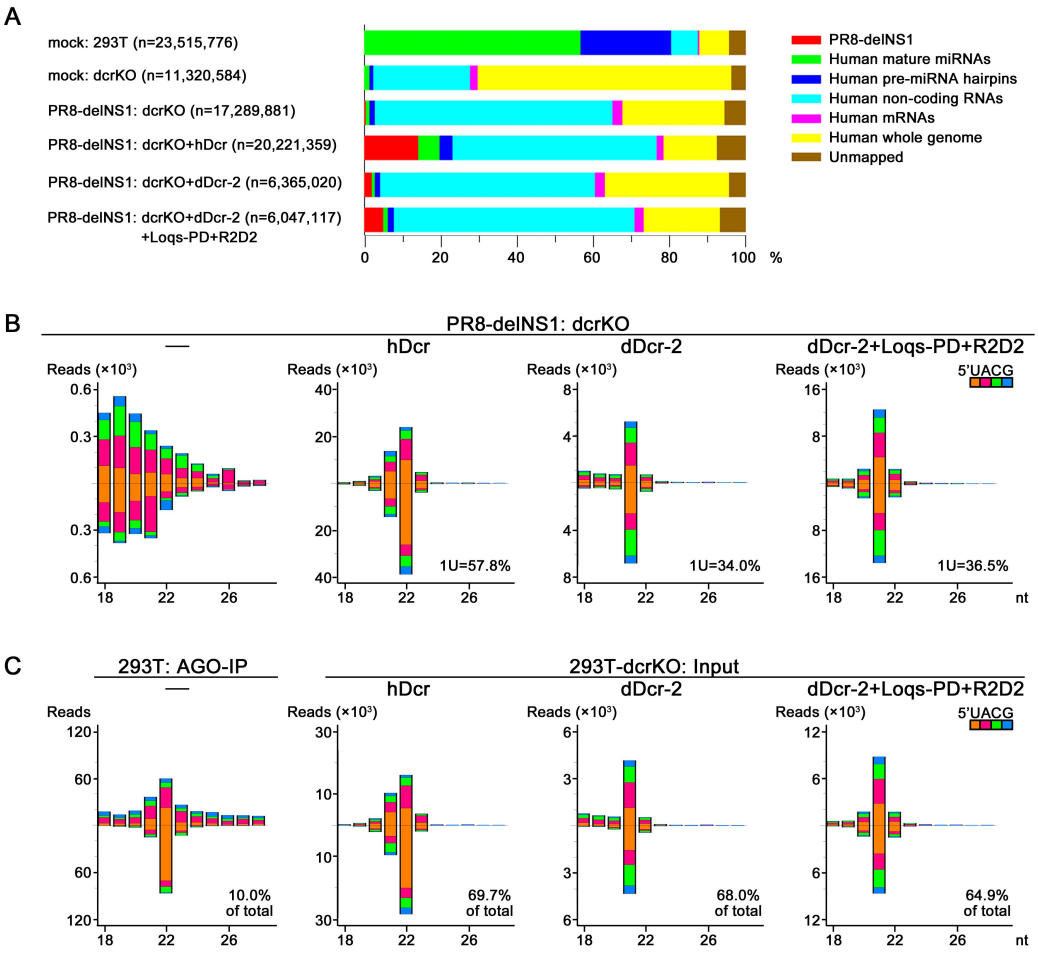

Figure 3.12 Properties of small RNA libraries sequenced from human Dicer knockout 293T cells. (A) Origins and total read numbers of small RNAs in each library sequenced from 293T cells and Dicer-knockout (hDicer-KO) cell lines either before or after infection with PR8-delNS1 after 24 hours. 18- to 28-nt small RNA reads were mapped to each category (indicated by colors) allowing 1-nt mismatch, and the proportions were presented by lengths of the bars. **(B)** Size distribution, abundance (shown as reads per million of total reads) and 5-terminal nucleotide (indicated by colors) of total sequenced vsRNAs from hDicer-KO 293T cells and the cell lines ectopically expressing hDicer, dDicer2 or dDicer2+Loqs-PD+R2D2 after infection with PR8-delNS1 after 24 hours. The % of 22-nt 1U in the cells expressing human Dicer and those of 21-nt 1U in the cells expressing *Drosophila* Dicer-2 were shown. **(C)** Properties of vsRNAs mapped to internal regions of virion RNA segments (excluding 100-nt from both 5' and 3' terminals) from wild-type 293T cells by AGO co-IP and hDicer-KO 293T cell lines ectopically expressing hDicer, dDicer2 or dDicer2+Loqs-PD+R2D2 after infection with PR8-delNS1 after 24 hours. The %s of internal reads to total vsRNAs were shown.

Ectopically expressed dDicer-2 also rescued the production of PR8-delNS1 vsiRNAs in 293T dcrKO cells (Fig 3.12). Notably, a dominant size shift of the influenza vsiRNAs

to 21-nt was detected in cells ectopically expressing dDicer-2 compared to the 22-nt vsiRNAs in cells expressing hDicer (Fig 3.12). However, the distribution pattern of hot spot vsiRNAs over the viral genomic RNAs was highly similar for the 21- and 22-nt vsiRNAs made by dDicer-2 and hDicer, respectively (Figs 3.13, 3.14, and 3.15). I found that 98.7% of the total 21-nt vsiRNAs (90.7% in species) produced by dDicer-2 and 98.3% of the total 22-nt vsiRNAs (74.2% in species) produced by hDicer shared the same mapping positions in the genomic RNAs of PR8-delNS1 (Figs 3.13 and 3.14). This result suggests that a similar set of dsRNA precursors were recognized and processed by the two Dicer nucleases.

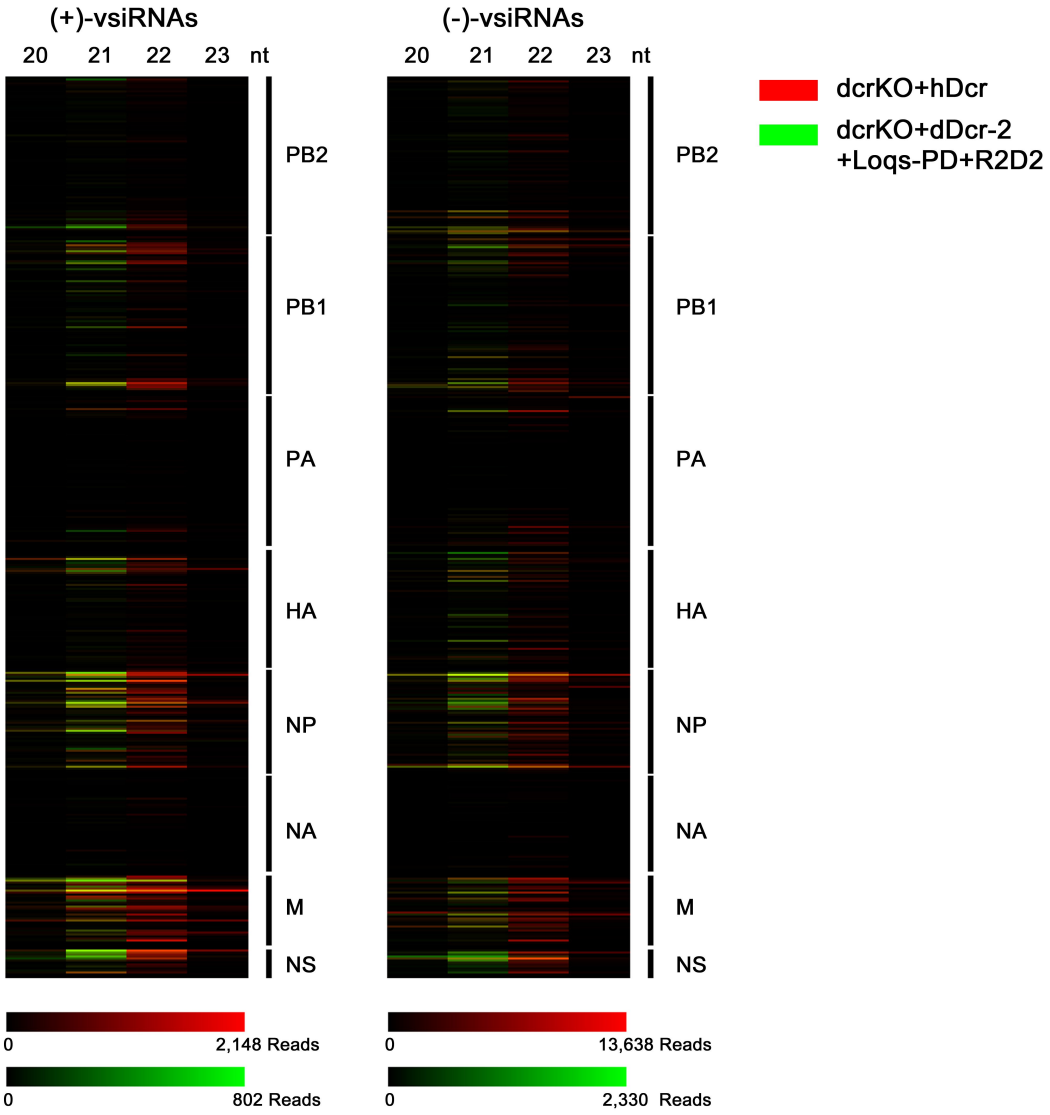

Figure 3.13 Heatmap of vsiRNAs produced by ectopically expressed Dicers in human Dicer knockout 293T cells. 20- to 23-nt PR8-delNS1 derived vsiRNAs sequenced from hDicer-KO 293T cell lines ectopically expressing hDicer (red) or dDicer2+Loqs-PD+R2D2 (green) were mapped to viral genome by their 5' ends. Each cell indicates a locus of 30 nucleotides along the viral genome segments shown in the direction of vRNA from the 3' end (top) to the 5' end (bottom). The overall number of the reads (per million of total reads) mapped to each locus were counted, and the reads abundance is presented by the brightness of the cell. The max reads number mapped to a single locus in either polarity of each library is shown.

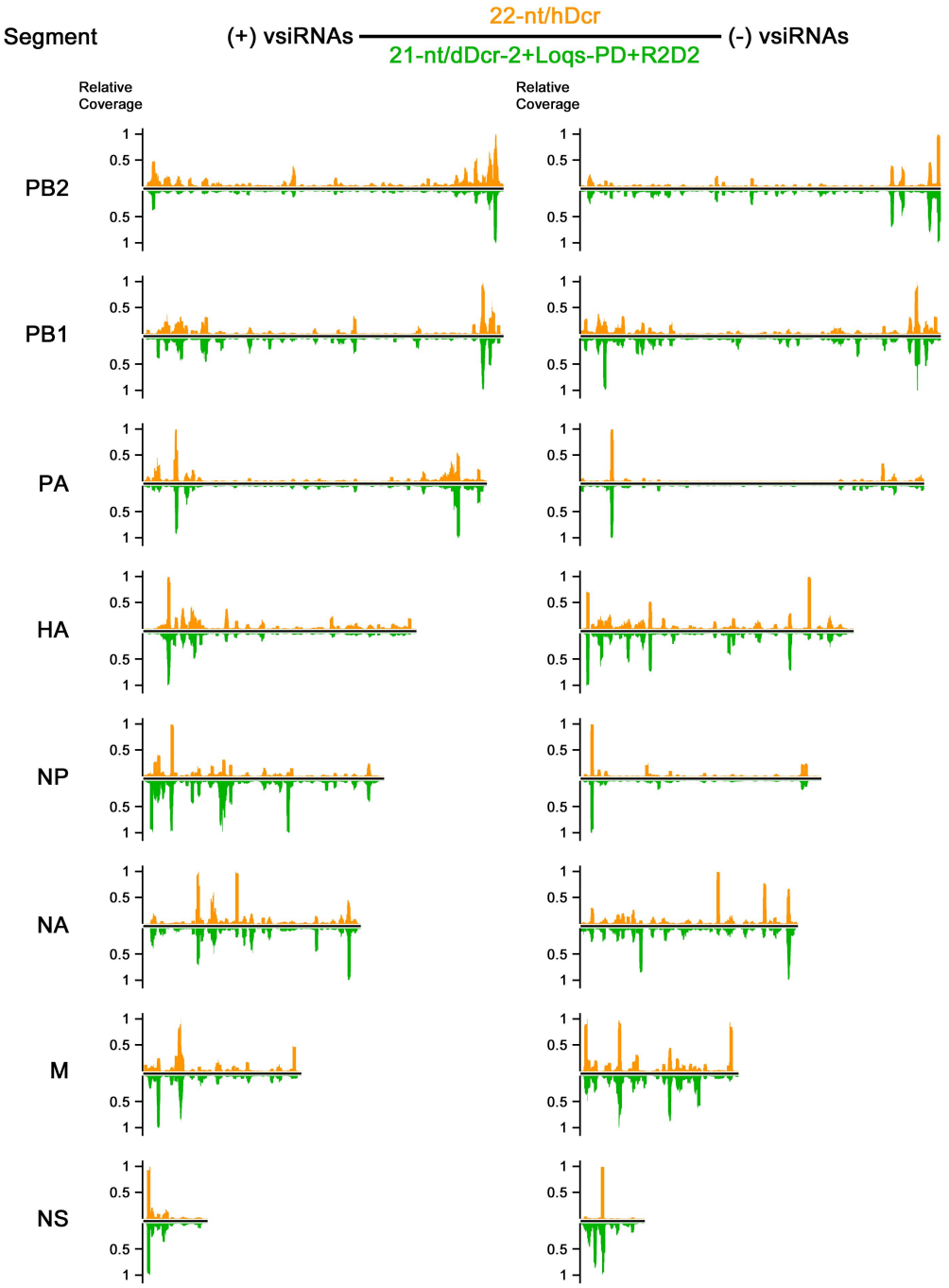

Figure 3.14 Genome distribution of PR8-delNS1 derived vsiRNAs produced by ectopically expressed Dicers in human Dicer knockout 293T cells. Distribution of positive and negative strand 22-nt (top) and 21-nt (bottom) vsiRNA reads along eight PR8-delNS1 genome segments from hDicer-KO 293T cells ectopically expressing hDicer and dDicer2+Loqs-PD+R2D2, respectively. The relative coverage to each nucleotide position by vsiRNAs was shown as a value normalized by the maximum coverage of each virion RNA segment in either polarity.

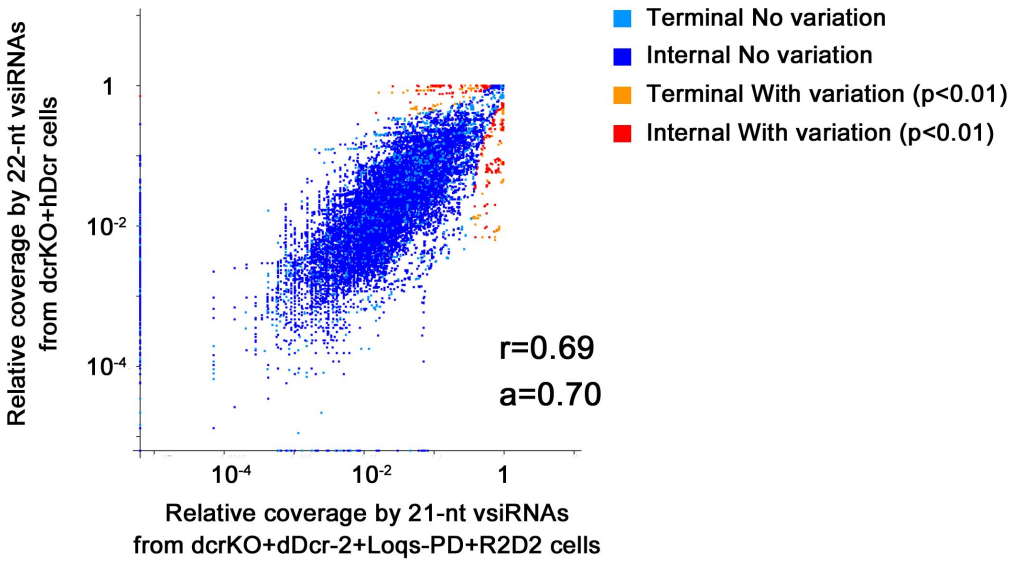

Figure 3.15 Correlation analysis of PR8-delNS1 derived vsiRNAs produced by ectopically expressed Dicers in human Dicer knockout 293T cells. Correlation analysis by scatter plot of 22-nt (y-axis) and 21-nt (x-axis) vsiRNA reads along eight PR8-delNS1 genome segments from hDicer-KO 293T cells ectopically expressing hDicer and dDicer2+Loqs-PD+R2D2, respectively. Each spot indicates the relative coverage normalized by the maximum coverage of each virion RNA segment in either polarity by vsiRNAs at the corresponding nucleotide position. The correlation coefficient and the regression coefficient through the origin are shown, and the relatively strong correlation indicates a similar distribution of vsiRNAs made by hDicer and dDicer2. Note that the correlation coefficient and the regression coefficient may have been attenuated due to the size difference between vsiRNAs made by hDicer and dDicer2. Whether the positions of the nucleotides are at the terminal (100-nt from either ends) or internal regions of the viral genomic RNAs and whether the variation is significant are indicated by colors.

3.3.7 Characterization of vsiRNAs in human 293T cells infected by IAV strains defective in dsRNA-binding ability of NS1

I next analyzed the vsRNA populations from different 293T cells 24 hours post infection with IAV-3841 or PR8-3841, two IAV mutant strains containing amino acid substitutions R38A and K41A known to result in defectiveness in dsRNA binding without affecting

protein dimerization (*201, 217*). IAV-3841 vsRNAs derived from 293T dcrKO cells ectopically expressing hDicer exhibited predominant peaks at 22-nt for both positive and negative strands, and were enriched for canonical siRNA duplexes with 2-nt 3' overhangs (Fig 3.16). However, IAV-3841 vsiRNAs were not enriched for 1U, represented 0.1% of the total reads in the library, and were less abundant compared to those in the same cells infected by PR8-delNS1 (Fig 3.16). Notably, mapping the IAV-3841 vsiRNAs to the eight genome segments yielded a distribution pattern of the vsiRNA hot spots different from that from PR8-delNS1 vsiRNAs (Fig 3.16). Moreover, abundant IAV-3841 vsiRNAs were mapped to segments NP, NA, M and NS, unlike PR8-delNS1 vsiRNAs (Fig 3.16).

The vsRNAs from wild-type 293T cells infected by PR8-3841 exhibited random size distribution and no 1U preference, but were enriched for canonical siRNA duplexes (Fig 3.16), suggesting that these vsRNAs included a subpopulation of canonical vsiRNAs. The genomic distribution of 21- to 23-nt PR8-3841 vsRNAs revealed abundant vsRNAs at the 5' terminal region of PB2 vRNA (Fig 3.16), which might correspond to the leader small RNAs reported by others (*180*). Indeed, removal of the vsRNAs mapped to the first 20 nts at the 5' terminal region of PB2 vRNA revealed a weak 22-nt peak for both positive and negative strands (Fig 3.17).

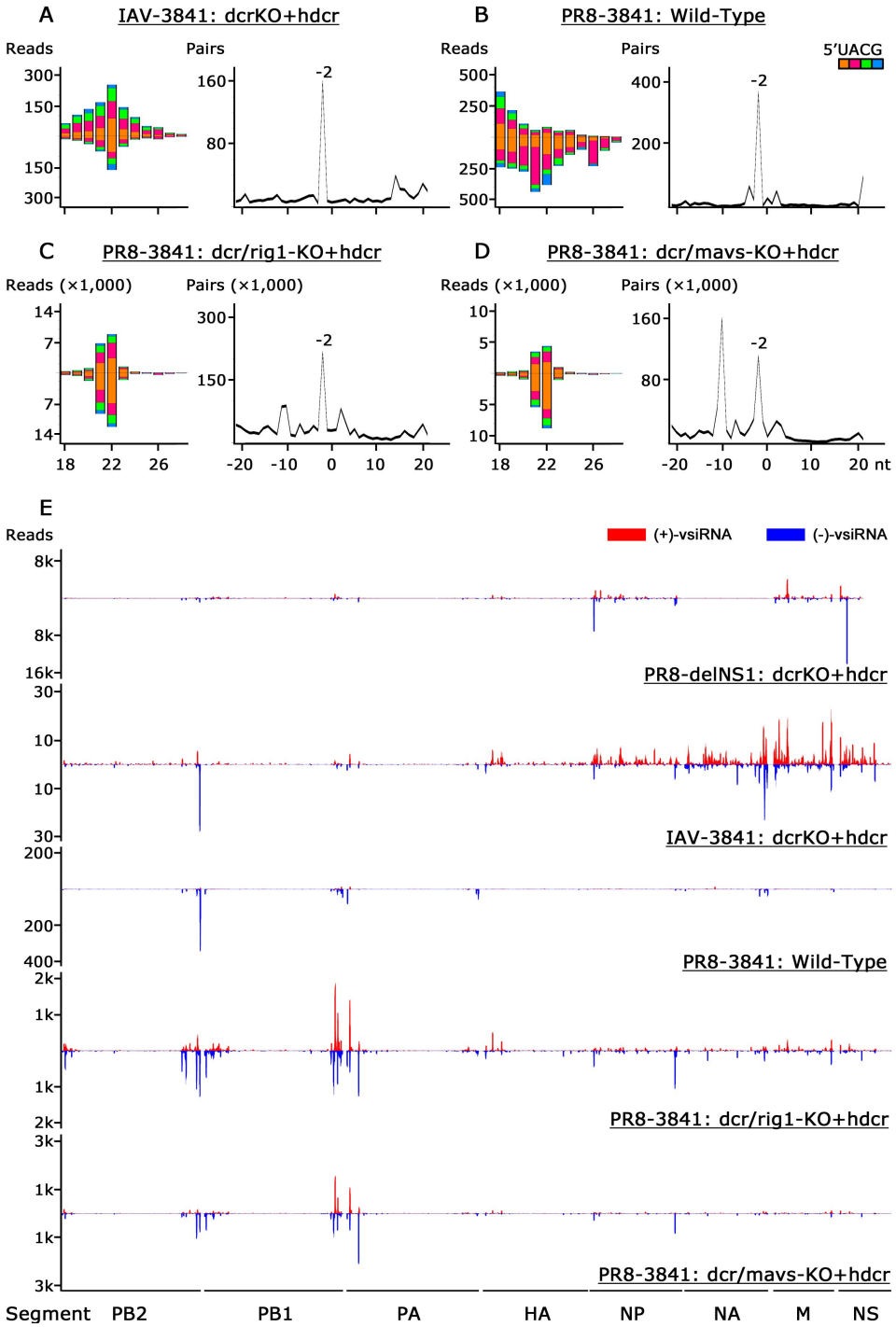

Figure 3-16 Properties of vsRNAs derived by NS1 deficient mutant IAV strain in 293T cells. **(A-D)** Size distribution, abundance, and total counts of pairs of complementary 22-nt reads in each distance category shown in nucleotides (shown as reads per million of total reads in each library) of IAV-3841 or PR8-3841 derived small RNAs sequenced from 293T cells infected by the virus at 1 dpi. The 5' terminal nucleotides of viral small RNAs are indicated by colors. The virus strain and genotype of the 293T cells for each library are indicated. **(E)** The coverage of each nucleotide position to the whole virus genome by 21- to 23-nt vsRNAs derived by IAV-3841 or PR8-3841 from 293T cells (shown as reads per million of total reads in each library). The strand sources of vsRNAs are indicated by colors, and the segment sources of vsRNAs are shown at bottom. As a comparison, the coverage distribution by vsiRNAs derived from dcrKO 293T cells ectopically expressing human Dicer infected by PR8-delNS1 at 1 dpi is shown.

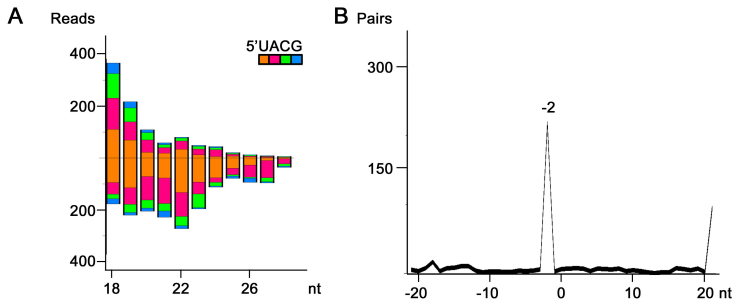

Figure 3.17 Properties of vsRNAs derived by PR8-3841 strain in 293T cells after removal of potential leader small RNAs. (A) Size distribution and abundance (shown as reads per million of total reads in the library) of PR8-3841 derived small RNAs sequenced from wild-type 293T cells infected by the virus at 1 dpi, excluding those generated from the first 20-nt at 5' terminal of PB2 vRNA to reduce the effect by leader small RNAs. The 5' terminal nucleotides of viral small RNAs are indicated by colors. **(B)** Total counts of pairs of complementary 22-nt viral small RNAs (per million of total sequenced reads) in each distance category (in nucleotides) show the enrichment for pairs of canonical vsiRNAs with 2-nt 3' overhangs (-2 peak).

Strikingly, PR8-3841 vsRNAs processed by ectopically expressed hDicer in 293T cells knocked out of both human Dicer and RIG-I (dcr/rig1-KO) or MAVS (dcr/mavs-KO) exhibited all of the known properties of the canonical siRNAs (Fig 3.16). PR8-3841 vsiRNAs in these two types of 293T cells were also abundant, representing 4.1% and 2.4% of the total small RNAs in dcr/rig1-KO and dcr/mavs-KO cells, respectively, and thus were comparable to PR8-delNS1 vsiRNAs processed by ectopically expressed human Dicer (Figs 3.12 and 3.16). Notably, the genome distribution pattern of PR8-3841 vsiRNAs in these cells differed from that of either PR8-delNS1 or IAV-3841 vsRNAs, since the termini of segments PB2, PB1 and PA were targeted by high densities of the positive and negative strand PR8-3841 vsiRNAs (Fig 3.16). Therefore, these results together demonstrate production of influenza vsiRNAs in human cells infected by IAV mutants carrying only point substitutions in segment NS to abolish the dsRNA-binding

activity, but the expression of NS1. This finding indicates a role of the dsRNA-binding activity of NS1 in the suppression of the vsiRNA biogenesis and suggests that the large deletion in segment NS is not essential for the induction of the vsiRNA biogenesis in human cells infected by IAV NS1-deletion strains.

3.3.8 Characterization of influenza vsRNAs bound to NS1 in 293T cells infected by wild-type influenza viruses

To investigate whether NS1 also sequesters vsiRNAs as NoV B2 as described in Chapter 2, I next analyzed the small RNA populations co-immunoprecipitated with the antibody specific to influenza NS1 protein from 293T cells 24 hours after infection by wild-type PR8 or WSN. PR8 and WSN vsRNAs found in NS1 exhibited random size distribution, and contained extremely low number of complementary duplexes, suggesting that no vsiRNAs were bound to NS1 during wild-type IAV infection unlike NoV (Fig 3.18). Although the size distribution patterns were different between the two virus strains, they were respectively consistent with those of the input vsRNAs (Fig 3.18). This result suggests different mechanisms of influenza NS1 and NoV B2 in the repression of the vsiRNA biogenesis during virus infection.

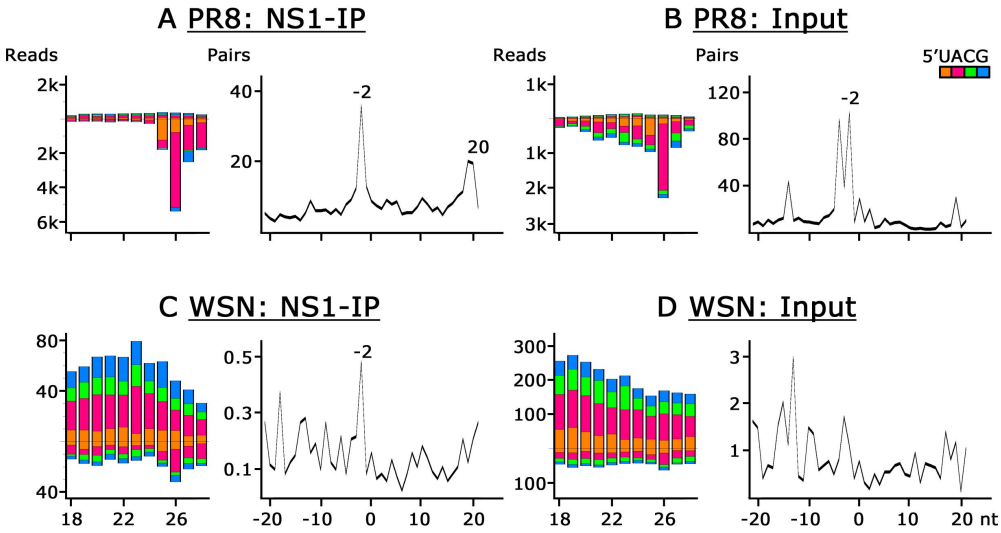

Figure 3.18 Properties of wild-type IAV strains derived vsRNAs bound to NS1 protein in human 293T cells. The NS1-bound vsRNAs derived from 293T cells infected by wild-type PR8 or WSN exhibit no properties of vsiRNAs and high similarity to input vsRNA populations. Size distribution, abundance (per million of total sequenced reads in the library), 5'-terminal nucleotide (indicated by colors), and the limited enrichment for pairs (-2 peak) of 22-nt vsRNAs with 2-nt 3' overhangs of the sequenced vsRNAs from 293T cells 24 hours after infection with wild-type IAV strains either without (input) or with co-immunoprecipitation by antibody specific to NS1 protein were shown.

3.4 Discussion and conclusions

Results of this chapter demonstrate innate immune detection of RNA virus infection by the RNAi pathway for the first time in mature human somatic cells. Similar to plants, invertebrates and mice (*128, 185*), the human vsiRNAs are produced from viral dsRNA precursors by Dicer and loaded abundantly into AGOs when the cognate VSR is inactive. These findings illustrate that the antiviral RNAi response is conserved in humans.

This work also reveals that either VSR depletion or AGO co-IP alone may not be

sufficient to remove the non-specific degradation products and to enrich the vsiRNA population for deep sequencing. Therefore, combining both VSR depletion and AGO co-IP will facilitate both the identification of canonical mammalian vsiRNAs and the characterization of human antiviral RNAi response.

Chapter 4: Conclusions

The results in this dissertation described the first *in vitro* and *in vivo* characterization of virus-derived siRNAs (vsiRNAs) in mammals. Upon infection with the VSR-defective mutant strains of NoV and IAV, cultured BHK-21 cells, human cells and suckling mice produced abundant vsiRNAs with the canonical siRNA properties, which include the preference for both 22-nt and 1U, approximately equal strand ratio, and the enrichment of canonical 22-nt siRNA duplexes with 2-nt 3' overhangs and 5' monophosphate. In contrast, previous studies by others examined mammalian cell infection by wild-type viruses and detected only virus-derived small RNAs (vsRNAs), which are non-specific degradation products from the abundant virus genomic RNAs (*179, 180*). The canonical siRNA properties of the vsiRNAs that I have found from mammalian cells infected with VSR-deficient NoV and IAV mutants suggest that they are the specific products processed by mammalian Dicer from viral dsRNA precursors. Consistently, the genetic study in human 293T cells illustrated the requirement of Dicer in the biogenesis of vsiRNAs targeting the Influenza A virus mutant defective in the expression of the viral NS1 protein. Therefore, these results demonstrate that the antiviral RNAi response previously described in fungi, plants, insects and nematodes (*128*) is also conserved in mammals.

The analysis of the small RNA population co-immunoprecipitated by anti-pan-AGO antibody illustrated both *in vitro* and *in vivo* loading of vsiRNAs in AGOs, similar to

mammalian miRNAs. Further analysis reveals that the VSR protein NS1 of Influenza A virus inhibits the biogenesis of viral siRNAs whereas the VSR protein B2 of Nodamura virus suppresses both the biogenesis and the Argonaute loading of viral siRNAs during infection. The mutational analysis indicated that the suppression of RNAi by the influenza and Nodaviral VSRs (*185*) depends on their dsRNA binding activity. The similarities in the induction and suppression of antiviral RNAi by virus infection in mammals and other eukaryotic hosts (*131, 134, 145, 162-163, 194, 210-211*) suggest an evolutionary conserved role of RNAi in antiviral defense in mammals. Indeed, studies by my colleagues in Ding lab demonstrated that NoV virulence both *in vitro* and *in vivo* requires the specific virus-encoded activity to suppress RNAi (*185*). Specifically, suckling mice produce abundant vsiRNAs and become completely resistant to the infection by NoV mutants either not expressing B2 or expressing a mutant B2 (R59Q) defective in dsRNA binding and RNAi suppression (*185*), and the clearance of NoVΔB2 in mouse embryonic stem cells is AGO2-dependent (*196*). These findings provide evidence supportive to the proposal that the vsiRNA-induced RNAi response functions as an innate antiviral immunity in mammals.

The bioinformatics analysis identified a typical population of vsiRNAs from the infected human somatic cells only after combining VSR deletion and Argonaute co-immunoprecipitation. In contrast, total virus-specific small RNAs sequenced directly from suckling mice infected with B2-deletion mutant NoV exhibited strong canonical siRNA properties, suggesting that the non-specific degradation products of the high

molecular weight viral RNAs do not accumulate to a level that interferes with the detection of vsiRNAs under *in vivo* conditions.

To summarize, this dissertation reports three major findings on mammalian antiviral RNAi response. First, it reports the first detection of Dicer-dependent mammalian vsiRNAs both *in vitro* and *in vivo*. Second, it establishes a strategy to identify canonical vsiRNAs from mammalian somatic cells by combining both VSR depletion and Argonaute co-immunoprecipitation. Third, it identifies a set of bioinformatic properties of vsiRNAs to distinguish them from non-specific degradation products of the high molecular weight viral RNAs. These findings together provide new insights into the innate and adaptive control of important viral pathogens in human and other mammals.

Bibliography

1. Eugene V. Koonin *et al.*, The ancient Virus World and evolution of cells. *Biology Direct*. **1**:29 (Sep 19, 2006)
2. Mya Breitbart and Forest Rohwer, Here a virus, there a virus, everywhere the same virus? *Trends Microbiol*. **13(6)**:278-84 (Jun, 2005)
3. Edward Rybicki, The classification of organisms at the edge of life, or Problems with virus systematics. *South African Journal of Science*. **86**:182-86 (April, 1990)
4. Mary Glenn Fowler *et al.*, Reducing the risk of mother-to-child human immunodeficiency virus transmission: past successes, current progress and challenges, and future directions. *Am J Obstet Gynecol*. **197(3 Suppl)**:S3-9 (Sep, 2007)
5. Yanping Chen *et al.*, Horizontal and vertical transmission of viruses in the honey bee, *Apis mellifera*. *J Invertebr Pathol*. **92(3)**:152-9 (Jun 21, 2006)
6. Robin A. Weiss, How Does HIV Cause AIDS? *Science*. **260(5112)**:1273-9 (May 28,1993)
7. Alan W. Hampson and John S. Mackenzie, The influenza viruses. *MJA*. **185(10)**:S39-S43 (Nov 20,2006)
8. Ajai A. Dandekar and Stanley Perlman, Immunopathogenesis of coronavirus infections: implications for SARS. *Nat Rev Immunol*. **5(12)**:917-27 (Dec, 2005)
9. S. Pattyn *et al.*, Isolation of Marburg-like virus from a case of haemorrhagic fever in Zaire. *Lancet*. **1(8011)**:573-4 (Mar 12, 1977)
10. E. T. W. Bowen *et al.*, Viral haemorrhagic fever in southern Sudan and northern Zaire: Preliminary studies on the aetiological agent. *Lancet*. **1(8011)**:571-3 (Mar 12, 1977)
11. zur Hausen H., Viruses in human cancers. *Science*. **254(5035)**:1167-73 (Nov 22, 1991)
12. Patrick Forterre, The origin of viruses and their possible roles in major evolutionary transitions. *Virus Res*. **117(1)**:5-16 (Feb 14, 2006)
13. F. H. C. Crick and J. D. Watson, Structure of Small Viruses. *Nature.* **177**:473-75 (Mar 10, 1956)
14. D. L. D. Caspar and A. Klug, Physical principles in the construction of regular viruses. *Cold Spring Harb Symp Quant Biol*. **27**:1-24 (1962)
15. David Baltimore, Expression of Animal Virus Genomes. *Bacteriol Rev*. **35(3)**:235-41 (Sep, 1971)

16. Yizhi Jane Tao and Qiaozhen Ye, RNA Virus Replication Complexes. *PLoS Pathog*. **6(7)**:e1000943 (Jul, 2010)

17. Kenneth K.-S. Ng *et al.*, Structure-function relationships among RNA-dependent RNA polymerases. *Curr Top Microbiol Immunol*. **320**:137-56 (2008)

18. Eugene V. Koonin, The phylogeny of RNA-dependent RNA polymerases of positive-strand RNA viruses. *J Gen Virol*. **72(Pt 9)**:2197-206 (Sep, 1991)

19. Anne Salonen *et al.*, Viral RNA replication in association with cellular membranes. *Curr Top Microbiol Immunol*. **285**:139-73 (2005)

20. Rocío Coloma *et al.*, The Structure of a Biologically Active Influenza Virus Ribonucleoprotein Complex. *PLoS Pathog*. **5(6)**:e1000491 (Jun 26, 2009)

21. Ervin Fodor *et al.*, Characterization of the RNA-Fork Model of Virion RNA in the Initiation of Transcription in Influenza A Virus. *J Virol.* **69(7)**:4012-9 (Jul, 1995)

22. S. P. J. Whelan *et al.*, Transcription and replication of nonsegmented negative-strand RNA viruses. *Curr Top Microbiol Immunol*. **283**:61-119 (2004)

23. Todd J. Green and Ming Luo, Structure of the vesicular stomatitis virus nucleocapsid in complex with the nucleocapsid-binding domain of the small polymerase cofactor, P. *Proc Natl Acad Sci U.S.A.* **106(28)**:11713-8 (Jul 14, 2009)

24. Junhua Pan *et al.*, Atomic structure reveals the unique capsid organization of a dsRNA virus. *Proc Natl Acad Sci U.S.A.* **106(11)**:4225-30 (Mar 17, 2009)

25. Sarah M. McDonald *et al.*, The ins and outs of four-tunneled Reoviridae RNA-dependent RNA polymerases. *Curr Opin Struct Biol.* **19(6)**:775-82 (Dec, 2009)

26. C. Cheng Kao *et al.*, De Novo Initiation of Viral RNA-Dependent RNA Synthesis. *Virology.* **287(2)**:251-60 (Sep 1, 2001)

27. Alberdina A. van Dijk *et al.*, Initiation of viral RNA-dependent RNA polymerization. *J Gen Virol*. **85(Pt 5)**:1077-93 (May, 2004)

28. Margarita Salas, Protein-Priming of DNA Replication. *Annu. Rev. Biochem*. **60**:39-71 (1991)

29. Moira Hagen *et al.*, The role of template-primer interactions in cleavage and initiation by the influenza virus polymerase. *J Gen Virol*. **76(Pt 3)**:603-11 (Mar, 1995)

30. Friedemann Weber *et al.*, Double-Stranded RNA Is Produced by Positive-Strand RNA Viruses and DNA Viruses but Not in Detectable Amounts by Negative-Strand RNA Viruses. *J Virol.* **80(10)**:5059-64 (May, 2006)

31. E. Domingo and J. J. Holland, RNA Virus Mutations and Fitness for Survival. *Ann. Rev. Microbiol.* **51**:151-78 (1997)

32. D. A. Steinhauer and J. J. Holland, Rapid Evolution of RNA Viruses. *Ann. Rev. Microbiol.* **41**:409-33 (1987)

33. John W. Drake and John J. Holland, Mutation rates among RNA viruses. *Proc Natl Acad Sci U.S.A.* **96(24)**:13910-3 (Nov 23, 1999)

34. Buonagurio D. A. *et al.*, Evolution of human influenza A viruses over 50 years: rapid, uniform rate of change in NS gene. *Science.* **232(4753)**:980-2 (May 23, 1986)

35. Manfred Eigen, Viral quasispecies. *Sci Am.* **269(1)**:42-9 (1993)

36. Stuart E. Turvey and David H. Broide, Innate immunity. *J Allergy Clin Immunol.* **125(Suppl 2)**:S24-32 (2010)

37. Katherine R. Spindler and Tien-Huei Hsu, Viral disruption of the blood-brain barrier. *Trends Microbiol.* **20(6)**:282-290 (June, 2012)

38. Francisco A. Bonilla and Hans C. Oettgen, Adaptive immunity. *J Allergy Clin Immunol.* **125(Suppl 2)**:S33-40 (2010)

39. Max D. Cooper and Matthew N. Alder, The evolution of adaptive immune systems. *Cell.* **124(4)**:815-22 (Feb 24, 2006)

40. Zeev Pancer and Max D. Cooper, The evolution of adaptive immunity. *Annu Rev Immunol.* **24**:497-518 (2006)

41. Janet Stavnezer *et al.*, Mechanism and regulation of class switch recombination. *Annu Rev Immunol.* **26**:261-92 (2008)

42. Jonathan U. Peled *et al.*, The biochemistry of somatic hypermutation. *Annu Rev Immunol.* **26**:481-511 (2008)

43. Iris K. Pang and Akiko Iwasaki, Control of antiviral immunity by pattern recognition and the microbiome. *Immunol Rev.* **245(1)**:209-26 (Jan, 2012)

44. Charles A. Janeway, Jr. and Ruslan Medzhitov, Innate immune recognition. *Annu Rev Immunol.* **20**:197-216 (2002)

45. Bruce Beutler, Innate immunity: an overview. *Mol Immunol.* **40(12)**:845-59 (Feb, 2004)

46. Taro Kawai and Shizuo Akira, Toll-like receptors and their crosstalk with other innate receptors in infection and immunity. *Immunity*. **34(5)**:637-50 (May 27, 2011)

47. Kenya Honda *et al.*, Regulation of the type I IFN induction: a current view. *Int Immunol.* **(17)11**:1367-78 (Nov, 2005)

48. Ke Shuai and Bin Liu, Regulation of JAK–STAT signalling in the immune system. *Nat Rev Immunol.* **3(11)**:900-11 (Nov, 2003)

49. Catherine Dostert *et al.*, The Jak-STAT signaling pathway is required but not sufficient for the antiviral response of drosophila. *Nat Immunol.* **6(9)**:946-53 (Sep, 2005)

50. Grace Chen *et al.*, NOD-like receptors: role in innate immunity and inflammatory disease. *Annu Rev Pathol.* **4**:365-98 (2009)

51. Christopher Lupfer and Thirumala-Devi Kanneganti. The expanding role of NLRs in antiviral immunity. *Immunol Rev.* **255(1)**:13-24 (Sep, 2013)

52. Thirumala-Devi Kanneganti *et al.*, Critical role for Cryopyrin/Nalp3 in activation of caspase-1 in response to viral infection and double-stranded RNA. *J Biol Chem*. **281(48)**:36560-8 (Dec 1, 2006)

53. Ahmed Sabbah *et al.*, Activation of innate immune antiviral responses by Nod2. *Nat Immunol.* **10(10)**:1073-80 (Oct, 2009)

54. Minsun Hong *et al.*, Structure and functional characterization of the RNA-binding element of the NLRX1 innate immune modulator. *Immunity.* **36(3)**:337-47 (Mar 23, 2012)

55. Yueh-Ming Loo and Michael Gale Jr., Immune signaling by RIG-I-like receptors. *Immunity.* **34(5)**:680-92 (May 27, 2011)

56. Hiroki Kato *et al.*, Differential roles of MDA5 and RIG-I helicases in the recognition of RNA viruses. *Nature.* **441(7089)**:101-5 (May 4, 2006)

57. Martin Schlee *et al.*, Recognition of 5' triphosphate by RIG-I helicase requires short blunt double-stranded RNA as contained in panhandle of negative-strand virus. *Immunity.* **31(1)**:25-34 (Jul 17, 2009)

58. Delphine Goubau *et al.*, Antiviral immunity via RIG-I-mediated recognition of RNA bearing 5'-diphosphates. *Nature.* **514(7522)**:372-5 (Oct 16, 2014)

59. Kathy Triantafilou *et al.*, Visualisation of direct interaction of MDA5 and the dsRNA replicative intermediate form of positive strand RNA viruses. *J Cell Sci*. **125(Pt 20)**:4761-9 (Oct 15, 2012)

60. Simon Rothenfusser *et al.*, The RNA helicase Lgp2 inhibits TLR-independent sensing of viral replication by retinoic acid-inducible gene-I. *J Immunol.* **175(8)**:5260-8 (Oct 15, 2005)

61. Takashi Satoh *et al.*, LGP2 is a positive regulator of RIG-I- and MDA5-mediated antiviral responses. *Proc Natl Acad Sci U.S.A.* **107(4)**:1512-7 (Jan 26, 2010)

62. Akiko Iwasaki and Ruslan Medzhitov, Regulation of adaptive immunity by the innate immune system. *Science.* **327(5963)**:291-5 (Jan 15, 2010)

63. Akiko Iwasaki and Ruslan Medzhitov, Toll-like receptor control of the adaptive immune responses. *Nat Immunol.* **5(10)**:987-95 (Oct, 2004)

64. Noah W. Palm and Ruslan Medzhitov, Pattern recognition receptors and control of adaptive immunity. *Immunol Rev*. **227(1)**:221-33 (Jan, 2009)

65. Joseph C. Sun and Lewis L. Lanier, Natural killer cells remember: an evolutionary bridge between innate and adaptive immunity? *Eur J Immunol.* **39(8)**:2059-64 (Aug, 2009)

66. Megha Ghildiyal and Phillip D. Zamore, Small silencing RNAs: an expanding universe. *Nat Rev Genet.* **10(2)**:94-108 (Feb, 2009)

67. Witold Filipowicz *et al.*, Post-transcriptional gene silencing by siRNAs and miRNAs. *Curr Opin Struct Biol.* **15(3)**:331-41 (Jun, 2005)

68. Carolyn Napoli *et al.*, Introduction of a Chimeric Chalcone Synthase Gene into Petunia Results in Reversible Co-Suppression of Homologous Genes in trans. *Plant Cell.* **2(4)**:279-89 (Apr, 1990)

69. Alexander R. van der Krol *et al.*, Flavonoid genes in petunia: addition of a limited number of gene copies may lead to a suppression of gene expression. *Plant Cell.* **2(4)**:291-9 (Apr, 1990)

70. Rosalind C. Lee *et al.*, The C. elegans heterochronic gene lin-4 encodes small RNAs with antisense complementarity to lin-14. *Cell.* **75(5)**:843-54 (Dec 3, 1993)

71. Benjamin P. Lewis *et al.*, Conserved seed pairing, often flanked by adenosines, indicates that thousands of human genes are microRNA targets. *Cell.* **120(1)**:15-20 (Jan 14, 2005)

72. Yoontae Lee *et al.*, MicroRNA maturation: stepwise processing and subcellular localization. *EMBO J*. **21(17)**:4663-70 (Sep 2, 2002)

73. J. Graham Ruby *et al.*, Intronic microRNA precursors that bypass Drosha processing. *Nature.* **448(7149)**:83-6 (Jul 5, 2007)

74. Katsutomo Okamura *et al.*, The mirtron pathway generates microRNA-class regulatory RNAs in Drosophila. *Cell*. **130(1)**:89-100 (Jul 13, 2007)

75. Eugene Berezikov *et al.*, Mammalian Mirtron Genes. *Mol Cell.* **28(2)**:328-36 (Oct 26, 2007)

76. Yoontae Lee *et al.*, MicroRNA genes are transcribed by RNA polymerase II. *EMBO J.* **23(20)**:4051-60 (Oct 13, 2004)

77. Xuezhong Cai *et al.*, Human microRNAs are processed from capped, polyadenylated transcripts that can also function as mRNAs. *RNA.* **10(12)**:1957-66 (Dec, 2004)

78. Yoontae Lee *et al.*, The nuclear RNase III Drosha initiates microRNA processing. *Nature.* **425(6956)**:415-9 (Sep 25, 2003)

79. Donald L. Court *et al.*, RNase III: Genetics and function; structure and mechanism. *Annu Rev Genet.* **47**:405-31 (2013)

80. Tomoko Kawamata and Yukihide Tomari, Making RISC. *Trends Biochem Sci.* **35(7)**:368-76 (2010)

81. Gunter Meister, Argonaute proteins: functional insights and emerging roles. *Nat Rev Genet.* **14(7)**:447-59 (Jul, 2013)

82. Richard I. Gregory *et al.*, Human RISC couples microRNA biogenesis and posttranscriptional gene silencing. *Cell.* **123(4)**:631-40 (Nov 18, 2005)

83. Keita Miyoshi *et al.,* Characterization of the miRNA-RISC loading complex and miRNA-RISC formed in the Drosophila miRNA pathway. *RNA.* **15(7)**:1282-91 (Jul, 2009)

84. Dianne S. Schwarz *et al.*, Asymmetry in the Assembly of the RNAi Enzyme Complex. *Cell*. **115(2)**:199-208 (Oct 17, 2003)

85. David P. Bartel, MicroRNAs: target recognition and regulatory functions. *Cell*. **136(2)**:215-33 (Jan 23, 2009)

86. Sam Griffiths-Jones *et al.*, miRBase: tools for microRNA genomics. *Nucleic Acids Res.* **36(Database issue)**:D15-8 (Jan, 2008)

87. Sihem Cheloufi *et al.*, A dicer-independent miRNA biogenesis pathway that requires Ago catalysis. *Nature.* **465(7298)**:584-9 (Jun 3, 2010)

88. Daniel Cifuentes *et al.*, A novel miRNA processing pathway independent of Dicer requires Argonaute2 catalytic activity. *Science.* **328(5986)**:1694-8 (Jun 25, 2010)

89. Andrew Fire *et al.*, Potent and specific genetic interference by double-stranded RNA in Caenorhabditis elegans. *Nature.* **391(6669)**:806-11 (Feb 19, 1998)

90. Feng Qu *et al.*, RDR6 has a broad-spectrum but temperature-dependent antiviral defense role in Nicotiana benthamiana. *J Virol.* **79(24)**:15209-17 (Dec, 2005)

91. Olivier Voinnet, Use, tolerance and avoidance of amplified RNA silencing by plants. *Trends Plant Sci.* **13(7)**:317-28 (Jul, 2008)

92. Emily Bernstein *et al.*, Role for a bidentate ribonuclease in the initiation step of RNA interference. *Nature.* **409(6818)**:363-6 (Jan 18, 2001)

93. Edwards Allen *et al.*, microRNA-directed phasing during trans-acting siRNA biogenesis in plants. *Cell.* **121(2)**:207-21 (Apr 22, 2005)

94. Antti Nykänen *et al.*, ATP requirements and small interfering RNA structure in the RNA interference pathway. *Cell.* **107(3)**:309-21 (Nov 2, 2001)

95. Haidi Zhang *et al.*, Human Dicer preferentially cleaves dsRNAs at their termini without a requirement for ATP. *EMBO J.* **21(21)**:5875-85 (Nov 1, 2002)

96. Thomas Tuschl *et al.*, Targeted mRNA degradation by double-stranded RNA in vitro. *Genes Dev.* **13(24)**:3191-7 (Dec 15, 1999)

97. Phillip D. Zamore *et al.*, RNAi: double-stranded RNA directs the ATP-dependent cleavage of mRNA at 21 to 23 nucleotide intervals. *Cell.* **101(1)**:25-33 (Mar 31, 2000)

98. Aimee L. Jackson *et al.*, Widespread siRNA "off-target" transcript silencing mediated by seed region sequence complementarity. *RNA.* **12(7)**:1179-87 (Jul, 2006)

99. John G. Doench *et al.*, siRNAs can function as miRNAs. *Genes Dev.* **17(4)**:438-42 (Feb 15, 2003)

100. Chi Zhang *et al.*, The Caenorhabditis elegans RDE-10/RDE-11 complex regulates RNAi by promoting secondary siRNA amplification. *Curr Biol.* **22(10)**:881-90 (May 22, 2012)

101. Patrick Provost *et al.*, Ribonuclease activity and RNA binding of recombinant human Dicer. *EMBO J.* **21(21)**:5864-74 (Nov 1, 2002)

102. Nuo Yang and Haig H. Kazazian, Jr., L1 retrotransposition is suppressed by endogenously encoded small interfering RNAs in human cultured cells. *Nat Struct Mol Biol.* **13(9)**:763-71 (Sep, 2006)

103. Takashi Sasaki *et al.*, Identification of eight members of the Argonaute family in the human genome. *Genomics.* **82(3)**:323-30 (Sep, 2003)

104. Dongmei Wang *et al.*, Quantitative functions of Argonaute proteins in mammalian development. *Genes Dev.* **26(7)**:693-704 (Apr 1, 2012)

105. Gunter Meister *et al.*, Human Argonaute2 mediates RNA cleavage targeted by miRNAs and siRNAs. *Mol Cell.* **15(2)**:185-97 (Jul 23, 2004)

106. Jidong Liu *et al.*, Argonaute2 is the catalytic engine of mammalian RNAi. *Science.* **305(5689)**:1437-41 (Sep 3, 2004)

107. Young Sik Lee *et al.*, Distinct roles for Drosophila Dicer-1 and Dicer-2 in the siRNA/miRNA silencing pathways. *Cell.* **117(1)**:69-81 (Apr 2, 2004)

108. Benjamin Czech *et al.*, Hierarchical rules for Argonaute loading in Drosophila. *Mol Cell.* **36(3)**:445-56 (Nov 13, 2009)

109. Peter Sarkies and Eric A. Miska, Small RNAs break out: the molecular cell biology of mobile small RNAs. *Nat Rev Mol Cell Biol.* **15(8)**:525-35 (Aug, 2014)

110. Scott W. Knight and Brenda L. Bass, A role for the RNase III enzyme DCR-1 in RNA interference and germ line development in Caenorhabditis elegans. *Science.* **293(5538)**:2269-71 (Sep 21, 2001)

111. René F. Ketting *et al.*, Dicer functions in RNA interference and in synthesis of small RNA involved in developmental timing in C. elegans. *Genes Dev.* **15(20)**:2654-9 (Oct 15, 2001)

112. Alla Grishok *et al.*, Genes and mechanisms related to RNA interference regulate expression of the small temporal RNAs that control C. elegans developmental timing. *Cell.* **106(1)**:23-34 (Jul 13, 2001)

113. Susan Parrish and Andrew Fire, Distinct roles for RDE-1 and RDE-4 during RNA interference in Caenorhabditis elegans. *RNA.* **7(10)**:1397-402 (Oct, 2001)

114. Colin C. Conine *et al.*, Argonautes ALG-3 and ALG-4 are required for spermatogenesis-specific 26G-RNAs and thermotolerant sperm in Caenorhabditis elegans. *Proc Natl Acad Sci U.S.A.* **107(8)**:3588-93 (Feb 23, 2010)

115. Weifeng Gu *et al.*, Distinct argonaute-mediated 22G-RNA pathways direct genome surveillance in the C. elegans germline. *Mol Cell.* **36(2)**:231-44 (Oct 23, 2009)

116. Yukio Kurihara and Yuichiro Watanabe, Arabidopsis micro-RNA biogenesis through Dicer-like 1 protein functions. *Proc Natl Acad Sci U.S.A.* **101(34)**:12753-8 (Aug 24, 2004)

117. Yukio Kurihara *et al.*, The interaction between DCL1 and HYL1 is important for efficient and precise processing of pri-miRNA in plant microRNA biogenesis. *RNA.* **12(2)**:206-12 (Feb, 2006)

118. Minju Ha and V. Narry Kim *et al.*, Regulation of microRNA biogenesis. *Nat Rev Mol Cell Biol.* **15(8)**:509-24 (Aug, 2014)

119. Ian R. Henderson *et al.*, Dissecting Arabidopsis thaliana DICER function in small RNA processing, gene silencing and DNA methylation patterning. *Nat Genet.* **38(6)**:721-5 (Jun, 2006)

120. Rajendran Rajeswaran *et al.*, Sequencing of RDR6-dependent double-stranded RNAs reveals novel features of plant siRNA biogenesis. *Nucleic Acids Res.* **40(13)**:6241-54 (Jul, 2012)

121. Daniel Zilberman *et al.*, Role of Arabidopsis ARGONAUTE4 in RNA-directed DNA methylation triggered by inverted repeats. *Curr Biol.* **14(13)**:1214-20 (Jul 13, 2004)

122. Ho-Ming Chen *et al.*, 22-Nucleotide RNAs trigger secondary siRNA biogenesis in plants. *Proc Natl Acad Sci U.S.A.* **107(34)**:15269-74 (Aug 24, 2010)

123. Rebecca Schwab and Olivier Voinnet, RNA silencing amplification in plants: size matters. *Proc Natl Acad Sci U.S.A.* **107(34)**:14945-6 (Aug 24, 2010)

124. Travis Thomson and Haifan Lin, The biogenesis and function of PIWI proteins and piRNAs: progress and prospect. *Annu Rev Cell Dev Biol.* **25**:355-76 (2009)

125. Jonathan B. Preall *et al.*, shutdown is a component of the Drosophila piRNA biogenesis machinery. *RNA.* **18(8)**:1446-57 (Aug, 2012)

126. Julius Brennecke *et al.*, Discrete small RNA-generating loci as master regulators of transposon activity in Drosophila. *Cell.* **128(6)**:1089-103 (Mar 23, 2007)

127. Weifeng Gu *et al.*, CapSeq and CIP-TAP identify Pol II start sites and reveal capped small RNAs as C. elegans piRNA precursors. *Cell.* **151(7)**:1488-500 (Dec 21, 2012)

128. Shou-wei Ding. RNA-based antiviral immunity. *Nat Rev Immunol.* **10(9)**:632-44 (Sep, 2010)

129. Frank Ratcliff *et al.*, A similarity between viral defense and gene silencing in plants. *Science.* **276(5318)**:1558-60 (Jun 6, 1997)

130. Andrew J. Hamilton and David C. Baulcombe. A species of small antisense RNA in posttranscriptional gene silencing in plants. *Science.* **286(5441)**:950-2 (Oct 29, 1999)

131. Roghiyh Aliyari *et al.*, Mechanism of induction and suppression of antiviral immunity directed by virus-derived small RNAs in Drosophila. *Cell Host Microbe.* **4(4)**:387-97 (Oct 16, 2008)

132. Qingfa Wu *et al.*, Virus discovery by deep sequencing and assembly of virus-derived small silencing RNAs. *Proc Natl Acad Sci U.S.A.* **107(4)**:1606-11 (Jan 26, 2010)

133. Xuemin Zhang *et al.*, Characterization of hypovirus-derived small RNAs generated in the chestnut blight fungus by an inducible DCL-2-dependent pathway. *J Virol.* **82(6)**:2613-9 (Mar, 2008)

134. Xiao-Hong Wang *et al.*, RNA interference directs innate immunity against viruses in adult Drosophila. *Science.* **312(5772)**:452-4 (Apr 21, 2006)

135. Marie-Anne Félix *et al.*, Natural and experimental infection of Caenorhabditis nematodes by novel viruses related to nodaviruses. *PLoS Biol.* **9(1)**:e1000586 (Jan 25, 2011)

136. Angéliqu Deleris *et al.*, Hierarchical action and inhibition of plant Dicer-like proteins in antiviral defense. *Science.* **313(5783)**:68-71 (Jul 7, 2006)

137. Jennifer L. Umbach and Bryan R. Cullen, The role of RNAi and microRNAs in animal virus replication and antiviral immunity. *Genes Dev.* **23(10)**:1151-64 (May 15, 2009)

138. Heather L. Chotkowski *et al.*, West Nile virus infection of Drosophila melanogaster induces a protective RNAi response. *Virology.* **377(1)**:197-206 (Jul 20, 2008)

139. Robert A. Zambon *et al.*, RNAi is an antiviral immune response against a dsRNA virus in Drosophila melanogaster. *Cell Microbiol.* **8(5)**:880-9 (May, 2006)

140. Margot Karlikow *et al.*, RNAi and antiviral defense in Drosophila: setting up a systemic immune response. *Dev Comp Immunol.* **42(1)**:85-92 (Jan, 2014)

141. Esther Schnettler *et al.*, Knockdown of piRNA pathway proteins results in enhanced Semliki Forest virus production in mosquito cells. *J Gen Virol.* **94(Pt 7)**:1680-9 (Jul, 2013)

142. Joël T. van Mierlo *et al.*, Defense and counterdefense in the RNAi-based antiviral immune system in insects. *Methods Mol Biol.* **721**:3-22 (2011)

143. Leah R. Sabin *et al.*, Ars2 regulates both miRNA- and siRNA- dependent silencing and suppresses RNA virus infection in Drosophila. *Cell.* **138(2)**:340-51 (Jul 23, 2009)

144. Maria-Carla Saleh *et al.*, Antiviral immunity in Drosophila requires systemic RNAi spread. *Nature.* **458(7236)**:346-50 (Mar 19, 2009)

145. R. Lu *et al.*, Animal virus replication and RNAi-mediated antiviral silencing in Caenorhabditis elegans. *Nature.* **436(7053)**:1040-3 (Aug 18, 2005)

146. Courtney Wilkins *et al.*, RNA interference is an antiviral defence mechanism in Caenorhabditis elegans. *Nature.* **436(7053)**:1044-7 (Aug 18, 2005)

147. Marie-Anne Félix *et al.*, Natural and experimental infection of Caenorhabditis nematodes by novel viruses related to nodaviruses. *PLoS Biol.* **9(1)**:e1000586 (Jan 25, 2011)

148. R. Lu *et al.*, An RIG-I-Like RNA helicase mediates antiviral RNAi downstream of viral siRNA biogenesis in Caenorhabditis elegans. *PLoS Pathog.* **5(2)**:e1000286 (Feb, 2009)

149. Mark G. Sterken *et al.*, A Heritable Antiviral RNAi Response Limits Orsay Virus Infection in Caenorhabditis elegans N2. *PLoS One.* **9(2)**:e89760 (2014)

150. Peter Sarkies and Eric A. Miska, RNAi pathways in the recognition of foreign RNA: antiviral responses and host-parasite interactions in nematodes. *Biochem Soc Trans.* **41(4)**:876-80 (Aug, 2013)

151. Nicolas Boché *et al.*, An antagonistic function for Arabidopsis DCL2 in development and a new function for DCL4 in generating viral siRNAs. *EMBO J.* **25(14)**:3347-56 (Jul 26, 2006)

152. Xiuren Zhang *et al.*, Cucumber mosaic virus-encoded 2b suppressor inhibits Arabidopsis Argonaute1 cleavage activity to counter plant defense. *Genes Dev.* **20(23)**:3255-68 (Dec 1, 2006)

153. Jean-Benoit Morel *et al.*, Fertile hypomorphic ARGONAUTE (ago1) mutants impaired in post-transcriptional gene silencing and virus resistance. *Plant Cell.* **14(3)**:629-39 (Mar, 2002)

154. Feng Qu *et al.*, Arabidopsis DRB4, AGO1, AGO7, and RDR6 participate in a DCL4-initiated antiviral RNA silencing pathway negatively regulated by DCL1. *Proc Natl Acad Sci U.S.A.* **105(38)**:14732-7 (Sep 23, 2008)

155. Atsushi Takede *et al.*, The mechanism selecting the guide strand from small RNA duplexes is different among argonaute proteins. *Plant Cell Physiol.* **49(4)**:493-500 (Apr, 2008)

156.Xian-Bing Wang *et al.*, RNAi-mediated viral immunity requires amplification of virus-derived siRNAs in Arabidopsis thaliana. *Proc Natl Acad Sci U.S.A.* **107(1)**:484-9 (Jan 5, 2010)

157.Attila Molnar *et al.*, Small silencing RNAs in plants are mobile and direct epigenetic modification in recipient cells. *Science.* **328(5980)**:872-5 (May 14, 2010)

158.Patrice Dunoyer *et al.*, Small RNA duplexes function as mobile silencing signals between plant cells. *Science.* **328(5980)**:912-6 (May 14, 2010)

159.Todd Blevins *et al.*, Four plant Dicers mediate viral small RNA biogenesis and DNA virus induced silencing. *Nucleic Acids Res.* **34(21)**:6233-46 (2006)

160.Priya Raja *et al.*, Viral genome methylation as an epigenetic defense against geminiviruses. *J Virol.* **82(18)**:8997-9007 (Sep, 2008)

161.Qingfa Wu *et al.*, Viral suppressors of RNA-based viral immunity: host targets. *Cell Host Microbe.* **8(1)**:12-5 (Jul 22, 2010)

162.Hongwei Li *et al.*, Induction and suppression of RNA silencing by an animal virus. *Science.* **296(5571)**:1319-21 (May 17, 2002)

163.Chao *et al.*, Dual modes of RNA-silencing suppression by Flock House virus protein B2. *Nat Struct Mol Biol.* **12(11)**:952-7 (Nov, 2005)

164.Andreas Lingel *et al.*, The structure of the flock house virus B2 protein, a viral suppressor of RNA interference, shows a novel mode of double-stranded RNA recognition. *EMBO Rep.* **6(12)**:1149-55 (Dec, 2005)

165.JN Leonard and DV Schaffer, Antiviral RNAi therapy: emerging approaches for hitting a moving target. *Gene Ther.* **13(6)**:532-40 (Mar, 2006)

166.Priya S. Shah and David V. Schaffer, Antiviral RNAi: translating science towards therapeutic success. *Pharm Res.* **28(12)**:2966-82 (Dec, 2011)

167.Jiehua Zhou and John J. Rossi, Progress in RNAi-based antiviral therapeutics. *Methods Mol Biol.* **721**:67-75 (2011)

168.Walter de Vries and Ben Berkhout, RNAi suppressors encoded by pathogenic human viruses. *Int J Biochem Cell Biol.* **40(10)**:2007-12 (2008)

169.Stephanie Korber *et al.*, Structure of the RNA-binding domain of Nodamura virus protein B2, a suppressor of RNA interference. *Biochemistry.* **48(11)**:2307-9 (Mar 24, 2009)

170.Etienne Bucher *et al.*, The influenza A virus NS1 protein binds small interfering RNAs and suppresses RNA silencing in plants. *J Gen Virol.* **85(Pt 4)**:983-91 (Apr, 2004)

171.Joost Haasnoot *et al.*, The Ebola Virus VP35 protein is a suppressor of RNA silencing. *PLoS Pathog.* **3(6)**: e86. (Jun, 2007)

172. Yamina Bennasser *et al.*, Evidence that HIV-1 encodes an siRNA and a suppressor of RNA silencing. *Immunity.* **22(5)**:607-19 (May, 2005)

173. Pavan Kumar Kakumani *et al.*, Role of RNA interference (RNAi) in dengue virus replication and identification of NS4B as an RNAi suppressor. *J Virol.* **87(16)**:8870-83 (Aug, 2013)

174. Alexey A. Matskevich and Karin Moelling. Dicer is involved in protection against influenza A virus infection. *J Gen Virol.* **88(Pt 10)**:2627-35 (Oct, 2007)

175. Motoyuki Otsuka *et al.*, Hypersusceptibility to vesicular stomatitis virus infection in Dicer1-deficient mice is due to impaired miR24 and miR93 expression. *Immunity.* **27(1)**:123-34 (Jul, 2007)

176. Robinson Triboulet *et al.*, Suppression of microRNA-silencing pathway by HIV-1 during virus replication. *Science.* **315(5818)**:1579-82 (Mar 16, 2007)

177. Bryan R Cullen. Is RNA interference involved in intrinsic antiviral immunity in mammals? *Nat Immunol.* **7(6)**:563-7 (Jun, 2006)

178. Sébastien Pfeffer *et al.*, Identification of microRNAs of the herpesvirus family. *Nat Methods.* **2(4)**:269-76 (Apr, 2005)

179. Poornima Parameswaran *et al.*, Six RNA viruses and forty-one hosts: viral small RNAs and modulation of small RNA repertoires in vertebrate and invertebrate systems. *PLoS Pathog.* **6(2)**:e1000764 (Feb 12, 2010)

180. Jennifer L. Umbach *et al.*, Influenza A virus expresses high levels of an unusual class of small viral leader RNAs in infected cells. *MBio.* **1(4). pii**: e00204-10 (Sep 14, 2010)

181. Kyle L. Johnson *et al.*, Nodamura virus nonstructural protein B2 can enhance viral RNA accumulation in both mammalian and insect cells. *J Virol.* **78(12)**:6698-704 (Jun, 2004)

182. Wan-Xiang Li *et al.*, Interferon antagonist proteins of influenza and vaccinia viruses are suppressors of RNA silencing. *Proc Natl Acad Sci U.S.A.* **101(5)**:1350-5 (Feb 3, 2004)

183. Christopher S. Sullivan and Don Ganem. A virus-encoded inhibitor that blocks RNA interference in mammalian cells. *J Virol.* **79(12)**:7371-9 (Jun, 2005)

184. Kathryn C. Johnson *et al.*, Conserved microRNAs in Chinese hamster ovary cell lines. *Biotechnol Bioeng.* **108(2)**:475-80 (Feb, 2011)

185. Yang Li *et al.*, RNA interference functions as an antiviral immunity mechanism in mammals. *Science.* **342(6155)**:231-4 (Oct 11, 2013)

186. Jeffery K. Taubenberger and David M. Morens. The pathology of influenza virus infections. *Annu Rev Pathol.* **3**:499-522 (2008)

187. Boguslaw Szewczyk *et al.*, Introduction to molecular biology of influenza a viruses. *Acta Biochim Pol.* **61(3)**:397-401 (2014)

188. Adolfo García-Sastre *et al.*, Influenza A virus lacking the NS1 gene replicates in interferon-deficient systems. *Virology.* **252(2)**:324-30 (Dec 20, 1998)

189. Chaolin Zhang and Robert B. Darnell. Mapping in vivo protein-RNA interactions at single-nucleotide resolution from HITS-CLIP data. *Nat Biotechnol.* **29(7)**:607-14 (Jun 1, 2011)

190. I-Chueh Huang *et al.*, Distinct patterns of IFITM-mediated restriction of filoviruses, SARS coronavirus, and influenza A virus. *PLoS Pathog.* **7(1)**:e1001258 (Jan 6, 2011)

191. Ji-Hong Yang *et al.*, Real-time RT-PCR for quantitation of hepatitis C virus RNA. *J Virol Methods.* **102(1-2)**:119-28 (Apr, 2002)

192. Caifu Chen *et al.*, Real-time quantification of microRNAs by stem-loop RT-PCR. *Nucleic Acids Res.* **33(20)**:2179 (Nov 27, 2005)

193. L. Andrew Ball *et al.*, Replication of nodamura virus after transfection of viral RNA into mammalian cells in culture. *J Virol.* **66(4)**:2326-34 (Apr, 1992)

194. Yanhong Han *et al.*, RNA-based immunity terminates viral infection in adult Drosophila in the absence of viral suppression of RNA interference: characterization of viral small interfering RNA populations in wild-type and mutant flies. *J Virol.* **85(24)**:13153-63 (Dec, 2011)

195. Yang Li *et al.*, Mechanism of influenza A virus NS1 protein interaction with the p85beta, but not the p85alpha, subunit of phosphatidylinositol 3-kinase (PI3K) and up-regulation of PI3K activity. *J Biol Chem.* **283(34)**:23397-409 (Aug 22, 2008)

196. P. V. Maillard *et al.*, Antiviral RNA interference in mammalian cells. *Science.* **342(6155)**:235-8 (Oct 11, 2013)

197. Matyas Flemr *et al.*, A retrotransposon-driven dicer isoform directs endogenous small interfering RNA production in mouse oocytes. *Cell.* **155(4)**:807-16 (Nov 7, 2013)

198. Michelle Quinlivan *et al.*, Attenuation of equine influenza viruses through truncations of the NS1 protein. *J Virol.* **79(13)**:8431-9 (Jul, 2005)

199. Hal P. Bogerd *et al.*, Derivation and characterization of Dicer- and microRNA-deficient human cells. *RNA.* **20(6)**:923-37 (Jun, 2014)

200. Min Zheng *et al.*, An A14U Substitution in the 3' Noncoding Region of the M Segment of Viral RNA Supports Replication of Influenza Virus with an NS1 Deletion by Modulating Alternative Splicing of M Segment mRNAs. *J Virol.* **89(20)**:10273-85 (Oct 15, 2015)

201. Weirong Wang *et al.*, RNA binding by the novel helical domain of the influenza virus NS1 protein requires its dimer structure and a small number of specific basic amino acids. *RNA*. **5(2)**:195-205 (Feb, 1999)

202. Xiang Liu *et al.*, Dicer-2 and R2D2 coordinately bind siRNA to promote assembly of the siRISC complexes. *RNA.* **12(8)**:1514-20 (Aug, 2006)

203. Xiang Liu *et al.*, Dicer-1, but not Loquacious, is critical for assembly of miRNA-induced silencing complexes. *RNA.* **13(12)**:2324-29 (Dec, 2007)

204. Gurman Singh Pall *et al.*, Carbodiimide-mediated cross-linking of RNA to nylon membranes improves the detection of siRNA, miRNA and piRNA by northern blot. *Nucleic Acids Res.* **35(8)**:e60 (Apr 2, 2007)

205. Kyung-No Son *et al.*, Double-Stranded RNA Is Detected by Immunofluorescence Analysis in RNA and DNA Virus Infections, Including Those by Negative-Stranded RNA Viruses. *J Virol.* **89(18)**:9383-92 (Sep, 2015)

206. Stéphanie Anchisi *et al.*, RIG-I ATPase activity and discrimination of self-RNA versus non-self-RNA. *MBio.* **6(2)**:e02349 (Mar 3, 2015)

207. Yongzhi Cui *et al.*, The Stat3/5 locus encodes novel endoplasmic reticulum and helicase-like proteins that are preferentially expressed in normal and neoplastic mammary tissue. *Genomics.* **78(3)**:129-34 (Dec, 2001)

208. Juan A. Diaz-Pendon *et al.*, Suppression of antiviral silencing by cucumber mosaic virus 2b protein in Arabidopsis is associated with drastically reduced accumulation of three classes of viral small interfering RNAs. *Plant Cell.* **19(6)**:2053-63 (Jun, 2007)

209. Xian-Bing Wang *et al.*, The 21-nucleotide, but not 22-nucleotide, viral secondary small interfering RNAs direct potent antiviral defense by two cooperative argonautes in Arabidopsis thaliana. *Plant Cell.* **23(4)**:1625-38 (Apr, 2011)

210. Xunyang Guo *et al.*, Silencing of host genes directed by virus-derived short interfering RNAs in Caenorhabditis elegans. *J Virol.* **86(21)**:11645-53 (Nov, 2012)

211. Delphine Galiana-Arnoux *et al.*, Essential function in vivo for Dicer-2 in host defense against RNA viruses in drosophila. *Nat Immunol.* **7(6)**:590-7 (Jun, 2006)

212. Vira Bitko *et al.*, Inhibition of respiratory viruses by nasally administered siRNA. *Nat Med.* **11(1)**:50-5 (Jan, 2005)

213. Kyle L. Johnson *et al.*, Recovery of infectivity from cDNA clones of nodamura virus and identification of small nonstructural proteins. *Virology.* **305(2)**:436-51 (Jan 20, 2003)

214. A. Schneemann, L. A. Ball, C. Delsert, J. E. Johnson, T. Nishizawa, in *Virus Taxonomy—Eighth Report of the International Committee on Taxonomy of Viruses*

C. M. Fauquet *et al.*, Eds. (Elsevier, San Diego, CA, 2005), pp. 865–872.

215. Bryan R. Cullen. RNA interference does not function as an innate antiviral response in mammalian somatic cells. *Future Virology*. **6(12)**:1381-4 (2011).

216. Bryan R. Cullen. Viruses and RNA interference: issues and controversies. *J Virol*. **88(22)**:12934-6 (Nov, 2014).

217. Nicola R. Donelan *et al.*, A recombinant influenza A virus expressing an RNA-binding-defective NS1 protein induces high levels of beta interferon and is attenuated in mice. *J Virol*. **77(24)**:13257-66 (Dec, 2003).

218. Jasmine T. Perez *et al.*, Influenza A virus-generated small RNAs regulate the switch from transcription to replication. *Proc Natl Acad Sci U.S.A.* **107(25)**:11525-30 (Jun 22, 2010)

219. Daniel Marc. Influenza virus non-structural protein NS1: interferon antagonism and beyond. *J Gen Virol*. **95(Pt 12)**:2594-611 (2014).

220. Benjamin Czech and Gregory J. Hannon. Small RNA sorting: matchmaking for Argonautes. *Nat Rev Genet.* **12(1)**:19-31 (Jan, 2011)

221. Ross C. Wilson and Jennifer A. Doudna. Molecular mechanisms of RNA interference. *Annu Rev Biophys*. **42**:217-39 (2013)

222. Arindam Chakrabarti *et al.*, New insights into the role of RNase L in innate immunity. *J Interferon Cytokine Res.* **31(1)**:49-57 (Jan, 2011)

223. Amiya K. Banerjee and Sailen Barik. Gene expression of vesicular stomatitis virus genome RNA. *Virology.* **188(2)**:417-28 (Jun, 1992)

224. Brandon S. Huneycutt *et al.*, Central neuropathogenesis of vesicular stomatitis virus infection of immunodeficient mice. *J Virol*. **67(11)**:6698-706 (NoV, 1993)